Volume 2 | Issue 2 | 2020

Technical Journal

Engineering excellence around the globe

N LAVALIN

Foreword

Chris Hendy

Editor-in-Chief SNC-Lavalin
Technical Journal

Professional Head of Bridge
Engineering and Transportation
Technical Director, EDPM

Welcome to the fourth edition of our SNC-Lavalin Technical Journal, established to showcase the fantastic depth and breadth of our engineering expertise across a wide range of disciplines and domains and to demonstrate that technical excellence is at the heart of everything we do. This fourth edition highlights the impressive work we have been doing from the improvement of existing design standards and development of new concepts, to the development of innovative designs and construction methods which enhance the environment and improve constructability, and the management of existing assets to extend service life and improve performance. And at this strangest of times, in the midst of a pandemic, we have run simulations to predict how to best manage the spread of COVID-19 whilst simultaneously preserving our global economies.

At concept design stage, we have produced the concept design for the most high-profile viaduct on the UK's HS2 high speed rail line, which intentionally sets the benchmark for quality and environmentally sensitive design for other structures to match across the entire scheme. We have also driven improvements in bridge design standards for light weight footbridges by enhancing the guidance and requirements for design to better limit vibrations such that adequate comfort is afforded to pedestrians using footbridges in a wide variety of common situations.

In design, we have significantly improved the efficiency of bored pile design in Denmark through our collaborative working with a piling contractor to correlate new design methods with site testing. And on the Elizabeth Line of the UK's Crossrail project we have analysed the success of prototyping the GFRC tunnel cladding to de-risk construction and improve quality, construction safety and whole-life performance.

In the field of asset management, we have extended the life of the suspension cables on the UK's longest suspension bridge through an innovative selective-replacement and testing regime which can be deployed on other suspension bridges around the world. And in Florida, working with FDOT we have established a new tidal connection in an area of Old Tampa Bay which dramatically improves water quality and creates ecological conditions that are conducive to seagrass recovery and benthic habitat.

The above examples provide only a small insight into the wealth of innovative papers presented in this journal and the far wider contribution that SNC-Lavalin makes day to day.

I hope you enjoy the selection of technical papers included in this edition as much as we have enjoyed compiling them.

Editor-in-Chief

Chris Hendy
Editor-in-Chief

FREng, MA (Cantab) CEng FICE Eur Ing
Technical Director, Atkins Fellow,
Professional Head of Bridge
Engineering
Engineering, Design and Project
Management
Epsom, UK

2020 Editorial Board Members

Ramy Azar
Ph.D, Ing.

Vice-President of Engineering and CTO
- Grid Solutions & Renewables
Power, Grid and Industrial Solutions
Infrastructure
Montreal, Canada

Vinod Batta
Ph.D., P.Eng.

Vice President & General Manager,
Power Solutions - Western Canada
Power, Grid & Industrial Solutions
Infrastructure
Vancouver, Canada

Donna Huey
GISP

Atkins Fellow and Sr. Vice President,
Client Technology Director
Engineering, Design and Project
Management
Orlando, FL, USA

Matt Keys
PhD BEng CEng

Fellow, Technical Director, Global
Technical Authority – Offshore
Structures
Oil & Gas
Perth, Australia

Adrian Lindon
BA(Hons) Dip. Arch, ARB, RIBA

Senior Technical Director - Atkins
Fellow, Design and Engineering
(Middle East and Africa)
Engineering, Design and Project
Management
Dubai, UAE

Navil Shetty
PhD, DIC, FIAM

Atkins Fellow and Technical Chair for
Asset Management
Centre of Excellence for Digital Asset
Management & Operations
Bangalore, India

Patrick Sikka
P. Eng

Vice-President
Mining & Metallurgy – North America
Toronto, Canada

Richard Moura
P.Eng.

Director, Business Development Rail
& Transit
Global Business Development,
Transportation-Major Projects
Infrastructure
Toronto, Canada

Tim Milner
CSci CChem MRSC

Atkins Fellow and Chief Technology
Officer
Nuclear
Columbia, SC, USA

Samuel Fradd

Technology Manager
Engineering, Design and Project
Management
Epsom, UK

Akshaye Sikand
MS, P.Eng.

Manager, Knowledge Management
Project Oversight
Toronto, Canada

Production Team

Dorothy Gartner
MLIS

Librarian
Project Oversight
Montreal, Canada

Samantha Morley
CAPM

Operations Coordinator
Technical Professional Organization,
Atkins North America
Denver, CO, USA

Cheryl Law
MEng CEng MICE

Associate Engineer, Infrastructure
Engineering, Design and Project
Management
Epsom, UK

Graphic Design Team

Montreal, Canada

About the Cover

Visualisation of the HS2 Colne Valley Viaduct crossing Harefield Lake, UK. Image was produced by Hays Davidson Ltd in conjunction with Knight Architects as an output to the Atkins-led specimen design development work for High Speed 2 Limited.

New Rules for Design of Footbridges Susceptible to Lateral and Torsional Vibration

José L de la Cuesta Padilla

MReS, CEng, MICE, Eur Ing
Group Engineer
Engineering, Design and Project Management
Swansea, UK

Benjamin Lau

BSc (hons), MSc PhD CEng FICE MIStructE
Associate Engineer
Engineering, Design and Project Management
Swansea, UK

Ian Ward

BSc (hons), MSc CEng FIMechE
Technical Director
Engineering, Design and Project management
Epsom, UK

Abstract

Modern footbridges are typically slender structures, often with low natural frequencies and low damping ratio. These structures are often prone to vibrations induced by the actions of the pedestrians and sometimes also wind. Recommendations for pedestrian comfort as well as for safety are included in Eurocodes BS EN 1990 and also, in the UK, within the UK National Annexes to BS EN 1990 [1] and BS EN 1991-2 [2], and UK Published Document PD 6688-2 [3]. However, these design codes have not been consistent in defining acceptance comfort criteria for the situations when a dynamic analysis needs to be undertaken, resulting in a high degree of ambiguity for UK applications. In particular, the treatment of bridges with lateral and torsional vibration generated by vertical loading on the bridge is not adequately covered.

This paper discusses the ambiguities and omissions in the UK suite of codes in the context of one particular half-through truss footbridge with unexpectedly lively lateral and torsional vibration and proposes amendments to the code requirements, which have now been implemented in NA+A1:2020 to BS EN 1991-2:2003 Incorporating Corrigendum No. 1 [4].

Keywords

Lateral Torsional Vibration; Natural Frequency; Footbridges; Comfort Criteria; Acceleration; Eurocodes

Chris Hendy

FREng MA(Cantab) CEng FICE Eur Ing
Technical Director, Atkins Fellow,
Head of Bridge Engineering
Engineering, Design and Project Management
Epsom, UK

1. Introduction

Modern footbridges are typically slender structures, often with low natural frequencies and low damping ratio. These structures are often prone to vibrations induced by the actions of the pedestrians and sometimes also wind. Recommendations for pedestrian comfort as well as for safety are included in Eurocodes BS EN 1990 and also, in the UK, within the UK National Annexes to BS EN 1990 [1] and BS EN 1991-2 [2], and UK Published Document PD 6688-2 [3]. However, these design codes have not been consistent in defining acceptance comfort criteria for the situations when a dynamic analysis needs to be undertaken, resulting in a high degree of ambiguity for UK applications. In particular, the treatment of bridges with lateral and torsional vibration generated by vertical loading on the bridge is not adequately covered.

This paper discusses the ambiguities and omissions in the UK suite of codes in the context of one particular half-through truss footbridge with unexpectedly lively lateral and torsional vibration and proposes amendments to the code requirements, which have now been implemented in NA+A1:2020 to BS EN 1991-2:2003 Incorporating Corrigendum No. 1 [4].

2. The Studied Bridge

The footbridge considered for the study is a three-span steel truss structure with spiral ramps at each end. The bridge superstructure comprises three simply supported half-through warren truss spans, prefabricated in hot rolled hollow steel sections with a longitudinally stiffened steel deck plate. The main span, which crosses a trunk road, is approximately 30.0 m long. The adjacent back spans are each 6.5 m long. The walkway has a width of 2.0 m.

The bridge is on a vertical curve with varying height (increasing in depth from supports to mid-span) and splayed outwards in plan.

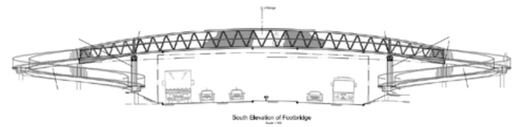

Figure 1: Footbridge south elevation

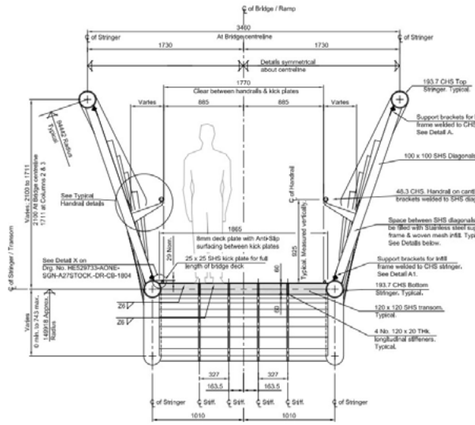

Figure 2: Typical section through deck

Before opening the footbridge to the public, concerns were expressed regarding the magnitude of vibrations experienced by construction workers in the course of completing the works. A detailed review of the bridge design was undertaken which identified that the critical lateral and torsional vibration mode being excited was not adequately covered by the standards and hence no limiting criteria and had been applied in the design. Nevertheless, the excitation was significant and so a modification of the structure was designed and installed. The modification included additional U-shape stiffeners welded to the columns and changing the bridge deck condition from simply supported to continuous deck over the main span supporting columns through connecting the bottom chords by welding; see Figure 3. The purpose of the modification was to increase the natural frequency for the excited lateral and torsional mode and to reduce the lateral acceleration causing the discomfort. The analysis that led to this action is described in Section 3.

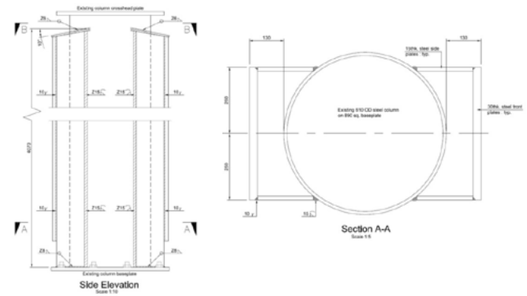

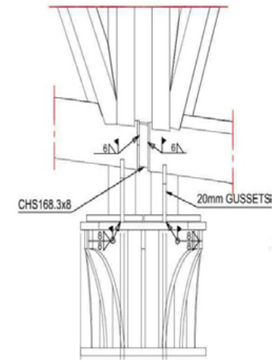

Figure 3: Column and bottom chord strengthening “with additional stiffening installed”

3. Analysis of the Footbridge

3.1 Determination of Natural Frequencies and Mode Shapes

The software LUSAS Bridge was used to idealise the structure and determine natural frequencies and mode shapes. Beam elements were used to model the truss members and the cross-girders. 4-node quadrilateral shell elements were used to model the deck plate, longitudinal stiffeners, columns heads and columns. The modelled fixity of the columns was fully fixed at the base given the relatively high stiffness of the foundations in comparison with the columns.

For the case with the retrofitted stiffening applied, the additional columns stiffeners were also modelled with shell elements.

As Initially Designed		
Mode No.	**Natural Frequency Hz**	**Mode Shape**
1	1.9	Lateral torsional
3	4.6	Longitudinal
5	5.9	Vertical
With Additional Stiffening Installed		
Mode No.	**Natural Frequency Hz**	**Mode Shape**
1	2.6	Lateral torsional
2	6.0	Longitudinal
3	6.1	Vertical

Table 1: Natural frequency values

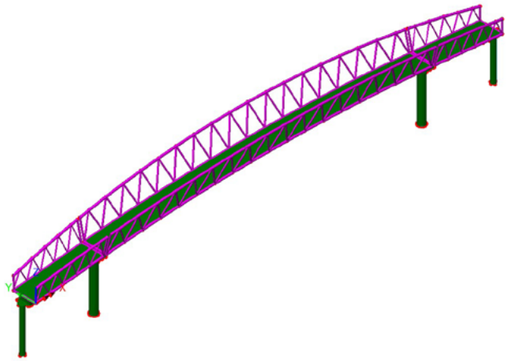

Figure 4: Model as initially designed

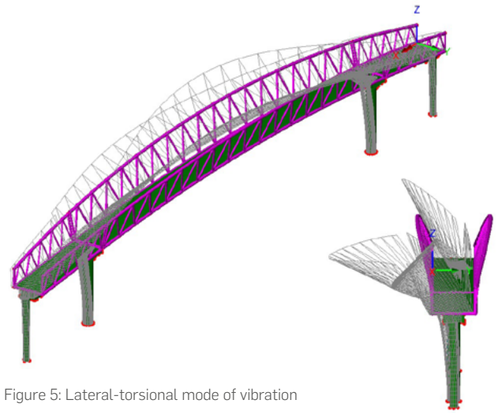

Figure 5: Lateral-torsional mode of vibration

To perform an evaluation of vibration performance under pedestrian loading using Eurocode BS EN 1991-2 [2], analysis of the structure must be performed to identify the relevant modes of vibration and associated natural frequencies of the footbridge. These relevant modes are vertical, lateral and torsional modes of vibration, and combinations of these. The LUSAS models were used to determine relevant modes of vibration for both the as initially designed case and the retrofitted stiffening case. A summary is shown in Table 1 and the critical vibration mode (mode 1) is illustrated in Figure 5 below.

The lowest mode, the lateral and torsional mode, is associated with a low torsional stiffness of the open bridge cross-section and rotation about the bridge's shear centre which is located below deck level. This mode can be excited by the vertical loading from pedestrians walking with an offset to the centreline of the footway.

3.2 Requirements of the Existing Standards Relevant in the UK

The standard way to evaluate footbridge performance is to compare natural frequencies of relevant modes to limiting values of frequency. If all frequencies exceed the limiting values then the bridge may be deemed to be unlikely to be excited by pedestrian loading and no further provision is required. If these limiting values cannot be met, then it is necessary to determine the accelerations produced under specified pedestrian dynamic forces and compare them to limiting values of acceleration, known as comfort criteria. For design to Eurocodes in the UK, the follow standards apply:

- Eurocode 1990 and associated UK National Annex [1]
- Eurocode 1991-2 and associated UK National Annex [2]
- BSI Published Document, PD 6688-2 [3]

However, these standards were found to be in conflict during the study.

Eurocode BS EN 1990 Cl A2.4.3.2(2) [1] requires that a verification of the comfort criteria must be performed if the fundamental frequency of the deck is less than that described in Table 2.

Vibration Mode	Natural Frequency
Vertical Vibration	5 Hz
Lateral Vibration	2.5 Hz
Torsional Vibration	2.5 Hz

Table 2: Natural frequency criteria BS EN 1990 [1]

In addition to the criteria included in Table 2, Eurocode BS EN 1990 cl A2.4.3.2 (1) [1] defines comfort criteria in terms of limits to the maximum acceleration that should be experienced in any part of the bridge deck. Table 3 summarises these maximum accelerations. The combined lateral and torsional mode for the bridge in this study had a natural frequency below the value of 2.5 Hz from Table 2 and hence required a check of comfort criteria in accordance with Table 3.

Vibration Mode	Acceleration Limit
Vertical Vibration	0.7 m/s^2
Lateral Vibration	0.2 m/s^2
Exceptional Crowd Condition	0.4 m/s^2

Table 3: Maximum accelerations EC 1990 [1]

The limiting values included in Table 2 are revised in the UK National Annex to Eurocode BS EN 1991-2 within clause NA 2.44.7(2) [2]. This changes the limiting natural frequency for transverse vibration to 1.5Hz, but this was intended to be the limit to prevent synchronous lateral vibration caused by lateral forces from footfall which occur at half the frequency of vertical footfall forces. It was not intended to cover the lateral and torsional mode relevant to the footbridge in this paper, which can be excited by vertical loading. The limiting frequency for torsional motion is not covered. Hence the natural frequency limits in the UK National Annex can be summarised in Table 4. Application of these criteria could incorrectly suggest that the footbridge in this paper need not be checked for lateral and torsional vibration as its lowest natural frequency in the lateral and torsional mode is greater than 1.5 Hz and no explicit frequency limit is given for torsional modes.

Vibration Mode	Natural Frequency Requirement - BS EN 1991-1-2 UK NA [4]
Vertical Vibration	5 Hz
Lateral Vibration	1.5 Hz
Torsional Vibration	Not specifically covered

Table 4: Natural frequency UK National Annex to Eurocode BS EN 1991 [2]

Where frequency limits are not met, serviceability comfort criteria need to be satisfied. Table NA.7 in the UK National Annex to BS EN 1991-2 [2] provides different loadings to be considered for different bridge classes based on likely usage. Three load models are described: a group of pedestrians walking, a group of people jogging and a crowd load model. The footbridge in this paper is classified as Class C (urban route) and the three relevant load models to consider for the analysis are given in Table 5.

Load Model	Size
Load Model C.1	Group of 8 people walking
Load Model C.2	Group of 2 people jogging
Load Model C.3	Crowd load of 0.8 persons/m^2

Table 5: Recommended crowd densities for design

3.3 Dynamic Analysis

To assess the discomfort actually experienced when using the bridge, a dynamic analysis was conducted using the loading specified in the UK NA to EN 1991-2 [2] and the maximum accelerations were evaluated.

The accelerations were determined using a Generalised Single Degree of Freedom approach using DynamAssist [5]. The equivalent single degree of freedom mass, M_{eq}, spring stiffness, K_{eq}, and driving force F_{eq} are evaluated based on energy considerations using the actual distribution of mass in the bridge and the critical vibration mode shape. The system is provided with the specified damping and then external dynamic force is applied.

The excitation of the footbridge occurred when people were walking on the structure. Hence Load Model 1 (group of 8 pedestrians walking – see Table 5) was used for the analysis. The travelling load for the analysis was applied eccentrically from the centreline of the bridge with a path 500mm offset from the bottom chord along the full length of the bridge.

The results of the acceleration checks are summarised in Table 6.

	Mode of Vibration	Lateral Natural Frequency (Hz) (LUSAS)	Lateral Acceleration m/s^2
As Initially Designed	Lateral Torsion	1.96	0.43
With Additional Stiffening Installed		2.57	0.23

Table 6:- Maximum acceleration on the deck

Based on the results shown on Table 6, the original design without the additional strengthening exceeded the comfort criteria specified in BS EN 1990 [1] for lateral accelerations. This helps explains why the vibration experienced during finalising construction was so noticeable and suggests that a limit, as proposed in Table 3, is required for lateral acceleration caused by vertical loading and the UK National Annex to EN 1991-2 [2] and PD 6688-2 [3] requires amendment to include this. A summary of natural frequency requirements from the different design documents is listed in Table 7 below.

	Code	Cut-off Lateral Natural Frequency Limit (Hz)	Natural Frequency of the Footbridge (Hz)	Comfort Criteria Check Required
As Initially Designed	BS EN 1990 [1]	2.5	1.9	Yes
	BS EN 1991 UK NA [2]	1.5	1.9	No
	PD 6688-2 [3]	1.5	1.9	No

Table 7: Comfort test summary

After the structure was retrofitted with the new elements the comfort was markedly improved. The natural frequency for the lateral-torsional mode increased to a value of 2.57 Hz with a maximum acceleration of 0.23m/s^2. This value improved the comfort criteria for the structure to the borderline of tolerance.

3.4 Site Measurement

Natural frequency was measured on the stiffened footbridge using a smart phone App with accelerometer and gyroscope functions built in. The App called Vibration from Diffraction Limited Design LLC was used to obtain the measurements from the smart phone. The test was conducted under the effect of a pedestrian walking randomly on the bridge deck. The measured natural frequency of the bridge was 2.45HZ and the computed natural frequency for the same lateral-torsional mode of vibration was 2.6Hz; the discrepancy between the computed and measured natural frequencies was only 6%. A measurement of acceleration was not taken, but the stiffened bridge exhibited no significant motion during the test.

4. Recommendations

This paper highlights that the current UK National Annex and Published Document are not adequate to assess the comfort of structures with low lateral and torsional vibration modes, such as half-through footbridges. Therefore, the following recommendations are suggested for the design of pedestrian bridges:

(i) All torsional and lateral modes of a type in Figure 2 should be checked for comfort criteria in accordance with Eurocode EN 1990 clause A2.4.3.2 (2) [1]. This requires comfort criteria to be verified if the vertical natural frequency is lower than 5 Hz or less than 2.5 Hz for lateral and torsional modes excited by vertical loading.

(ii) The limiting lateral excitation for comfort should be taken from Eurocode EN 1990 clause A2.4.3.2(1) [1] as 0.2 m/s^2 under the loading from a single pedestrian or group of pedestrians in the UK NA to EN 1991-2 [2].

(iii)However, it must be noted that lateral excitations due to deliberate excitation may be far higher than above (with much larger deflections). This could lead to the perception that the bridge is unacceptable dynamically. Therefore, if the lateral acceleration exceeds 0.2 m/s^2 under the vertical loading, then discussion should be held with the Technical Approval Authority (TAA) about possible measures to reduce accelerations to 0.2 m/s^2 or to increase the natural frequency of the structure. This may require the installation of tuned mass dampers or stiffening of the bridge. In the absence of conversations with the TAA, where the calculated fundamental frequency of the bridge is less than 3 Hz for lateral and torsional vibrations, provision should be made in the design for the possible installation of dampers in the bridge after its completion.

These recommendations have now been implemented in in NA+A1:2020 to BS EN 1991-2:2003 Incorporating Corrigendum No. 1 [4].

5. Conclusions

This paper has highlighted ambiguities and inconsistencies between Eurocode BS EN 1990 and the UK National Annexes to BS EN 1990 [1] and BS EN 1991-2 [2], and also UK Published Document PD 6688-2 [3]. It has shown that these inconsistencies can lead to important lateral and torsional vibration modes not being identified as requiring evaluation against comfort criteria and has proposed amendments to the code requirements to address this. These proposals have now been implemented in NA+A1:2020 to BS EN 1991-2:2003 Incorporating Corrigendum No. 1 [4].

References

1. BS EN 1990:2002+A1:2005 as modified by UK National Annex, “Eurocode - Basis of structural design”.

2. BS EN 1991-2:2003 as modified by UK National Annex, “Eurocode 1: Actions on structures - Part 2: Traffic loads on bridges”.

3. PD 6688-2: 2011, “Background to the National Annex to BS EN 1991-2, Traffic loads on bridges”

4. NA+A1:2020 to BS EN 1991-2:2003 Incorporating Corrigendum No 1, “UK National Annex to Eurocode 1: Actions on Structures - Part 2: Traffic loads on bridges”.

5. DynamAssist. Structural dynamics software (www.DynamAssist.com).

Humber Bridge Hanger Replacements and Testing

Andrew Arundel

BEng (Hons), CEng, FICE
Chief Operating Officer at Humber Bridge Board, E Riding
Yorkshire, UK

David Bishop

MEng (Hons), CEng, MIStructE, MICE
Principal Engineer
Engineering, Design and Project Management
Edinburgh, UK

Chris R. Hendy

FREng, MA(Cantab), CEng, FICE, Eur Ing,
Head of Bridge Engineering, Technical Director
Engineering, Design and Project Management
Epsom, UK

Abstract

The Humber Bridge is an iconic Grade 1 Listed structure which remains one of the longest single span suspension bridges in the world. It has a main span of 1410 m and a total span length of 2220 m. The bridge deck is connected to the main suspension cables by spiral wire rope hangers with socketed end connections.

This paper discusses the global analysis of the bridge to identify the predicted stresses in the hangers, which was complicated by the triangulation of the hangers. It then covers the selection of three trial hangers to be replaced, the specification of the replacement hangers and the testing specified to determine the residual life of the original hangers. The design, fabrication, and installation of the works involved in replacing the hangers is described and the paper concludes with a discussion of the results of the hanger testing and how this has informed the strategy for management of the remaining hangers.

Keywords

Humber; Suspension bridge; Spiral wire

Dr. Chris Mundell

MEng (Hons), PhD, CEng MICE
Head of Civil Engineering Structures
Engineering, Design and Project Management
Bristol, UK

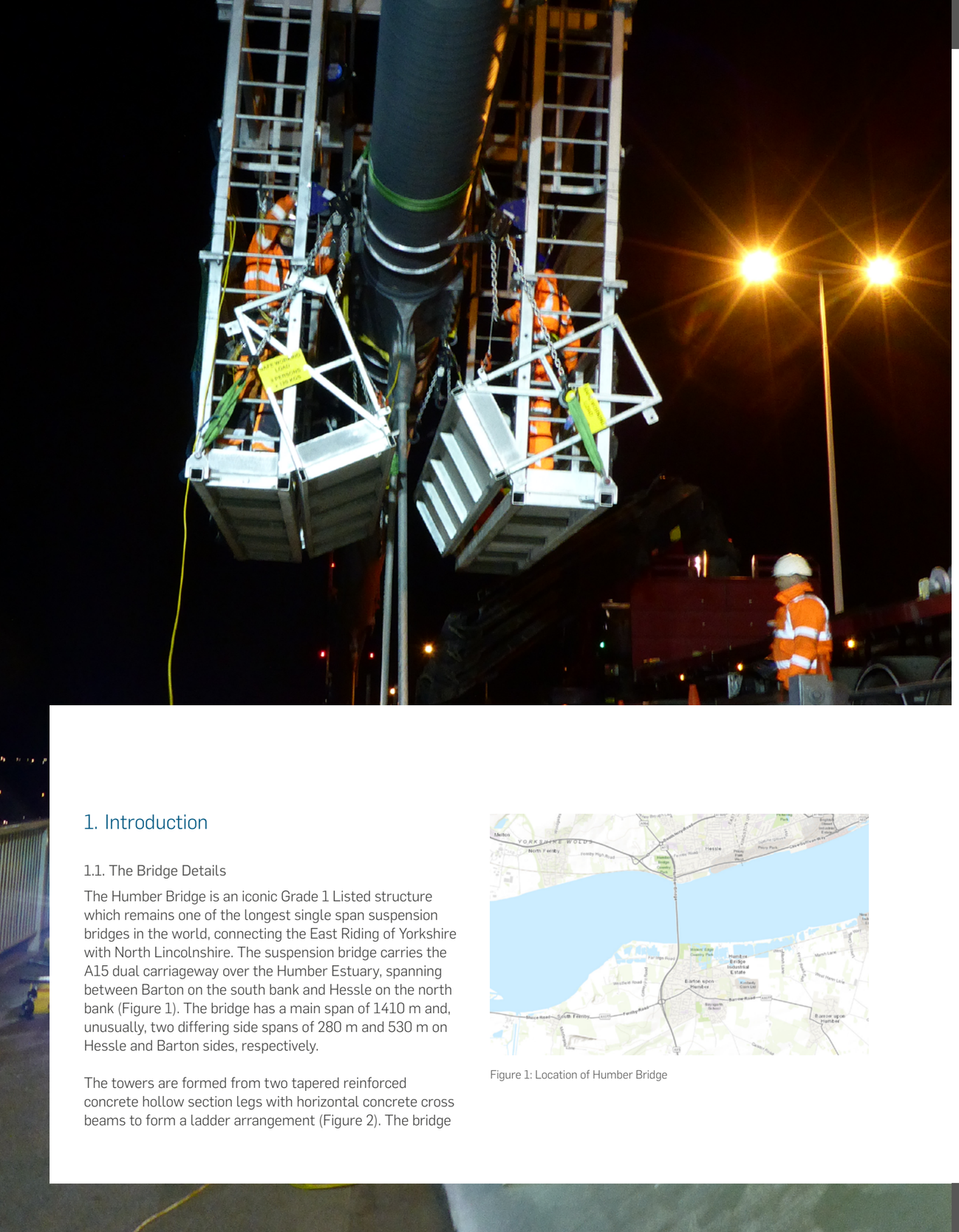

1. Introduction

1.1. The Bridge Details

The Humber Bridge is an iconic Grade 1 Listed structure which remains one of the longest single span suspension bridges in the world, connecting the East Riding of Yorkshire with North Lincolnshire. The suspension bridge carries the A15 dual carriageway over the Humber Estuary, spanning between Barton on the south bank and Hessle on the north bank (Figure 1). The bridge has a main span of 1410 m and, unusually, two differing side spans of 280 m and 530 m on Hessle and Barton sides, respectively.

The towers are formed from two tapered reinforced concrete hollow section legs with horizontal concrete cross beams to form a ladder arrangement (Figure 2). The bridge

Figure 1: Location of Humber Bridge

superstructure comprises a stiffened steel box girder with an orthotropic deck roadway and internal diaphragms at 4.525 m c/c. The box sections were erected in 18.1 m long sections and are 22 m wide and 4.5 m deep, with 3 m wide cantilever panels incorporated along each side of the boxes to carry the walkways and cycle tracks.

Figure 2: Humber Bridge

The suspension cables on the main span and Barton side span are 0.684 m in diameter and each contains 14948 galvanised steel wires of 5 mm diameter, while the cables on the Hessle side span are 0.702 m in diameter and each contain 15748 wires of 5 mm diameter. The tensile strength of the wires varies between 1540 -1770 N/mm^2 and have a 0.2% proof stress of 1180 N/mm^2. The cable anchorages on both sides of the bridge are of a gravity type, with each cable anchored into a solid block of concrete.

The bridge deck is connected to the main suspension cables by 484 spiral wire rope hangers (sometimes referred to as suspenders) with socketed end connections. The hangers are inclined, rather than vertical. The hangers were manufactured by Bruntons of Musselburgh Limited from 62.3 mm diameter spiral strand bridge rope. The hanger cables are attached to the deck via a welded stool with an articulated socket. The shorter cables have double articulation to permit rotation of the cable both longitudinally and transversely which may be caused by thermal and wind-induced movement of deck and main cables, together with vibration and misalignment of the hangers themselves.

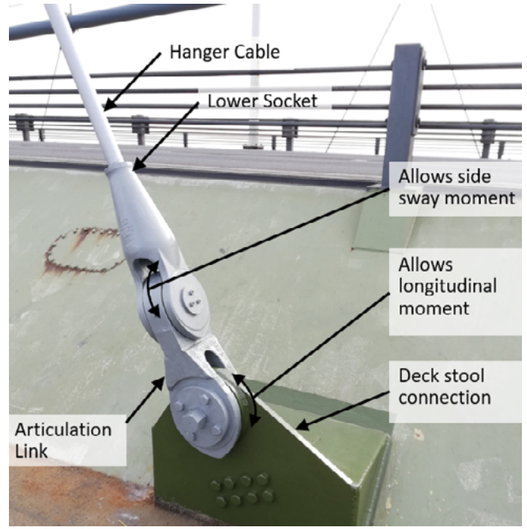

Figure 3: Hanger deck connection

Each rope is composed of 105 No x 5 mm Ø wire, 5 No x 4 mm Ø wire and 1 No x 2.5 mm Ø wire distributed as follows:

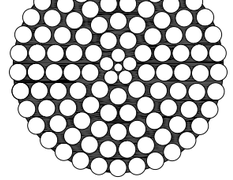

Layer 1 = 33 No. x 5mm dia. (outer layer)
Layer 2 = 27 No. x 5mm dia.
Layer 3 = 21 No. x 5mm dia.
Layer 4 = 15 No. x 5mm dia.
Layer 5 = 9 No. x 5mm dia.
Layer 6 = 5 No. x 4mm dia.
Layer 7 = 1 No. 2.5mm dia. (central wire).

Figure 4: Spiral wire rope

The hanger ropes are internally lubricated with Bruntons “BM” compound and externally coated with Metalcoat, supplied by Bridon of Doncaster. The individual wires are galvanised. The minimum guaranteed breaking strength of each spiral rope hanger is 2900 kN and the Young’s Modulus of the hanger based on its total cross-sectional area is 140 kN/mm^2, the low value compared to an individual wire being due to the spiral arrangement of the wires in the rope.

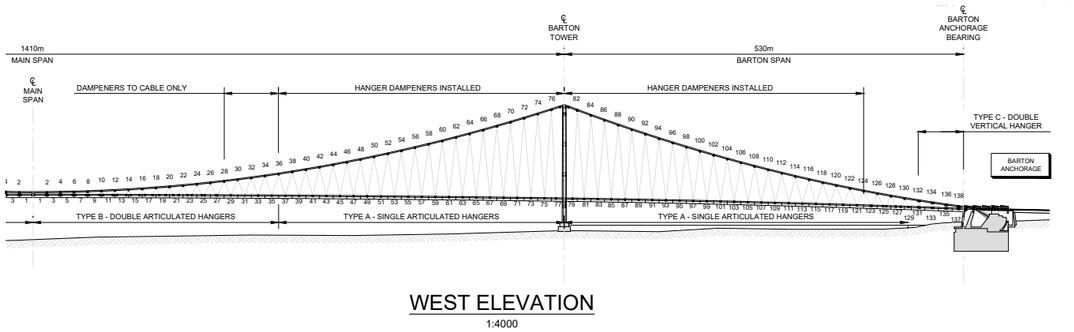

Figure 5: Hanger referencing and location - Barton and Main Span (symmetrical)

1.2. The Objective of the Hanger Replacement Project

The two next longest-spanning UK suspension bridges, the Severn Bridge (opened in 1966) and the Forth Road Bridge (opened in 1964), had all their hangers replaced after 23 to 24 years and 33 to 36 years of service life, respectively. This was driven by concerns over their deterioration and a wider industry belief that the life of hangers was typically limited to around 25 years. The Humber Bridge had 37 years of post-opening service by 2018 with all but two of the original hangers still present. Therefore it was decided that a programme of hanger investigation should be undertaken.

Additional detailed visual inspections were carried out on the hangers which suggested that the condition remained generally good. A few wires were seen out of lay (which could indicate broken wires within a hanger), there was some water seepage, and there were a number of cracks in the Metalcoat paint system, but little evidence of significant corrosion on the outside of the hangers. However, corrosion, fatigue damage, wire embrittlement or wire breaks in the interior of the hangers could not be detected through visual inspection and hence more detailed investigation was required to create a management plan for the hangers and to inform decisions on when and how many of the hangers should be replaced.

To gather more detailed information about the condition of the hangers and their residual life and hence produce a hanger management plan, it was decided that three hangers should be selected for trial replacement and testing.

Figure 6: Typical hanger defects

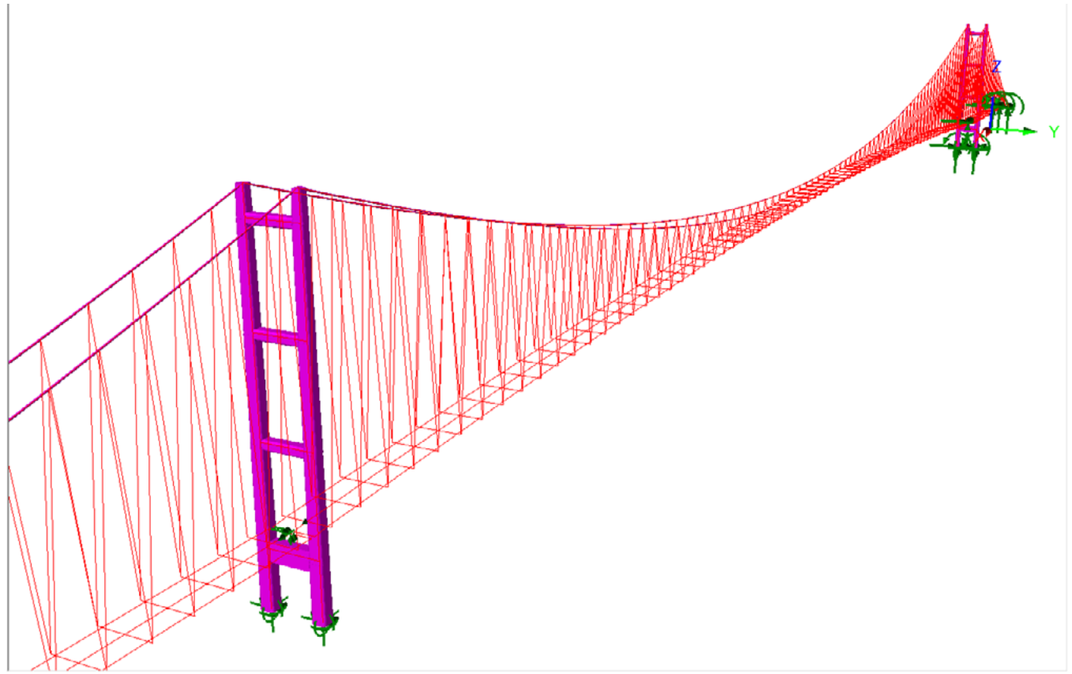

Figure 7: Global analysis idealisation of bridge

2. Global Analysis and Selection of Trial Hangers to Replace and Test

2.1. Global Analysis for Dead Loads

In order to enable the identification of the most highly stressed hangers and those with the greatest fatigue demand, and also to prepare specifications for testing existing hangers and procuring new replacement hangers, a 3D finite element model of the bridge was created in the LUSAS modelling software as shown in Figure 7.

The inclination of the hangers sets up a truss action in the bridge under load, tending to put the deck into global tension and reducing the tensile force in the main suspension cables slightly. Adjacent hangers carry significantly different loads due to the inclination and truss action, one tending to increase its tension and one tending to reduce its tension. For the complete bridge, this distribution of forces between hangers under a given load case can be modelled with confidence. However, the distribution of forces generated in the hangers during construction is less certain and very sensitive to the assumed construction sequence. The bridge records show that the deck unit erection in the main span progressed from the centre of the span back towards the towers (Figure 8). In the side spans, deck erection started at the abutments and progressed to the towers. The sections of deck were first connected with rotational pins, allowing for movement during the construction, with those units later fully fixed once the catenary shape of the main cable had been achieved. In order to model the construction sequence, geometrically non-linear staged-construction analysis was undertaken to derive the forces in the hanger cables.

Figure 8: Bridge during construction

The construction sequence and the inclined cables had a very significant effect on the calculated cable forces as can be seen in Table 1, which compares the original designers' estimate for the cable dead load force, the dead load force predicted by the current analysis, and the actual measured jacking force ultimately required to release the pins connecting the cable end sockets to the deck gusset plates during replacement. The table shows that the original design did not consider the effects of the diagonal hanger arrangement as the dead load forces are all the same. The predicted dead loads vary significantly due to the push-pull nature of the forces generated by the inclined hangers, whilst the actual measured jacking loads followed the same pattern but the loads were all higher. The higher jacking loads measured on site were expected because of the temporary works design which gripped the cable above the pin connection and therefore required a greater force than the actual cable force to reduce the reaction on the pin to zero – see section 5. For hangers 10-9 and 16-17 this accounted for the majority of the difference to the predicted loads and the rest was attributed to variations in surfacing thickness and a small effect of the traffic running on the bridge during jacking. However, hanger 18-17 was found to be significantly higher loaded than predicted which was caused by the original fabrication length of the hanger being shorter than the adjacent hanger which was verified by detailed pin to pin site measurements.

Table 1: Predicted and Actual Dead Loads in the Three Replaced Hangers

	Freeman Fox & Partners (kN) Dead Load.	Predicted Nominal Dead Loads (kN)	Actual Jacking Loads (kN)
Hanger 10-9	410	793	950
Hanger 16-17	410	137	290
Hanger 18-17	410	774	1100

2.2. Live Load Analysis

To determine the hangers with greatest maximum service stress, both Eurocode design live loading to EN 1991-2 and Bridge Specific Assessment Live Loading, derived from weigh-in motion equipment, were applied to the bridge. Hanger 10-9 was identified as having the greatest maximum service stress.

Hanger 16-17, pre-selected based on its condition, was noted to theoretically just be able to go slack under maximum live load and so certainly had the lowest minimum service load of all the hangers.

2.3. Fatigue Analysis

To determine the hangers with the greatest fatigue demand, simplified fatigue loading based on Eurocode BS EN 1991-2 (BSI 2003) fatigue load model FLM3 together with the damage equivalent factors in BS EN 1993-2 (BSI 2006) were applied. This resulted in the determination of an applied fatigue stress range which, if applied over 2 million cycles, would cause the same damage as the real traffic spectrum. This approach is particularly useful in producing a fatigue testing specification – see section 4. The maximum service stress expected under normal operation was also determined because fatigue testing would be carried out by cycling the stress down from the maximum value by an amount equal to the calculated fatigue stress range. Hanger 18-17 was identified as having the greatest fatigue stress range which, based on the application of FLM3, was 78 MPa. New cables/tension components are tested to $\Delta\sigma = 150$ MPa in accordance with BS EN 1993-1-11 (BSI 2006) with an additional 1.25 additional safety factor, so this indicated that the actual fatigue demand on the bridge cables was much less than that required to be demonstrated for a new cable.

There is no obtainable detailed background to the λ_1 damage equivalent factor for fatigue load model FLM3 provided in BS EN 1993-2, and the fatigue assessment produced is generally considered to be conservative. There is also some uncertainty around the application to a cable element. EN 1993-2 proposes the use of a critical length of the influence line equal to twice the hanger spacing for arch bridges, but this assumes that the majority of the load comes from the two adjacent bays between hangers. The influence line for the Humber hangers is very different to this because of the triangulation of the hanger system; Figure 9 shows the variation of a typical hanger force as the FLM3 vehicle traverses the bridge, where it is clear that the influence line is much more extensive than the hanger spacing. However, additional unpublished research by CEN/TC250/SC3/WG13 (the group responsible for maintaining EN 1993-2) suggested that FLM3 is particularly inaccurate for large loaded lengths and could be unconservative in some cases. Therefore, an additional assessment was carried out using fatigue load model FLM4, which uses a traffic spectrum defined in the UK National Annex to BS EN 1991-2 (BSI 2020), for comparison to the fatigue stress ranges derived from FLM3.

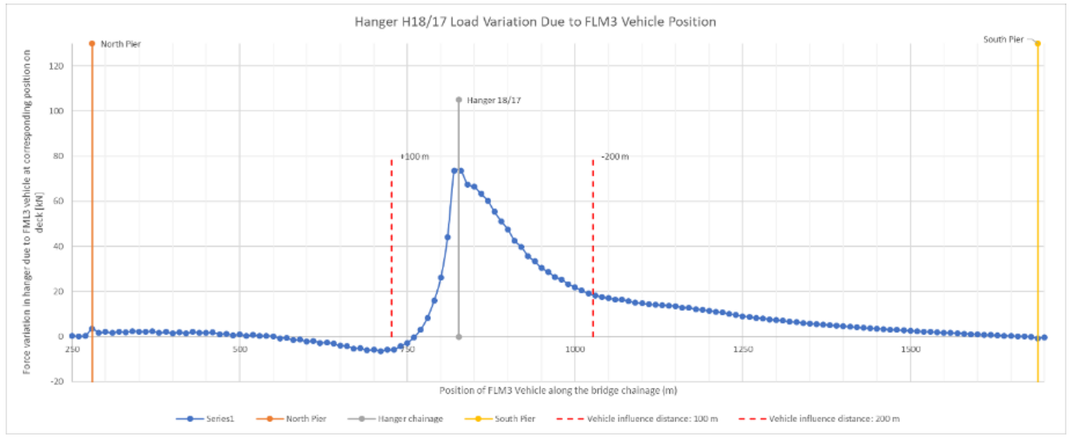

Figure 9: Hanger force variation due to FLM3 vehicle position

The use of FLM4 requires significantly more analysis because of the need to traverse the bridge with a variety of different vehicles alone and in convoy and therefore is not normally used for design, but the approach can be advantageous for assessment of existing structures as it is likely to demonstrate a greater life. The application of FLM4 for bridge structures and elements subjected to fatigue is outlined in Eurocode BS EN 1991-2 and the UK National Annex. Four separate load cases are outlined in the National Annex:

1. Lane 1 traffic only with 80% of lane 1 lorry numbers;
2. Lane 1 traffic is to run in convoy with vehicles at 40 m spacing, with 20% of lane 1 lorry numbers;
3. Lane 2 traffic only with 80% of lane 2 lorry numbers; and,
4. Lane 2 traffic in convoy with vehicles at 40 m spacing, with 20% of lane 2 lorry numbers

FLM4 in the UK National Annex comprises 23 different vehicles designations with a specified number of cycles for each vehicle, then used to calculate the damage summation. The fatigue damaging stress cycles due to the transit of Fatigue Load Model 4 lorries were assessed and counted using the rain flow counting procedure described in BS EN 1993-1-9.

For 1 and 3, one single FLM4 vehicle is run at regular intervals across the full length of the structure in the respective lane until the whole spectrum has been traversed.

For 2 and 4, a convoy of FLM4 vehicles runs at regular intervals from one end of the structure to the other. Detailed guidance is not provided in either the UK National Annex or clause 8.4.2.1 of BS5400 Part 10 (BSI 1980) on the simultaneous presence of vehicles or combination of vehicles in the load spectrum. For example, with the length of influence line shown in Figure 10, if the vehicles are applied as a continuous convoy with vehicles at 40 m spacing, then there is very little fatigue stress range generated as each vehicle departing the bridge is replaced with one joining and a quasi-permanent load is generated; the passage of a single vehicle alone creates a greater stress range. However, if the vehicles are applied in convoy until the influence line is filled and then all the vehicles are allowed to leave the bridge before any more vehicles are applied, then a cyclic load case is created which is greater than the full characteristic live load, which clearly is unrealistic.

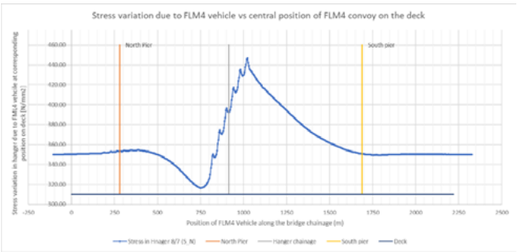

Figure 10: Hanger force variation due to FLM4 vehicle convoy position

Table 2: Selected Hangers and Outline Testing Proposed

Hanger Reference	Testing Selection Criteria
H10-9	High fatigue load range amongst central span hangers but with the greatest maximum hanger load under permanent load + Fatigue loading out of the 5 maximum ranges identified. > 4.3 m long; > No visible signs of corrosion but appears to have wires out of lay (indicative of possible fractured wires); > Hanger tested for its residual fatigue life and ultimate tensile strength (if sufficient fatigue life).
H16-17	Hanger with the lowest permanent load and subjected to theoretical decompression under live loading of the entire structure. > 7.7 m long; > In the worst physical condition whereby, it has corrosion and wires out of lay; > Hanger proposed to be tested to destruction; > Fatigue testing was not initially proposed for this hanger as it is in the worst physical condition and it may have had a limited fatigue life. Failure under fatigue testing alone would provide no information on the minimum tensile strength of all cables.
H18-17	Greatest fatigue load range. > 9.2 m long; > Hanger tested for its residual fatigue life and ultimate tensile strength (if sufficient fatigue life).

As there is no guidance within the UK National Annex for the derivation of a discrete vehicle convoy for load cases 2 and 4, the convoy was based on the recorded traffic data. The traffic data showed that between 2009 and 2016 the proportion of HGV's within the traffic had risen from 4.52% to 4.92%, so approximately 5%. Adopting 40 m vehicle spacing, there would be 30 vehicles maximum (conservatively assuming zero vehicle length) in the entire 1200 m length of the influence line. Based on the percentage of HGVs and observed traffic patterns, a convoy was formed from two vehicles running side by side with a third vehicle considered with 40 m spacing. The three vehicles were run across the structure, all clearing the influence line before running the next convoy. This approach showed that the damage from FLM3 was greater than that from FLM4 and hence the stress range from FLM3 was suitable for defining the fatigue testing requirements.

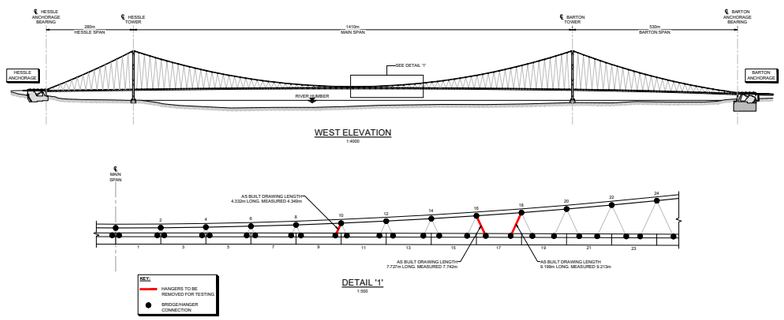

Figure 11: Locations of selected hangers

2.4. Selection of Trial Hangers to Replace and Test

The choice of hangers to be replaced and tested were selected based on identifying cables with the greatest maximum service stress, the greatest fatigue loading, and the worst physical condition. In addition, hangers were all chosen on the same side (west side) for construction purposes and hangers with attached structural health monitoring were avoided. The selected hangers and their reason for selection are summarised in Table 2. Their locations are shown in Figure 11.

3. Digital Image Correlation Measurement of Hanger Service Stress Range

As part of the project, Digital Image Correlation (DIC) measurements were undertaken on the cable with the highest predicted stress range to check whether the predictions made by the analysis model reflected the true behaviour. The outer layer of strands was exposed and a camera used to track the movement of pixels and thereby measure strain, which could be converted to stress. This was done both during the day with unrestricted traffic and at night with an 11 T vehicle, for which the results were within +/-10% of those generated by the analysis model. The technique is well-established and has been used to determine live load stresses in a variety of bridges (Winkler and Hendy, 2016) and also specifically to monitor hanger vibrations on the Great Belt Bridges (Winkler and Hendy, 2018).

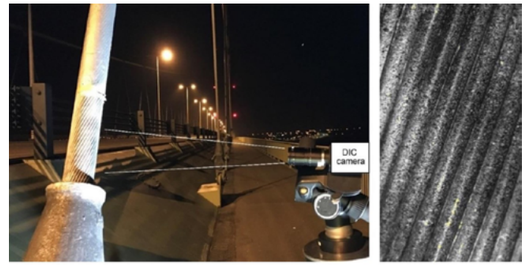

Figure 12: Daytime DIC measurement with unrestricted traffic and night measurement with 11 T vehicle

4. Hanger Testing Specification

4.1. Overview of Testing Requirements

A wide range of testing, both non-destructive and destructive, was specified to be carried out on the three extracted hangers in order to provide as much information as possible on their condition and potential future life expectancy to facilitate producing the optimal management strategy. The testing schedule is shown in Table 3.

Table 3: Hanger Testing Schedule

Hanger Information		Test to be Conducted						
Hanger reference for West span of Main Elevation	Length of hanger pin to pin (mm)	Visual Examination	Fatigue Test	Ultimate Tensile Strength	Fracture Surface Inspection	Examination of individual wires	Individual Wire Ultimate Strength	Chemical Analysis
9-10	4332	☑	☑	☑	☑	☑	x	☑
16-17	7727	☑	x	☑	☑	☑	x	☑
17-18	9199	☑	☑	☑	☑	☑	x	☑

The properties of a hanger and its constituent wires are listed in Table 4 below.

Table 4: Hanger Properties

Type of Steel	Diameter [mm]	Tensile Strength [MPa]	Cross-section [mm²]	Minimum Breaking Force FMUTS [kN]	Nominal Breaking Force [kN]	95% of Minimum Breaking Force [kN]
Suspender Rope	62.3	1416	2271 (effective)	2900	3216 (328000kgf)	2755
5 mm wire	5	To be determined by testing	19.63	-	To be determined by testing	-
4 mm wire	4		12.56	-		-
2.5 mm wire	2.5		4.90	-		-

Table 5: Fatigue Axial Test Stress Range Per Hanger

Hanger reference	Upper load limit [kN]	Upper stress limit σ_{sup}* [MPa]	Lower load limit [kN]	Lower stress limit σ_{inf}* [MPa]	Stress range (MPa)
9-10	1,118 (39% of minimum breaking load)	493	849	374	119
17-18	883 (30% of minimum breaking load)	388	705	310	78

Note: *Stresses are derived from the calculated wire rope effective area of 2271mm²

4.2. Residual Fatigue Life Testing and Tensile Testing

Two original, complete fully assembled hanger specimens were identified for fatigue testing as specified in Table 5. Each specimen was fully representative of the actual system and the conditions of use, including the actual anchorage systems of the hangers with the pin connection and corrosion protection. The tests were performed at ambient temperature between 10°C and 35°C, with a test frequency of 0.67 Hz, which was the fastest test speed practical.

Each specimen was subjected to two million cycles of the following coexisting effects:

- Sinusoidal variation of the axial stress between σ_{sup} and σ_{inf} as given in Table 5.
- Coexisting flexural loading induced by wedge-shaped shim plates introducing a 0.6° or 10 mrad misalignment of the terminations with the axis of the hanger. Hanger reference 9-10 was tested under configuration 2 and hanger 17-18 was tested under configuration 1 as shown in Figure 13 below.

The stress range of 78 MPa specified for hanger 17-18 was that derived from the use of FLM3 as described in section 2.3. It was considered unlikely that the cables would be able to withstand anywhere near the same levels of stress as required for a new cable (typically 150 MPa) because of the fatigue damage likely to have occurred in service to date and due to corrosion. Due to this concern, the 1.25 factor mentioned in section 2.3 was not applied to the 78 MPa stress range. The specified stress range for hanger 9-10 was initially derived and specified the same way. However, as discussed in section 7.2, the fatigue test for hanger 17-18 easily demonstrated adequate fatigue performance at the specified stress level, so the opportunity was taken to increase the stress range for the test of hanger 9-10 so that the test would give information at a different point on the S-N curve. A value of 119 MPa was chosen because a draft second generation version of EN 1993-1-11 was, at the time, considering specifying two possible S-N curves, one with a stress range requirement of 119 MPa at 2 million cycles and another with 145 MPa at 2 million cycles. It was again considered that the existing hanger could not tolerate the higher stress range, so the lower was chosen, noting that this achieved a factor of safety greater than the specified 1.25 as 1.25 x 78 = 98 MPa < 119 MPa.

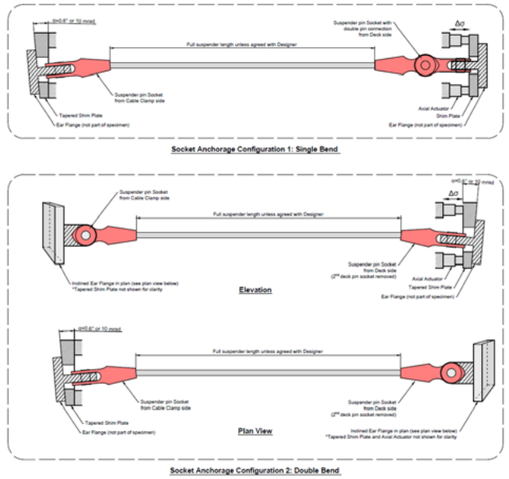

Figure 13: Fatigue test set-up

The fatigue test result was deemed to be satisfactory if:

- The specimen survived two million cycles of fatigue loading without detected breakage of more than 2% of the wires of which the hanger is made; and,
- No failure occurred in the anchorage material or in any component of the anchorage during the fatigue test.

An ultimate tensile-strength (UTS) test was also carried out after the fatigue test on each specimen. It was carried out in accordance with BS ISO 2408:2017 method 1 with the existing pin sockets used to support the hangers during the testing.

As per BS EN 1993-1-11 Appendix A4, the ultimate tensile test results of fatigue tested hanger was deemed to be satisfactory if it reached:

- A force of at least 95% of the minimum ultimate tensile strength FMUTS of the cable, defined from the characteristic strength of the strand and its nominal cross-sectional area from Table 4; and,
- A strain under the maximum load not less than 1.5%, allowing for deformation inherent to the operation of the anchorages (such as working-in of jaws).

For hanger 16-17, which was not first subjected to fatigue testing, the test was deemed satisfactory if the measured breaking force, F_m, reached or exceeded the minimum breaking force, F_{MUTS} given in Table 4.

UTS testing of the complete hanger assembly was followed by examination of the fracture surface to determine type of failure (i.e., brittle or ductile).

5. Temporary Works for Replacing the Hangers

The hangers were removed and replaced without installation of temporary works to support the deck, under two lane traffic management. This required verification of the existing structure, deck, and adjacent hangers to accommodate the additional loads during the removal process.

Hanger releasing equipment was provided by the contractor, Spencer Group, jacking up the deck to release the load from the hanger locking pin (Figure 14). The pin was removed and the deck was lowered gradually to remove the load from the hangers.

Load monitoring was conducted using proprietary vibrating wire strain gauges attached to adjacent hangers to ensure that the loads were not exceeded and to ensure that when the hangers were replaced this was at the correct load.

The assessment identified that existing welds within the hanger supporting stool would be overstressed during jacking and over-running the welds to adequately transfer loads form the jacking equipment to the orthotropic deck.

Due to the nature of the hanger replacement, the tolerance on hanger length was tighter than industry standards for new construction and, therefore, allowances for wedge draw-in were required during fabrication. Details of the new hanger can be seen in Figure 15 below.

Figure 15: Fabrication of replacement hanger

6. Results of the Testing for the Removed Hangers

6.1. Overview and Visual Inspection

After removing from the bridge, the hangers, including their sockets, were transported to Norway where inspection and testing was undertaken by DNV.GL.

Hanger 16-17 was generally in good condition with a few wires out of lay and breaks in the paint coating at several locations.

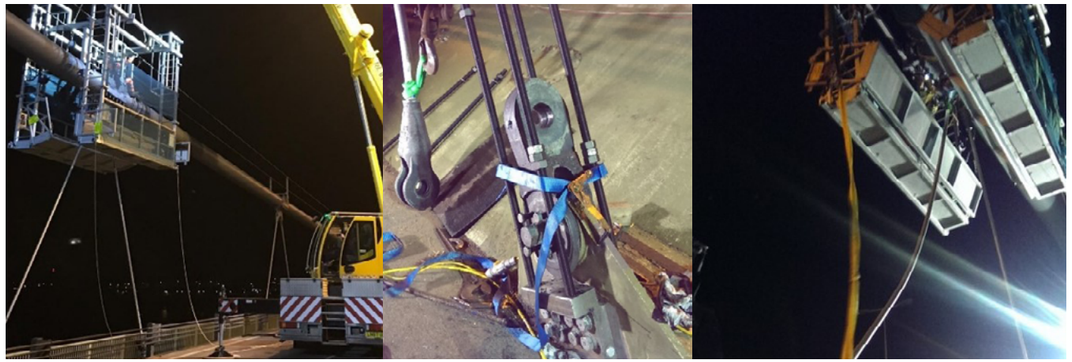

Figure 14: Hanger replacement – temporary access and removal

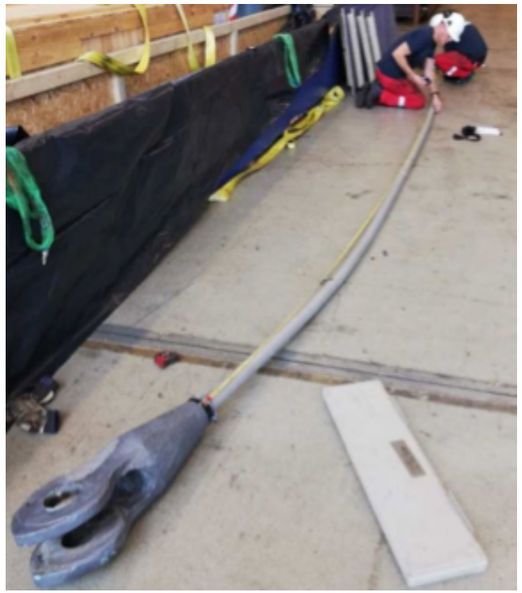

Figure 16: Testing hanger 16-17

Hanger 17-18 was in good condition. It was noted that the average thickness of the Metalcoat paint was thicker in the lower section of the cable at around 600 microns, probably because more maintenance painting had been conducted at the lower level of the hanger. The coating was cracked at one location but the wires below the Metalcoat appeared undamaged and free from any corrosion. The sockets appeared to be in good condition with no visible damage observed.

Hanger 9-10 was visually in a worse condition than hanger 17-18 with areas of exposed wires and corrosion, as shown in Figure 17 below. In addition, individual wires could be seen out of lay in several locations.

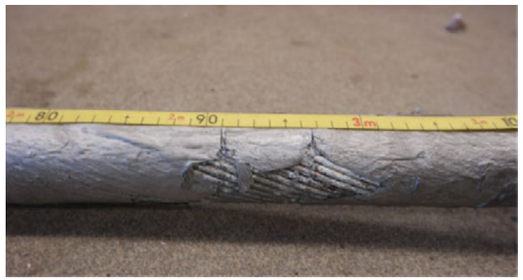

Figure 17: Testing hanger 9-10

6.2. Fatigue Testing

Hanger 17-18 was tested first in accordance with the stress range of 78 MPa and setup as described in section 4.2. The rig is shown in Figure 18. A fabricated adaptor tool with a threaded bar was used to maintain the required misalignment of the upper and lower hanger sockets such that this force was not transmitted to the hydraulic system. The test rig was set to a nominal 58kN (2% of minimum breaking load) to allow final inspection and measurement prior to the test starting and acoustic monitoring was installed to detect wire breaks occurring during the test, which took 35 days to complete. One possible wire break was detected by the monitoring system after approximately 89,000 cycles, but no wire break was evident on visual inspection after the test until subsequent dismantling as described in section 6.3.

Figure 18: Fatigue test rig (hanger 17-18)

Hanger 9-10 was tested second with the greater stress range of 119 MPa, greater maximum stress in the cycle and set-up described in section 4.2. The test was completed to 2 million cycles with no wire breaks detected.

6.3. Ultimate Tensile Testing

All hangers were tested in a 2,900 T tensile test machine (as shown in Figure 19) before the protective mat was placed over the hanger.

Figure 19: Tensile test rig (hanger 16-17)

Hanger 16-17 was tested first and had not undergone prior fatigue testing. Failure occurred adjacent to the cable top anchorage (see Figure 21 and Table 6) at 3.4% average strain, which was greater than the minimum value specified of 2%. The measured breaking load also exceeded the 95% minimum breaking load as required.

All wire failures were ductile and no other wire failures were visible away from the anchorage. Upon dismantling hanger 16-17, the socket was cut through by laser and the condition of the socket and wires inside were studied (Figure 20). There was no visible corrosion and the condition of individual wire strands was very good. There were some minor air pockets within the zinc filler in the socket, but these had clearly not adversely affected the corrosion protection or the structural adequacy of the connection. The free length of the cable itself had isolated corrosion in wire layers 2 and 3 only, with two wire breaks noted away from the location of failure in the ultimate tensile test. These wire breaks were assumed to have occurred in service. It was also noted that the lubrication introduced when the cable was manufactured was absent in the three outer layers, but present in the inner four.

Figure 20: Cut socket for hanger 16-17

Hanger 17-18 was tested after fatigue testing. Failure again occurred adjacent to the cable top anchorage at 3.2% average strain which was greater than the minimum value specified of 2%. The measured breaking load also exceeded the 95% minimum breaking load as required. All wire failures were ductile and no other wire failures were visible away from the anchorage but, on dismantling, five wire breaks were found in layer three. These wire breaks were subject to fracture surface investigation as discussed in section 6.5. Only one potential wire break was detected in the fatigue test, so it was concluded that the other breaks had either occurred in service or had occurred during the tensile test.

Hanger 9-10 was also tested after fatigue testing. Failure once more occurred adjacent to the cable top anchorage at 2.9% average strain (greater than the minimum value specified of 2%) and the measured breaking load exceeded 95% of the minimum breaking load as required. All wire failures were ductile and no other wire failures were visible away from the anchorage.

A summary of all the tensile test results is shown in Table 6. All failures occurred near the top anchorage and it was suggested that this was due to bending stresses during service near the upper anchorage for bending in the plane of the pin combined with a lack of lubrication at the top of the cable since it had flowed down to the bottom of the cable. There is also a trend indicating that greater fatigue cycling may reduce ductility as measured by the average strain at failure, but this is not pronounced.

Table 6: Tensile Test Results

Hanger	Nominal Breaking Force (kN)	Minimum Braking Load (MBL) (kN)	Actual Breaking Load (kN)	Failure Location	Strain (Approximate from Load Graphs)
16-17	3216	2900	3016	Close to upper socket (~60mm)[2]	3.4%
17-18[1]	3216	2900	3070	Close to upper socket (~60mm) [2]	3.2%
9-10[1]	3216	2900	3025	Close to upper socket (~60mm) [2]	2.9%

Note:

1. Tensile test results following fatigue testing.
2. Failure location for all hangers tested in 2019/20 were close to the upper socket. No specific measurements were taken. However, from photographic records, it appears to be approximately 60 mm from the socket.

Figure 21: Tensile test failure in hanger 16-17 (other hanger failures similar)

6.4. Examination of Wire Surfaces Upon Completion of Testing

Following completion of the ultimate tensile testing of the complete hanger system in section 6.3, the ropes were dismantled into their constituent wires, keeping a record of which layer the wires came from. The wires were categorized visually by corrosion stage (as defined in the NCHRP report 534 (2004)) for which the four corrosion stages are characterized by the presence of the following:

1. New/spots of zinc oxidation on the wires;

2. Zinc oxidation on the entire wire surface;

3. Spots of brown rust covering up to 30% of the surface of a 75 mm to 150 mm length of wire; and,

4. Brown rust covering more than 30% of the surface of a 75 mm to 150 mm length of wire.

Previous experience on the main cable assessments of Humber, Severn (Hendy C., Mundell C., and Bishop D., 2014), and Forth bridges has shown that the likelihood of brittle fractures of wire increases significantly once stage 3 and stage 4 corrosion conditions are present as crack propagation is initiated at corrosion pits which behave as crack-like defects. Figure 22 below shows the change in tensile strength of a wire for each corrosion stage.

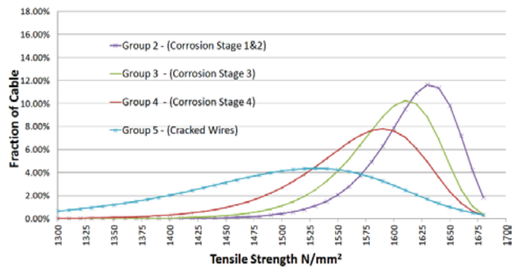

Figure 22: Extract from the management of the Severn Bridge Suspension Bridge paper

6.5. Fracture Surface Investigation

After the tensile test, five single wire breaks were found in the third layer of the hanger cable 17-18. These single wire failures are remote from the main breakage, which occurred close to the upper socket. These individual wire failure surfaces were subjected to a fracture surface investigation which suggested that, in three out of five wires, the breaks had occurred due to brittle fracture following fatigue crack propagation from a corrosion pit that generates a crack-like defect. A typical wire surface is shown in Figure 23. As mentioned in section 6.4, this phenomenon is usually linked with wires in corrosion stages 3 and 4

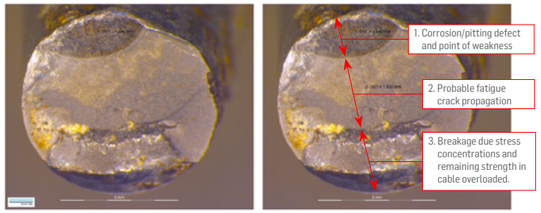

Figure 23: Typical fracture surface of broken wire from hanger 17-18, away from tensile test failure zone

7. Future Hanger Management Strategy

The implications of the test data obtained to date are that the Humber hangers may generally have significantly more residual life than initially anticipated. All the tensile test failures, after fatigue in service and after an additional fatigue loading simulating 120 years more service, were ductile and reached the minimum required test load. This means that the cables are suitable for monitoring because they currently have been shown to have adequate strength and ductility by testing but future reductions in strength will permit load shedding to adjacent hangers and the bridge has redundancy to accept failure of any one hanger.

Were it possible to freeze the corrosion in the hangers at current levels, the fatigue testing has indicated that replacements could be deferred for a very substantial period as it simulated the fatigue effects of 120 years of usage. However, corrosion has advanced in a small number of wires to the point where corrosion pitting may now begin to develop if the wires are not adequately protected by the paint system and the fatigue life of individual wires will start to reduce and the overall hanger strength will start to reduce. Given that the Metal Coat paint system is unlikely to be fully effective at preventing further corrosion, no matter how often and how well applied, it is likely that further deterioration will occur and this very high residual life cannot be achieved in practice without a different fully-effective corrosion protection system being installed, such as dry air.

As a result, the hangers will be managed by an increase in inspections of those in the worst visual condition, the painting regimen will be increased and a further set of hanger replacements and testing is recommended to be carried out in 10 years to understand the nature and consequences of any further deterioration. The cost-benefit of this approach, compared to wholesale replacement of hangers at present, is very substantial. Assuming a Net Present Value (NPV) of 4%, the comparable whole life costs over a 20-year period for carrying out the replacement now is £20.5 million compared to delaying the replacement by 10 years of £14.5 million.

8. Conclusion

The Humber hanger replacement and testing scheme has developed the detailed and repeatable methodology for hanger replacement through an increased understanding of the bridge behaviour and has justified extending the life of the existing hangers through adoption of a detailed management strategy. The minimal structural intervention adopted is both environmentally and economically advantageous. This paper provides guidance to other bridge owners wishing to pursue a similar reduction in structural intervention.

Acknowledgements

The authors would like to thank Humber Bridge Board for the support provided throughout the project. The Principal Contractor who removed the hanger was Spencer Group who were responsible for preparing the temporary works design. Replacement hangers and sockets were fabricated by Bridon-Bekaert The Ropes Group. The testing of the hangers was carried out by DNV.GL and report prepared for Humber Bridge Board by Ole Kristian Støylen Project Engineer, Andreas Tjørve Project Engineer Mads Arild Eidem Head of Section.

References

BSI (2003) BS EN 1991-2:2003: Eurocode 1: Actions on structures – Part 2: Traffic Loads on bridges. BSI, London, UK

BSI (2006) BS EN 1993-2:2006: Eurocode 3: Design of steel structures – Part 2: Steel bridges. BSI, London, UK

BSI (2006) BS EN 1993-1-11:2006: Eurocode 3: Design of steel structures – Part 1-11: Design of structures with tension components. BSI, London, UK

BSI (2020) UK National Annex NA+A1:2020 to BS EN 1991-2:2003: Eurocode 1: Actions on structures – Part 2: Traffic Loads on bridges. BSI, London, UK

BSI (1980) BS 5400:1980: Steel, concrete and composite bridges. Part 10. Code of practice for fatigue. BSI, London, UK

BSI (2011) BS EN 13411-4:2011: Terminations for steel wire ropes — Safety - Part 4: Metal and resin socketing. BSI, London, UK

Hendy C., Mundell C., and Bishop D. (2014) Management of the Severn Suspension Bridge, Bridge Maintenance, Safety, Management and Life Extension, Taylor & Francis Group, London, ISBN 978-1-138-00103-9

National Cooperative Highway Research Program (NCHRP) (2004), Mayrbaurl and Camo, Report 534, Guidelines for Inspection and Strength Evaluation of Suspension Bridge Parallel Wire Cables, Transportation Research Board of the National Academies.

Winkler J., Hendy C. (2016), Improved Structural Health Monitoring of Bridge Infrastructure using Digital Image Correlation, IABMAS June 26th – 30th 2016, Maintenance, Monitoring, Safety, Risk and Resilience of Bridges and Bridge Networks, Brazil. ISBN 978-1-138-02851-7

Winkler J., Hendy C. (2018), Monitoring of the Great Belt Bridge hanger vibrations and expansion joint movements using Digital Image Correlation, IABSE Conference 2018 – Engineering the Past, to Meet the Needs of the Future June 25-27 2018, Copenhagen, Denmark, ISBN 9781510892088

HS2 Colne Valley Viaduct – Developing a Successful Specimen Design

David A Smith

BEng CEng FICE
Technical Director
Engineering, Design and Project Management
Epsom, UK
Lead Discipline Engineer,
HS2 Ltd
London, UK

Louisa S Man

MEng CEng MICE
Formerly Senior Bridge Engineer
Engineering, Design and Project Management
Epsom, UK

Abstract

The HS2 Phase One route passes through a diverse and continuously changing British landscape. Structures along the route should be designed and constructed to respond to this diversity, becoming harmonious, memorable, and fitting additions to their sites. This is particularly true for the Colne Valley Viaduct, which, due to its scale, visibility, and the sensitivity of its site, forms one of the most important structures along the route. As such, it will become a beacon of HS2 Ltd's design-quality to onlookers and passengers alike. Colne Valley Viaduct offers an opportunity to celebrate the exceptional character of its surroundings and demonstrate how HS2 structures can combine local distinctiveness with route-wide identity.

This paper describes how HS2 Ltd chose to develop a specimen design for Colne Valley Viaduct, following the deposition of the Phase One hybrid Bill and before the subsequent granting of Royal Assent and award of a main works civil contract. It describes the reasons why such an approach was undertaken and what key aims were achieved.

Keywords

Concept design; Aesthetics' Local context; Bridges; Stakeholder engagement

Héctor Beade Pereda

ICCP MEng CEng MSpICE
Associate
Knight Architects
High Wycombe, UK

Tomás García

Head of Civil Structures
HS2 Ltd
London, UK

1. Introduction

The HS2 Phase One route passes through a diverse and continuously changing landscape. Structures along the route should be designed and constructed to respond to this diversity, becoming harmonious, memorable, and fitting additions to their sites.

This is particularly true for the Colne Valley Viaduct, which, due to its scale, visibility and the sensitivity of its site, forms one of the most important structures along the route. As such, it will become a beacon of HS2 Ltd's (HS2) design-quality to onlookers and passengers alike. It will portray the national scale of HS2's infrastructure whilst expressing its sensitive integration within the landscape. Colne Valley Viaduct offers an opportunity to celebrate the exceptional character of its surroundings and demonstrate how HS2 structures can combine local distinctiveness with route-wide identity.

Aspirations for the viaduct were set high as stated by the High Speed Rail (London – West Midlands) Bill Select Committee of the House of Commons[1]:

"181. ...the Colne Valley viaduct will be the most significant visible engineering feature of the HS2 Phase One route. It will have international significance and its design should reflect that. Having argued against a viaduct, local people deserve that its design be respectful and respectable... Sympathetically and imaginatively designed, the viaduct can become a suitable symbol for the country's future high-speed railway network."

Figure 1: Virtual image of CVV crossing Harefield No. 2 Lake

At the time the main Phase One civil engineering works contracts were being procured, the design development of all structures along the route was limited to just the initial maturity necessary for parliamentary design. By nature, these designs were concerned more with space-proofing and ensuring sufficient land was made available within the HS2 Act for construction and operation, without being overly restrictive on structural forms or potential construction methods, than specifying the precise quality aspirations for a preferred option. HS2 chose to develop a specimen design (Figure 1) for Colne Valley Viaduct for a number of reasons following the deposition of the Phase One hybrid Bill and before the subsequent granting of Royal Assent and award of a main works civil contractor. These key aims included the following:

1. Setting a design quality benchmark. When completed, Colne Valley Viaduct will be the longest viaduct in the UK in a highly environmentally sensitive area in close proximity to several settlements. The Parliamentary Select Committee recognised that this would therefore be a viaduct of international significance and that it should be a beacon structure for HS2, to be designed and delivered as an exemplar to the project.

2. Engaging with communities and making the most of the time to design. These represent points two and nine of the HS2 Design Vision[2], respectively, and were seen as being vital to address ahead of detailed design. It was expected that HS2 was unlikely to achieve the same depth of design development if concept design of the viaduct didn't commence until the main works construction contract procurement process had concluded. Once appointed, the contractor's designer was likely to be working under greater timescale and cost pressure, potentially compromising the ability to engage with affected communities to fully inform the early design development.

3. An early test of HS2's previously published standards and requirements. For viaducts, these included the Bridge Design Requirements[3], Aesthetic Approach[4] and Technical Standards[5, 6] to confirm that an appropriate solution could be achieved in response to the technical and aesthetic requirements and location specific constraints. It was hoped that the specimen design approach and some of the conclusions might be suitable for use in other contexts throughout Phases One, 2a, and 2b.

4. Developing a specimen design based on a tangible asset. Work and design aspirations to date were inevitably based on a subjective understanding of design intent.

Developing a design based on a tangible asset allowed this to be framed in a clearer context and allowed direct comparison for further design guideline development.

5. Continuous stakeholder engagement. Progressing a specimen design ahead of the main works contract award allowed time to gather and process local knowledge using an appropriate assessment approach. The time was used constructively to share information with all relevant stakeholders, to receive inputs, and to process them as part of the design.

6. An opportunity to inform stakeholders about technical issues of a structure of this scale. The development of a specimen design maximised the opportunity for stakeholders to consider the essential technical aspects alongside environmental, aesthetic, and emotional ones. The nature of high-speed railway traffic constrains the work of the designer. High-speed rail viaducts are subjected to heavier vertical and horizontal loads than road or conventional rail bridges and must comply with strict deflection and vibration limits to guarantee passenger comfort and traffic security. Due to these particularities, high-speed rail viaducts have a more robust appearance and shorter spans than the average of those carrying other types of traffic, which makes the design of elegant structures challenging. This challenge can be even higher if additional elements, such as noise barriers, need to be included in the design.

The ultimate aim of the process was to design a viaduct that responds to both the technical requirements of HS2 and the unique and sensitive nature of its location. It was important to stress throughout that the specimen design was developed as one *potential* solution that best satisfied the numerous requirements and aspirations, not necessarily *the* final solution.

2. Contractual Arrangements, Scope, and Programme

Through an existing framework contract with Atkins, HS2 appointed Knight Architects to develop a specimen design for Colne Valley Viaduct. Atkins remained closely involved in the design development, ensuring engineering robustness to the emerging concepts and advising on the array of relevant information already available and studies already undertaken as well as administering the framework contract and sub-consultancy contract.

In addition to evaluating a range of structural options to fulfil the location-specific demands of the Colne Valley, a major aspect of the scope for the specimen design development was to positively engage with the Colne Valley Regional Park Panel (CVRPP) and the HS2 Independent Design Panel (IDP) through a series of meetings, presentations, and workshops throughout the work. Such an approach ensured the key external stakeholders were involved in shaping the direction of the design development with the intention to ease subsequent planning consent ahead of construction.

The CVV specimen design was developed between July 2016 and March 2017 whilst the HS2 Phase One main works contracts were being tendered, evaluated, and procured. Consequently, release of developing aspirations, images, and conclusions into the pubic domain was supressed until the main works contract was awarded in July 2017. The specimen design work was commissioned to make the best use of the time available between deposition of the Phase One hybrid Bill, the subsequent granting of Royal Assent, and the award of a main works civil contractor.

3. Site Analysis

The Colne Valley Regional Park is located to the northwest of London, spanning Berkshire, Hertfordshire, Surrey and Hillingdon and is the first large green area (111 km^2) to the west of London. It is formed predominantly from parkland, farmland, and woodland, yet contains large reservoirs which surround the River Colne and the Grand Union Canal. The site of the Colne Valley Viaduct itself sits alongside the existing Chilterns railway line which runs into London Marylebone. The viaduct crosses several reservoirs, the Grand Union Canal as well as the A412 North Orbital Road and Moorhall Road. The site's heritage stems from quarrying and agriculture, which have now given way to mainly recreational uses surrounding the reservoirs. The combination of water courses, lakes, meadows, and woods makes the area highly valuable and environmentally sensitive in terms of landscape and wildlife (Figure 2).

Figure 2: Aerial view of Colne Valley and the viaduct alignment

The immediate surroundings of CVV can be broadly divided into two key landscape character areas: water and woodland. In order to successfully integrate within this landscape, it is important that the viaduct responds specifically to the varied characteristics of these two areas.

The water area is located above the reservoirs and covers the majority of the length of the viaduct (Figure 3). Whilst the bodies of water are fragmented with roads, canals, and the River Colne, visually, they combine to create a consolidated character which influence the design of the viaduct. Expanses of water provide open views to the surrounding vantage points.

Figure 3: Water character area

By contrast to the openness of the water, the woodland character area is defined by enclosure, with tree-lined roads permitting only restricted views of the structure which will pass through it (Figure 4). Whilst the woodland character area surrounds all edges of the water, it is primarily focused to the northwest of the water, with the viaduct entering the woodland after it has crossed the River Colne.

CVV will be most visible as it crosses the water character area. Here, the key viewpoints are from the elevated position of the existing railway line, as well the lower viewpoints surrounding the water's edge. Denham Green and Harefield are the nearest settlements, but views from these locations are restricted by woodland. The A412, Moorhall Road, and

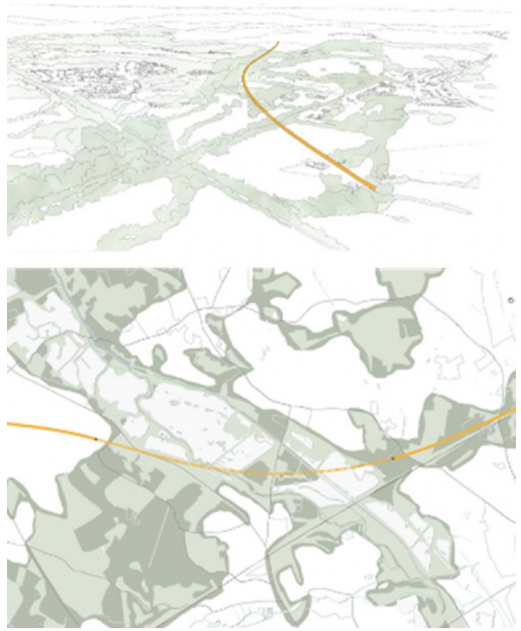

Figure 4: Woodland character area

the Grand Union Canal all permit axial views of the structure, predominantly framed by trees. CVV must respond to these wide range of viewpoints. The best vantage point is afforded from the existing railway, which will be both at speed and a reasonable distance away. By contrast, the low-level views from the footpaths and trails surrounding the water will permit a closer, and comparatively "slower" experience of the viaduct at a primarily pedestrian-scale.

A key characteristic of a well-integrated structure is how it responds to the infrastructure beneath it. Beyond the challenge of responding to the axial views created at the road, canal, and river crossings, the viaduct must formally address these crossings in its structural arrangement too. In order to form a positive addition to the site, as the CVV crosses over this range of existing infrastructure, its design must respond to the constraints that they create. The viaduct should "tread lightly" across this sensitive landscape: a significant challenge given that the range of typologies, alignments, and context of these crossings varies dramatically beneath the viaduct.

Most crossings are lined with trees (even in the water character area) which serves to restrict views to the axis of the crossing itself. Alignments range from the perpendicular arrangement at Moorhall Road to the high skew of the A412. Whilst the visibility of crossings within the woodland character area is limited (often to viewpoints on the road

itself) the crossings of the canal and river within the water character area can be viewed from a variety of surrounding vantage points. At these locations, the span arrangement, pier form, and alignment are of critical importance in establishing a structure which actively responds to the specific features of the site below it.

4. HS2 Constraints

The main constraint on the design of CVV is arguably its vertical alignment. The low, relatively consistent alignment creates a challenging relationship between the structure and the ground below it. Proportions, span length, and structural profiles all must be carefully considered to produce a fitting, elegant solution. This challenge is eased somewhat over the water, as reflections serve to increase the perception of height, allowing more light, transparency, and even views through the structure. In the woodland areas, the low vertical alignment places the deck within the treeline, which masks large portions of the structure from the majority of viewpoints. This alignment results in the viaduct passing through rather than over the woodland, which a successful design must respond to.

By contrast to the challenges of the vertical alignment, from an aesthetic standpoint, the effect of the gently curved plan alignment is generally positive. However, the curve eliminates "pure" elevational views, with neighbouring piers presenting different angles to most viewpoints. Combined with a low alignment, this can often produce a "forest of columns" effect, which must be avoided. As such, pier shaping and arrangement must carefully consider the plan-curve so as to achieve a well-co-ordinated, deliberate appearance.

If a successful pier arrangement is achieved, the eye will be drawn to lines of the deck. From most viewpoints, the plan curvature will generate a dynamic form, creating fluid, free-flowing lines that sit well within this natural setting. The viaduct's combination of length and plan curvature may also result in views of the structure for the passengers upon it. Even if only a brief glimpse is achieved, this will greatly enhance the passenger experience of the railway. CVV provides one of the best opportunities along Phase One for views of the open countryside for HS2 passengers. The experiences of speed, scale, and "journey" are all further enhanced if the structure (and even the train itself) can be a part of that view.

There are certain constraints to be taken into account when defining the sectional design (Figure 5). The viaduct cross section must accommodate two high-speed rail tracks with a cant due to the curved horizontal alignment and the slab track system. A derailment containment system must be used at both sides of the track area, and two evacuation/ maintenance routes must be arranged at both edges of the deck. Overhead lines are used for electrical power transmission to the trains, which means that overhead catenary system (OCS) masts will be arranged at certain longitudinal intervals (typically between 40 m and 60 m) at both sides of the track area. Their spacing and design should be consistent and co-ordinated across the viaduct, as changes in either disrupt the rhythm of the structure below. Noise barriers are required along most of the length of the viaduct, at least on one side of the deck, with heights varying from 3 m to 4 m depending on receptor proximity and noise model input parameter assumptions. A protection barrier is needed on the edges of the deck.

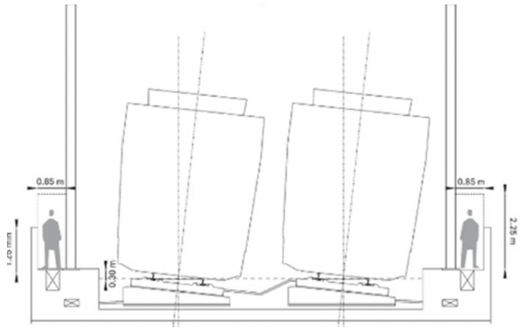

Figure 5: HS2 cross section requirements

Having just exited a tunnel from London, CVV offers an exciting opportunity to provide dramatic, open views to HS2 passengers, allowing the diverse changes in the landscape to be perceived. Across the route, these elevated vantage points are relatively rare and great care must be taken to not unnecessarily obstruct them with noise barriers. The location, height, and design of the barriers must seek to combine functional performance with transparency; to reduce noise whilst maximising views. In addition to the consideration of the view from the viaduct, the consideration of noise barrier impact on views of the viaduct is of critical importance. The flowing, understated lines that could be achieved in the primary structure can all too easily be broken with poorly designed barriers placed on top of it.

As many of the viewpoints of the viaduct are from below, the transverse position of the barriers is just as important as the longitudinal. Barriers which are placed in close proximity to the rail have less impact on the appearance of the structure. Once the broad position, height, and design of the barriers is established, its components must also be carefully co-ordinated so that the noise barrier appears as a logical, integral element of the viaduct design.

5. Design Aspirations

Colne Valley Viaduct is one of the most important structures on the HS2 Phase One route, set within one of the most sensitive landscapes. As such, it must represent the very best in contemporary design. It will form a "beacon" of HS2, and therefore must convey the route-wide aspiration to create a fitting, elegant, and long-lasting piece of national infrastructure.

There are broadly two design methodologies that can be used to achieve an aspiration for the design of a "beacon structure" – prominence or elegance. A prominent viaduct would take the form of a tall, eye-catching design, usually with above-deck structure. High vertical alignments such as those across deep valleys lend themselves to this approach, where massive forms can remain aesthetically pleasing due to the proportions offered by the vertical scale of the crossing itself. Achieving a beacon structure through elegance requires careful detailing, slender proportions, and keenly designed components via a reductive rather than an additive approach. This elegance approach is best suited to the low vertical alignment of Colne Valley Viaduct, where issues of deck depth, span length, structural proportions, and transparency are valued over height.

A low vertical alignment leaves less room for elaborate design. Where tall, prominent structures can readily accommodate elaborate eye-catching designs, low-lying solutions should strive for understated simplicity if they are to be considered elegant. A high viaduct can be easily visible and legible. It also may offer more options in terms of height versus span ratio choice. It is much easier to get an internationally recognised "beacon structure" with a high alignment than with a low one. A low viaduct is less likely to be visible and legible (especially in woodland areas). It offers less design versatility in terms of height versus span ratio. Achieving an internationally recognised beacon structure with a low alignment is challenging.

Given the low alignment, the aspiration must be for an "extraordinary" viaduct. This is intended both in the hyperbolic sense of achieving an exceptional structure, but also in the very literal sense of designing something out-of-the-ordinary. An "ordinary" structure will not be specific to the Colne Valley, nor will it be commensurate with the importance of this scheme.

One of the primary influences on an elegant design is what happens below the deck level. The curved plan alignment of CVV requires careful alignment of the piers in order to ensure that their arrangement is logical, simple, and fitting. Twin piers, which each support a bearing at a single cross section, will read as two separate objects. This is not suitable to a curved alignment where their rhythm will create interference patterns that create a cluttered appearance. As such, piers should be singular in their design, either "leaf" style elements or "V" piers. In doing so, their arrangement and rhythm will be more easily read from the variety of surrounding viewpoints, and the viaduct will appear to "tread lightly" across this sensitive landscape.

An elegant viaduct, particularly one with a low vertical alignment, must be well proportioned. The proportions of CVV should address the following three constraints:

1. **Span to Depth Ratio.** It is important that CVV appears to be "working" but without appearing to be an ordinary structure. This visual perception is usually based on the span to depth ratio, with overly short spans detracting from the drama and elegance of a structure. Whichever structural system is used, it must appear to be keen and efficient, even with an extraordinary design which positively portrays the forces running through it.

2. **Deck Depth to Clearance Ratio.** A low viaduct must strive to maximise the clearance that remains underneath it. Views, landscape permeability, and light all benefit from greater clearance. This distance will be viewed against the structural depth. A well-proportioned ratio between the two will ensure the viaduct delicately and respectfully crosses the landscape.

3. **Width to Clearance.** Visually, structures which are wide in the transverse direction need to have more clearance. This is to the same end as a good depth to clearance ratio – light, views, and permeability are worsened by structural width. Moreover, the width dramatically impacts the bearing locations, and, in turn, the pier size. Wide piers block views and increase the visual mass. Split piers increase the transparency but at the cost of adding clutter.

In response to the character areas described previously, longer spans are suited to the comparative openness of the water areas with the enclosure provided by the woodland areas permitting shorter spans. Reflections over the water require careful consideration to be given to the deck soffit, which will be readily visible from many vantage points. Pier form may also benefit from changing to suit the specific characteristics of each area. Whilst other elements of the structure will change across the landscape character areas, the deck edge will likely benefit by remaining consistent. This will give continuity across the viaduct, providing a steady datum, against which other structural changes can be read.

CVV will be viewed at a variety of distances and speeds and the quality of materials and detailing must respond to this. An understated, elegant solution must be exceptionally well detailed if it is to be perceived as an extraordinary structure.

It must be long-lasting, of the highest quality, and provide a material finish that is suited to the close proximity that can be achieved from many of the viewpoints on and surrounding the water.

Particularly below-deck, the structure must be designed with a “pedestrian-scale” in mind. Whilst CVV is indeed a large piece of railway infrastructure, it will form a critical component of the pedestrian environment beneath it. Piers will touch the water, provide access around them for walking routes, and the relatively low height of the deck soffit will make it easily visible. As such, all elements that face the pedestrian environment must be of a quality, scale, and texture commensurate with the up-close and low-speed scrutiny it will be subject to. Quality in this sense is related to overall geometric design, choice of materials (light grey concrete for the structure, and transparent acrylic sheets and stainless steel for noise barrier, as an example), use of texture for some of the surfaces (some areas of deck and piers with recessed patterns), how these materials are treated during construction (concrete finish, welding smoothness in steelwork, etc.), and the design of details (recessed stripes to direct water in a controlled way on the deck sides, or drainage conduit-pier coordination, for example).

For CVV to be considered a fitting structure that has been sensitively designed with the landscape in mind, it must directly address the features which it crosses. This is achieved to some extent by responding to the specific characteristics of the woodland and the water. However, the existing infrastructure also must be referenced. The Grand Union Canal, the River Colne, as well as the different roads and pathways crossed should be acknowledged in the design. This could be as simple as ensuring that these structures are positioned centrally within spans, or could extend to having their presence highlighted by “feature” spans.

6. Option Appraisal

Having established the design aspirations, concept design options were then assessed against them. In order to best address the separate constraints and opportunities of the woodland and the water character areas, options focussed on them separately. Many of the proportional constraints (span to depth, depth to clearance, etc.) are most restrictive in the woodland character area. As such, the cross-sectional design of the deck and piers was designed with a focus on this area so as to address the most constrained sections of the viaduct.

Within this area, the cross-section of the deck, its influence on the bearing location and, in turn, the pier width is of critical importance; there is a visual aspiration to increase the clearance underneath the deck. At several locations (such as over roads) this desire is reinforced with a functional clearance constraint.

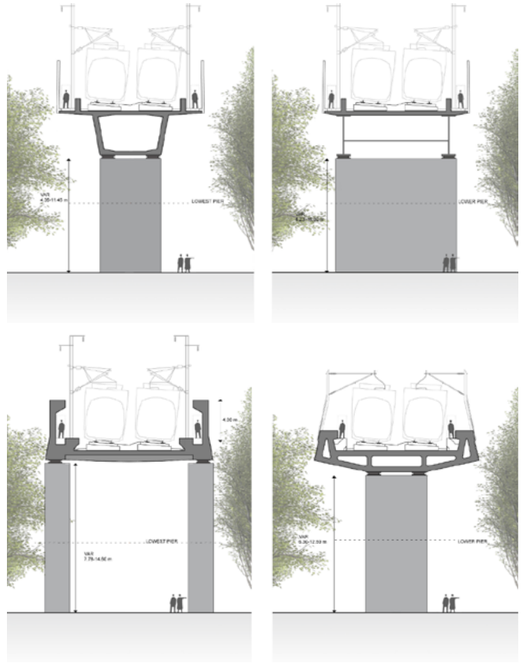

Figure 6 (a to d): Alternative deck cross-section and substructure forms considered

A traditional arrangement would position the vast majority of the structure below the level of the deck (Figure 6(a)). This reduces the clearance and also “stacks” elements such as derailment containment kerbs, noise barriers, parapets, and OCS structures on top of the structural depth, which leads to a further increase in the total perception of deck depth. Using a “through” structure arrangement has the benefit of moving a proportion of the structure above the deck. This improves the clearance below and also allows certain elements (noise barriers, kerbs, walkways, etc.) to exist within or behind this structural makeup, further reducing the visual depth of the “total” deck build-up. Of course, if this structure rises to the point where it begins to block the views of the passengers, any benefit achieved in views of the structure is eliminated with a negative effect on views from the structure.

Next, is the deck’s influence on the transverse distance between bearings. Traditional through-structures force the bearings to the edge of the deck, which results in either wide leaf piers (Figure 6(b)), twin-piers (Figure 6(c)) or cantilevered piers. These piers either appear overly large and block views or produce an irregular pattern which clutters the appearance of the viaduct and as such are not suitable for CVV. The proposed solution is shown in Figure 6(d), which combines above- and below-deck structure with enough torsional stiffness in order to maintain a close bearing proximity beneath the deck. The result is a structure with a good “total depth” to clearance ratio, which masks certain elements behind the structure, and permits transversely slender piers beneath.

Figure 8: Virtual image of CVV crossing Korda Lake

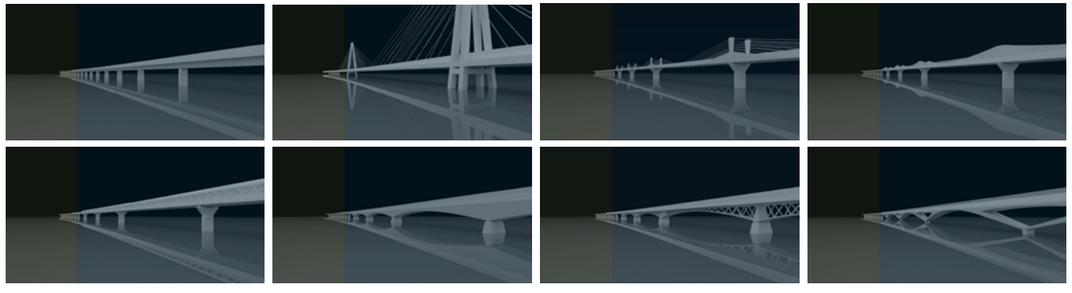

Figure 7 (a to h): Options evaluated to cross the main water bodies

Having established a deck cross-section preference, a number of general layout options were then tested against the site and HS2 constraints, ranging from a very conventional viaduct with 50 m to 60 m long typical spans (Figure 7(a)) to a multi-span cable-stayed viaduct (with 350 m typical spans, Figure 7(b)) that was used to explain the drawbacks of the design many people had in mind at the beginning of the work stage (inappropriate scale and conflicting with the close Denham aerodrome).

Structural forms considered included the following, as illustrated in Figure 7(a) to (h):

a) Multi-span continuous beam with a box girder with cantilevers (or U-shaped) constant depth cross-section;

b) Multi-span cable-stayed viaduct;

c) Extradosed Spans Over Main Lakes responding separately to the woodland and water character areas;

d) Multi-span beam with variable depth spans (above rail) over main lakes;

e) Multi-span beam with constant depth tubular cross section over main lakes;

f) Multi-span beam with variable depth spans (below rail) over main lakes;

g) Multi-span beam with variable depth truss spans (below rail) over main lakes; and,

h) Multi-span variable depth arched spans with v-shaped piers over main lakes.

Based on previous design assumptions, all the options had common features: a typical constant hybrid box girder-trough deck forming circa 50 m spans in the woodland area, complemented by other structural forms to achieve longer 100 m to 115 m spans over the lake areas, keeping as continuous a deck edge as possible.

The selected design (Figures 1, 7(h), 8, 11, and 12) is a multi-span concrete structure whose typical deck arrangement in the woodland areas smoothly turns, when crossing the lakes, into a series of 105 m spans with variable-depth, an arched soffit and triangular voids in the deepest areas (which can be seen as part of the V-shaped piers in Figures 8, 9, 11, and 12). This solution is the one that better responds to the different character areas and obstacles being crossed. It successfully uses the reflection on the water as a relevant feature of the design thanks to the sequence of arches, narrowing when closer to the water (Figure 7(h)). This arrangement also minimises the area in contact with the water, so as to tread lightly across this sensitive landscape and visually links the deck to the piers, adding clarity to the arrangement when viewed from oblique angles.

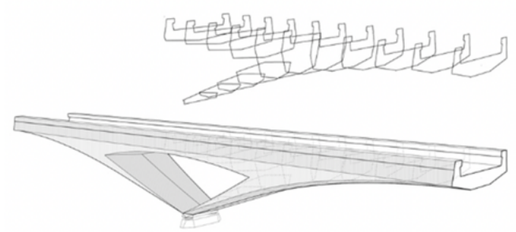

Figure 9: Detail of one of the triangular cells of the main span crossing the water bodies

Large perforations in the deeper areas of the deck maintain views and landscape flows through them. The deck soffit and the internal faces of the triangular cells are faceted, increasing the visual slenderness without noticeably reducing their mechanical properties (Figure 9).

Concrete was chosen as the main material for the bridge due to its appearance, natural ageing, benefits from a maintenance point of view, and to the mass and damping provided (that is, in general, beneficial to a high-speed rail viaduct with long spans). The typical construction-related drawbacks aren't a discouraging aspect in the case of CVV, due to accessibility of the site, the proximity of the deck to ground level, and the shallowness of the lakes (average depth of approximately 5 m).

The woodlands offer enough areas with lower visitor accessibility to place the required special substructure elements to create fixed points for stretches of the viaduct, or to allow room for expansion joints.

7. Specimen Design Features

The combination of some above-deck structure and torsional stiffness creates a deck that actively responds to the HS2 constraints, whilst maintaining good clearance below, as well as offering an opportunity for a consistent design element across the varied conditions of the viaduct. Applying a subtle taper to the piers, as well as simple "creases" to their face, creates a standard form which is well suited to the Colne Valley. The cross-sectional distance between the deck edge and the bearings also serves to cast the pier into shadow, drawing attention to the crisp edge of the deck, adding lightness to the appearance of the structure in both the water and woodland areas.

Whilst the general aim of achieving long spans on the water section is desired, it was found that a slight reduction in span, from 115 m to 105 m, resulted in a much better arrangement. The proposed 105 m spans formally address both the lakes and the canal below and create a structure which is both more legible and more deliverable.

For this elegant structure to become a beacon, it must be exceptionally detailed. Part of this is to ensure that its key features are refined designs which add to the interest and quality of the crossing. The parametrically refined forms facet the deck soffit and the internal faces of the triangular cells, increasing the visual slenderness without reducing their mechanical properties.

For any viaduct to be considered elegant, it must provide a holistic solution, which addresses the requirements of both the rail and the landscape. Even if the structure itself is beautiful, additional elements placed on top of it run the risk of adding clutter. As such, the proposal is for a holistic edge condition, which – with a single system – incorporates the noise barrier, parapet, fowl and bat protection, and the OCS masts. As opposed to large "frames" which abruptly start and stop and may thus disrupt the rhythm of the structure below, the proposal developed for the CVV specimen design was for a series of vertical elements which subtly modulate across the viaduct (see Figure 10). Their triangular cross-section gives the system a transparent appearance when seen from distance by CVRP visitors, and their arrangement and slenderness will make them almost invisible for HS2 users looking through the train window. The envelope created by the system is consistent regardless of whether a noise barrier is needed or not, with its angle dividing the external face of the deck into two, increasing its visual slenderness.

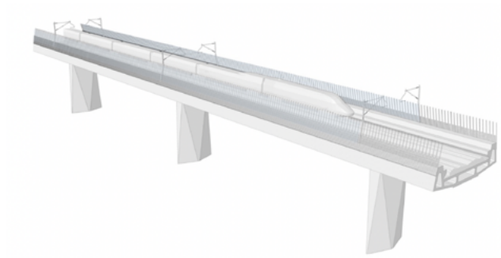

Figure 10: Concept of multi-purpose parapet noise barrier and flying fauna protection

The piers of the viaduct have an elegant, subtly tapered, and faceted design. Since every support is made up by a single body, instead of the two columns that would be typically used together with U-shaped cross sections, they will be compact and cast in shadows, avoiding the "forest of columns" effect. Facets break their volume and create attractive shade contrasts varying with the daytime, season, and position of the viewer. These are key features of the design, defining a high quality that suits the viaduct design aspirations. This general design approach can be further enhanced in specific areas by improving the material finish with the addition of texture when they can be seen in close proximity by pedestrians. The texture approach defined in the specimen design complements the pier design, with simple vertical recessed lines on the triangular faces whose bases are located at ground level. This adds a balanced degree of complexity and interest to the untextured design while enhancing its natural geometric features, intensifying facet contrast.

Figures 1, 8, 11, and 12 show key views of the viaduct crossing Harefield No.2 Lake and Korda Lake. The key features of the CVV specimen design can be appreciated in these images: elegance, subtlety, legibility, harmonious and sculpted concrete shapes, respect for the water bodies being crossed (minimum concrete volume in contact with the water), transparency, use of reflection, care for detail, and the holistic design of viaduct and edge conditions. The images show an extraordinary contextual structure, perfectly suited to the Colne Valley, which will become a beacon through its elegance.

Figure 11: Virtual image of CVV crossing Harefield No. 2 Lake

8. External Stakeholder and Panel Engagement

The CVV specimen design was developed interacting with the Colne Valley Regional Park Panel and the HS2 Independent Design Panel at different stages of the work. Both panels provided very valuable input that was taken into account to produce the specimen design. Both panels offered strong support for the content of the specimen design and especially the design approach. Specifically, both panels highlighted:

- The engagement and transparency with stakeholders throughout the process;
- The sensitivity to the context of the overall design;
- How the viaduct changes in span and geometry depending whether it is above water, woodland or roads, keeping design coherence and elegance at the same time;
- How the "hybrid" cross-section successfully balances noise reduction with views from the train;
- The elegantly proportioned shapes of the main spans over water bodies and the variable depth span over the A412;
- Having used the reflective properties of the water bodies as a relevant design parameter;
- The design considerations of the parapet and noise barrier and how the system becomes a fowl and bat protection barrier in the areas noise protection isn't needed; and,
- The intent to use ribbing to control water flow and staining and to add texture.

Both panels encouraged the design team to consider the user experience of the Colne Valley Park visitors when designing the viaduct. Some aspects of the design are directly consequences of this input including: the use of longer spans with arched shapes in the more visible areas; having an uncluttered pier arrangement with a single concrete body (instead of two columns) with refined shapes and dimensions; using textured surfaces when piers can be potentially in close proximity with pedestrians; and allowing the possibility of locally creating apertures to allow visitors to cross the piers when they are close to towpaths.

9. Conclusions

The process of developing a specimen design for Colne Valley Viaduct highlighted a number of positive aspects and its successful delivery was down to a number of key principles established from the outset. These included:

- Setting a clear definition of scope and outcomes from the start;
- The appointment of appropriate specialists – both engineering and architectural – collaborating harmoniously to develop the design;
- Engagement with relevant local stakeholders throughout the process, actively involving them in the design development and exploring what their key issues were and what compromises they would be more willing to make to achieve a structure capable of satisfying the numerous high-speed railway constraints;
- Always being cognisant of the need to develop a design that is respective and respectful of the location through which it runs;
- Establishing a well-defined and structured approach to the overall design process with clear milestones, articulated appropriately to all parties; and,
- Ensuring an openness with panels, members, and wider communities to explain design approach, technical challenges, and specific constraints of high-speed railway viaducts.

Developing a specimen design for Colne Valley Viaduct successfully made the most of the time available between hybrid Bill and award of a main works design and build contract. It enabled the diverse, sometimes conflicting requirements to be interpreted and the constraints and opportunities that are placed upon the viaduct to be explored. The work turned the design aspirations into a high-quality concept that meets HS2's technical standards and environmental requirements, capturing the views of the CVRPP and the HS2 IDP. The CVV specimen design received exceptionally positive support from both panels and the individual stakeholders and formed a reference and benchmark for the subsequent design stages.

The proposed viaduct responds to the scale and visual character of the different areas of the Colne Valley park, to the user experience along and below the structure, and to the environmental sensitivity of the location. What began being envisaged by many as an eye-catching, prominent structure, ended up being a beacon through its elegance. The combination of subtle, elegant arches, structural lightness, and exceptional proportions created a structure which would be a fitting addition to the landscape.

Figure 12: Virtual image of CVV crossing Korda Lake

Acknowledgements

This paper is published with the permission of HS2 Ltd. The authors acknowledge Billy Ahluwalia, HS2's senior project manager for Colne Valley Viaduct, for his valuable input throughout the specimen design development. The final visualisation images were produced by Hays Davidson Ltd in conjunction with Knight Architects. The authors would also like to acknowledge the contributions to a successful specimen design approach from the Colne Valley Regional Park panel, chaired by Jim Barclay, and the HS2 Independent Design Panel, chaired by Sadie Morgan and Tony Burton.

References

1. The Stationery Office, House of Commons Select Committee on the High Speed Rail (London – West Midlands) Bill, Second Special Report of Session 2015–16, The Stationery Office, London, 22 February 2016 (accessible via: https://publications.parliament.uk/pa/cmhs2/129/129.pdf)

2. High Speed 2 (HS2) Limited. HS2 Design Vision, HS2 Ltd, London, 2015 (accessible via: https://www.hs2.org.uk/documents/hs2-design-vision/)

3. High Speed 2 (HS2) Limited. Bridge Design Requirements, Project document HS2-HS2-BR-STD-000-000004, HS2 Ltd, London, 2015 (not publicly accessible)

4. High Speed 2 (HS2) Limited. Open Route Design Approach, Project document HS2-HS2-AR-GDE-000-000005, HS2 Ltd, London, 2016 (not publicly accessible)

5. High Speed 2 (HS2) Limited. Technical Standard – Bridge Design Basis, Project document HS2-HS2-BR-STD-000-000001, HS2 Ltd, London, 2015 (not publicly accessible)

6. High Speed 2 (HS2) Limited. Technical Standard – Viaducts, Project document HS2-HS2-BR-STD-000-000002, HS2 Ltd, London, 2015 (not publicly accessible)

Assessing Options for Getting Back to Work During the COVID-19 Pandemic

Stephen Bourne

P.E.
Atkins Fellow, Project Director
Engineering, Design and Project Management
Miami, FL, United States

Abstract

The recent COVID-19 pandemic and its resulting economic impacts have made clear the need for communities to find ways to continue to operate, even as outbreaks occur. Atkins has adapted its City Simulator tool – a software focused on climate change - to allow communities to explore their options in terms of coping with COVID-19. With City Simulator, a digital twin of the community is created and then simulated as the community evolves from present day to mid-century. An initial experiment is described where an infection strikes a virtual city, Optima, of 95,909 people. The base run shows that 79% of the population is infected in a massive first outbreak that reduces the engaged workforce of the city from 33,000 to fewer than 500 people. A social distancing measure is then simulated to explore the efficacy of such measures. The study shows that three factors impact efficacy of the measure: introduction time relative to initial infection, duration of implementation, and compliance of the population. The results show that it may be possible, with the application of mitigating and adapting measures, to continue to operate and avoid community shutdown and keep the working population productive.

Keywords

City Simulator; COVID-19; Pandemic; Social distancing

1. Introduction

The recent COVID-19 pandemic and its resulting economic impacts have made clear the need for communities to find ways to continue to operate, even as outbreaks occur. 33.0% and 20.4% drops in year-on-year GDP in the US and UK, respectively, point to devastating economic impacts of shutting down society to avoid infection (USBEA 2020, UKONS, 2020). Atkins has adapted its City Simulator tool to allow communities to explore their options. Initially developed to provide clients with a means to measure how resilient their communities are to climate change and sea level rise, City Simulator is a map-based software tool used to create a digital twin of the community and then evolve the community day-by-day into the future. Over the course of the simulation, the community is hit with projected disasters like storms, heat waves, and rises in sea levels.

The resulting impacts to community property and productivity are simulated and measured as key performance metrics. Stakeholders use these metrics as a basis for decision making in terms of any mitigation and adaptation actions they will take to become more resilient.

Though initially focused on climate change and the disaster types that it influences, through its agent-based design, the framework for City Simulator enables the ability to include other disasters such as cyber threats, terrorist attacks, and epidemics. The term “agent-based” refers to the fact that each individual person in a community is modeled as an avatar. Activities like commuting, shopping, stopping to get gas, etc. are all captured in the model daily. As these contact points are explicitly modeled within the context of a real community, the framework lends itself naturally to modeling the spread and recession of an epidemic. Moreover, given the capability within the framework to add adaptation/mitigation actions and simulate their influence on agent activities, testing options for epidemic mitigation, actions like social distancing, stay-at-home directives, regular disinfection of surfaces, and so on can be tested in terms of their effectiveness.

This paper will describe the recent development of an epidemic modeling capability within City Simulator and a first application to a virtualized city called Optima.

Optima – A virtual City

- = 95,099 people
  - = 31,129 workers
- = 20,030 buildings
  - ! Commercial – 3,125 buildings(single and multi-business)
  - ! **Residential – 16,905 buildings (single and multi-family)**
- = Central Business District in SW Quadrant
- = Daily Commutes to work

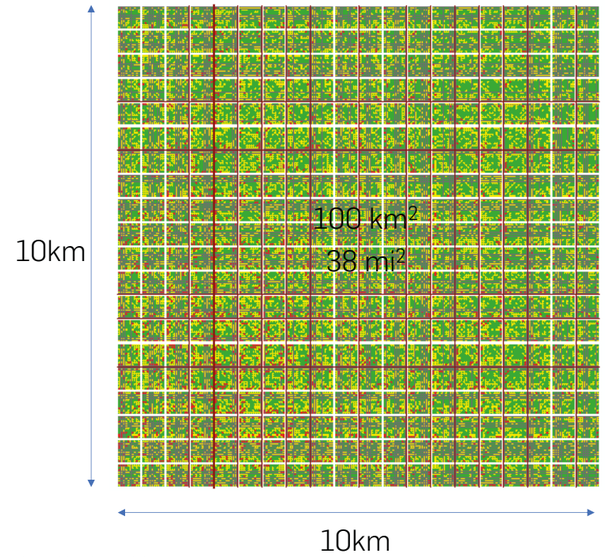

Figure 1: Optima is a virtual city generated within City Simulator to run the epidemic model

2. Optima

A virtual city called Optima was created with City Simulator to act as a test bed for epidemic model. This 95,099-person city covers 100 sq km (38 sq mi) as a great square, 10 km on a side. There are 20,030 buildings in the city, 3,125 of which are commercial. The workforce is 31,129 people, each of whom commute to work each day.

It should be noted that City Simulator was designed to work on real cities, and there are many examples of it being used around the world. Optima was created to help the Atkins team focus on infection dynamics and ensuring they are being simulated correctly. In future runs, real communities will be simulated, which will add complexity to the simulation and provide valuable insight to those communities.

3. Simulating Spread of Infection Through Travel Modeling

The simulation was based on the so-called SIR model, where buckets of susceptible, infected, and recovered populations are accounted for explicitly (Weisstein 2020). Given each building in the community is modeled as an object, a building-level SIR model was applied to each structure. Community-scale estimates of susceptible, infected, and recovered individuals are therefore a sum of the SIR models results at each building across the community.

The transfer of individuals from S to I to R was tracked through simulating infection occurring during explicit contacts between individuals as they traveled through the

community. The contacts were tracked through City Simulator's built-in travel model, which maps out the commute path of every worker in the community. Typically, these paths are used to understand the level of disruption felt by the community when, for example, a culvert or bridge is damaged due to flooding and the residents are not able to take their normal commute. In the case of epidemic modeling, the commute paths help to simulate how the infection spreads through daily travel. The figure below shows an example of a "commute footprint" for an individual commercial building in the central business district of Optima. The building, indicated by the white arrow, has 18 workers. Collectively, they live in homes that are reached by the set of highlighted road segments on the map. Given the City Simulator model has a commute footprint for every commercial building in the city, it can effectively map the spread of infection from building to building each day.

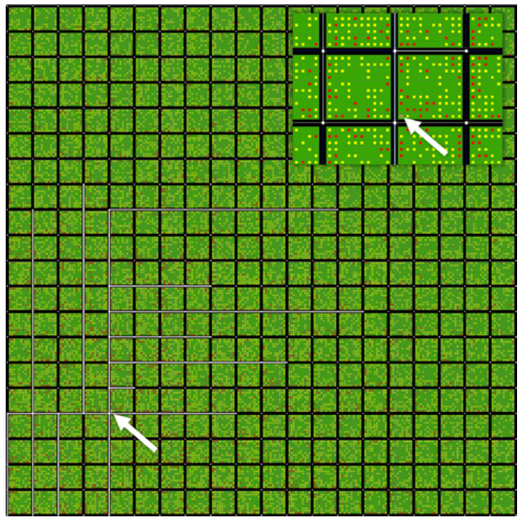

Figure 2: Each of the 3,125 commercial buildings in Optima has a commute footprint, which shows the road segments (white lines) used by workers in the building to get from home to work.

3.1 Measuring Vulnerability With the Base Run

To understand how vulnerable Optima is, a base run was first conducted where no mitigation actions were taken.

The contact model used was very simple. It only included commutes from home to work and back. At home, workers were assumed to make contact with their family members, one of whom may be a working spouse. At work, each worker was assumed to make contact with two sets of people in their building: close colleagues (up to six people they interact with regularly) and others within the building.

Other assumptions made included:

- The virus enters the community as a single infection case every 10 days. The person infected is selected at random from the pool of susceptible people. These are people that haven't had the virus yet at the time of infection.
- Infection lasts 14 days. This is from the time the person is infected until they recover and become immune. Note that no deaths were modeled in the initial model. All infected residents were assumed to recover.
- Each infected person is asymptomatic for five days. During this time, they continue to go to work and spread disease.
- 50% of people remain asymptomatic. This means they never stop going to work and continue spreading disease. The individuals are selected at random. The remaining 50% are assumed to stay at home or be admitted to the hospital.
- Probability of contact and transmission on any given day is:
  - Among family members: 25%.
  - Workers to close colleagues: 5%
  - Workers to others in building: 5% to 1%, depending on size of commercial building

Note that the assumptions made are intended to enable exploring the model performance. As such, the model was not calibrated exactly to the parameters of the current Coronavirus outbreak, particularly because those parameters are only starting to be known with accuracy as the epidemic plays out.

Further note that, in future runs, the commutes will be more realistically as "journeys," where avatars make stops, contact infected surfaces - fomites – and carry the disease with them. The model will also include contacts with surfaces at the workplace and residence and be calibrated to reflect the length of time each surface type remains infectious.

3.2 Base Run Results

The base run results are shown in the video and chart below. After an initial period of about 8 days, the infection (blue line) explodes, jumping to more than 75,000 cases out of the 95,000 people in Optima. The video shows the spread across the city day by day. Each blue dot is a building that contains at least one infected person. The red line in the chart shows the number of "sick" people as the infection plays out. These are people who have passed the initial five-day asymptomatic period and are now assumed to be staying at home or admitted to the hospital and are not causing further infection. The peak of the infection is reached on January 20 and then the infections cases drop quickly as the infected recover and immunity builds among the community.

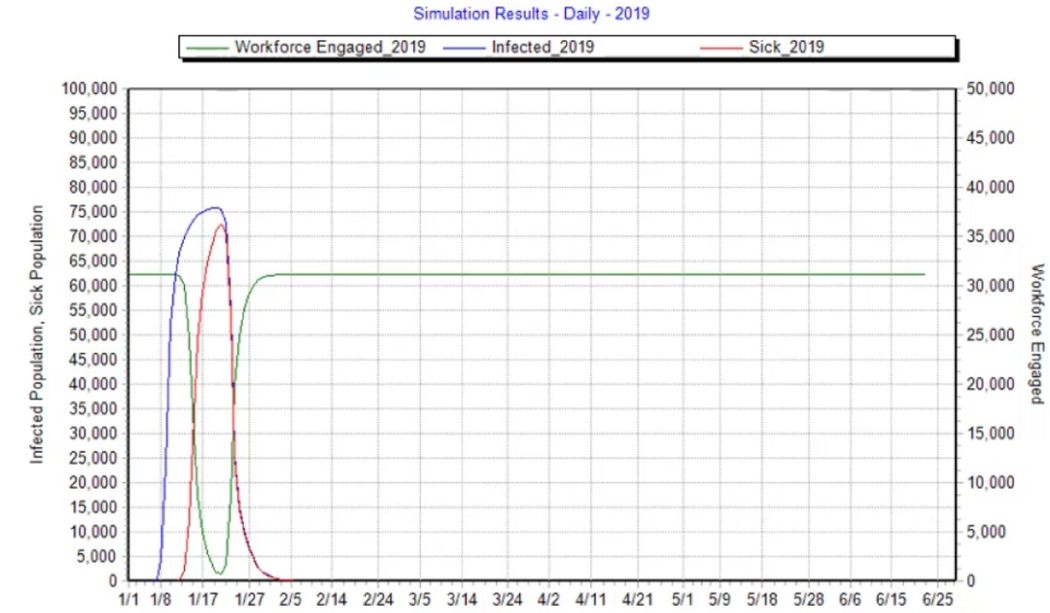

Figure 3: The base run shows a large peak in infected cases (blue line) impacting 75,000 of the 95,000 people in the city. Those immobilized by the infection (red line) remain asymptomatic for the first five days and then are confined to their homes and hospitals. The engaged workforce (green line) drops to nearly zero as almost all of the city's workers are impacted by infection.

The green line in the Figure 3 shows the engaged workforce, which starts out at 31,129 (see right axis) and drops to nearly zero as the infection impacts nearly the entire workforce, an enormous economic impact.

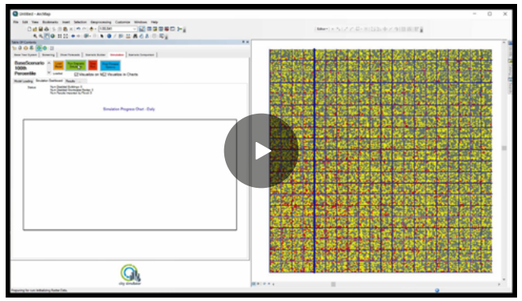

Video 1: Base-run

4. Using Social Distancing to Mitigate the Impacts of the Epidemic

Using City Simulator's scenario-based framework, a social distancing measures was added to evaluate the degree to which Optima's vulnerability could be reduced. Social distancing is the practice of separating yourself physically from others. Generally, a minimum distance guideline is provided to the public. For the current Coronavirus pandemic, it is often 6 ft (1.82 m). The experimental set up is described in Figure 4.

The impacts of social distancing are assumed to be:

- Probability of contact and transmission on any given day is:
  - Among family members: Would drop from 25% to 1%
  - Workers to close colleagues: Would drop from 5% to 0.5%
  - Workers to others in building: Would drop from a maximum of 5% to a maximum of 0.5%

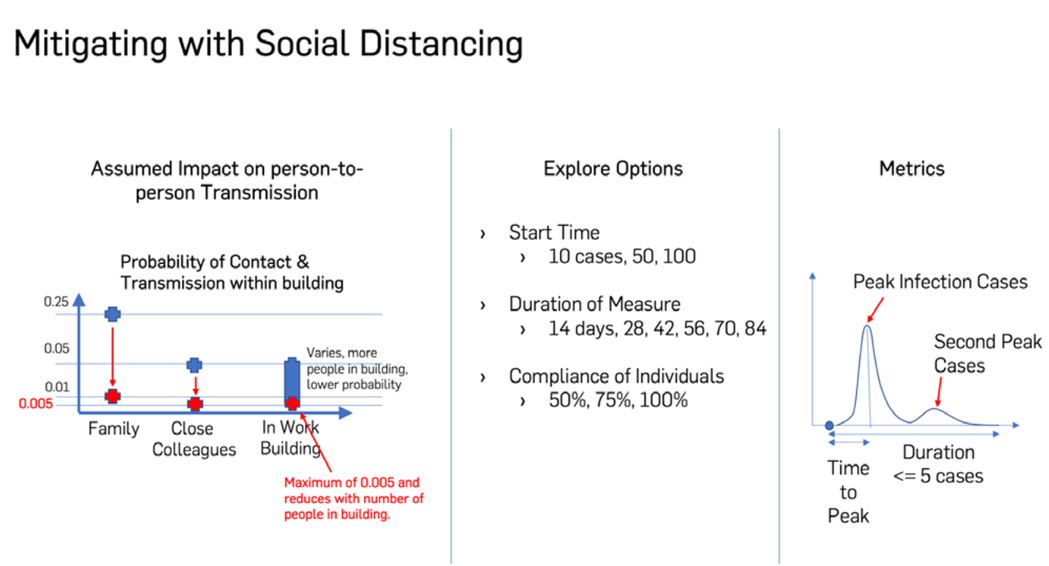

Figure 4: Experiment set up for social distancing

It should be noted the distance required for social distancing to achieve this level of reduction in infection probability is not specified within the experiment. It is assumed that this distance can be achieved in all interactions between agents. The specific distance would ideally be found through physical experiments.

The experiment explored three parameters:

- Start Time: The number of cases detected that triggers the social distancing measure. The values used were 10, 50, and 100 cases.
- Duration of Measure: The length of time in days that the measure would be in place. Values used were 14, 28, 42, 56, 70, and 84 days.
- Compliance of Individuals: The percentage of individuals that complied with the directive and kept their distance. Values used were 50%, 75%, and 100%.

Finally, the following key metrics were used:

- Peak Infection Cases – the maximum number of cases detected on a given day
- Time to Peak – the number of days since the first detected case and the day with peak cases
- Second Peak Cases – the maximum number of cases detected after the initial peak occurs.
- Duration of Epidemic – the number of days until the number infected drops to one.

Each variation of the three parameters was tested, creating 3 start times x 6 durations x 3 compliance levels, or 54 runs.

4.1 Impact of Social Distancing

Figure 5 compares the base run to a run that starts at 10 cases, has a 14-day social distancing duration, and includes 50% compliance. This was defined as the "minimum measure," as it had the lowest values of the three parameters. The measure is effective to some degree, with peak cases dropping from about 75,000 to about 63,000. About 10,000 of the engaged workforce remain working. Finally, and ominously, a second peak starts to form. This is due to the single "drip" of new infections every 10 days. The peak drops off rapidly due to the herd immunity that has been established in the first peak, but the trade-off of the lower initial peak to additional outbreaks in the future is clear.

4.2 Can Social Distancing Be Used to Allow Workers to Continue Working?

To explore the degree to which the peak can be reduced, all 54 runs were conducted and summarized in Figure 6. The chart shows the range of peak cases across the varying combinations of start triggers, duration, and compliance

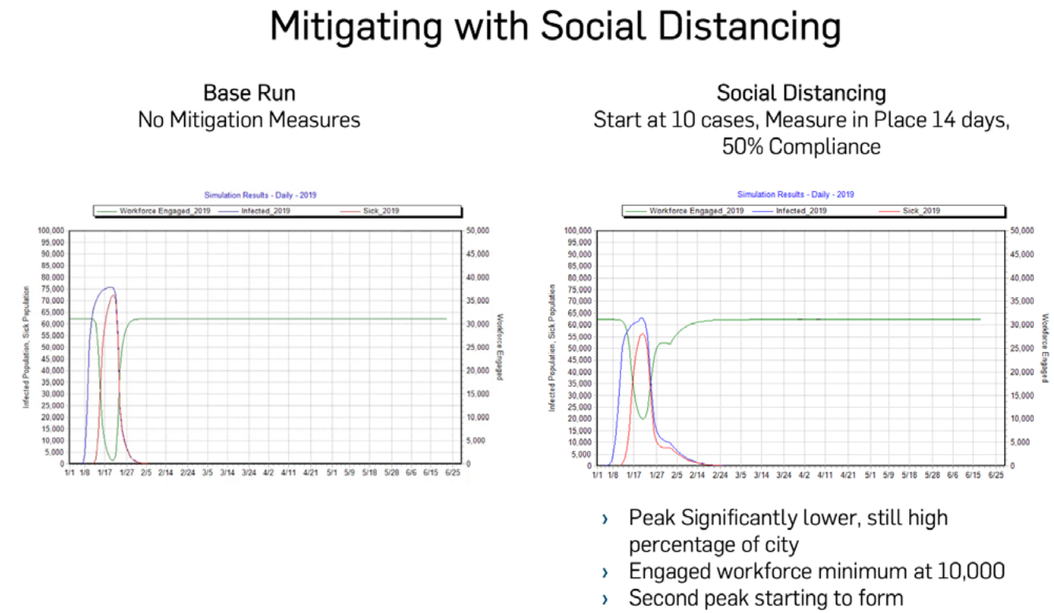

Figure 5: Minimum social distancing, where the public is 50% compliant and the social distancing is only in place for 14 days, results in a drop in peak cases from 75,000 to 63,000

levels. The top of the bar in each case represents the peak found using the 50% compliance level, whereas the bottom of the bar represents the peak found using the 100% compliance level. The 75% compliance level is indicated by the X in each bar.

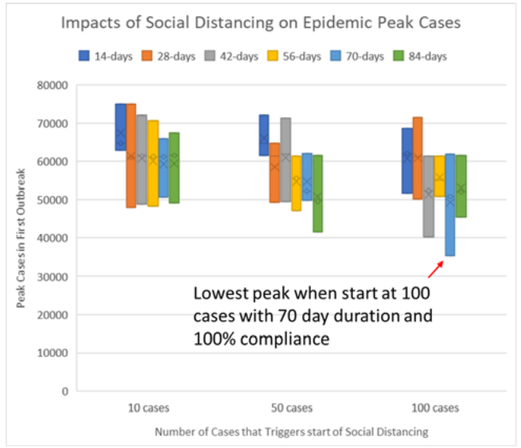

Figure 6: The highest peak infection metric ranges from around 75,000 cases to 35,000 cases depending on when the social distancing starts, how long it is enforced, and how compliant the population is. The height of the bars indicates the range of effectiveness that compliance has, with the upper edge of the bar representing the peak cases when 50% of the public are compliant and the lower edge for when 100% are compliant.

The chart shows clearly that:

- The minimum peak occurs when social distancing started at 100 cases with a 70-day duration and 100% compliance.
- In general, peak infections drop with duration of the measure; the longer the better.
- Somewhat non-intuitively, peak infections drop more if you start social distancing later, after a small population of infections have been established. This is due to allowing some of the population to develop immunity.
- With 50% compliance, the 14- and 28-day measures starting at 10 infection cases are ineffective, resulting in peak infections that are similar to the base run.
- The lowest peak found across all runs is approximately 35,000 people, or about 36% of Optima's population.

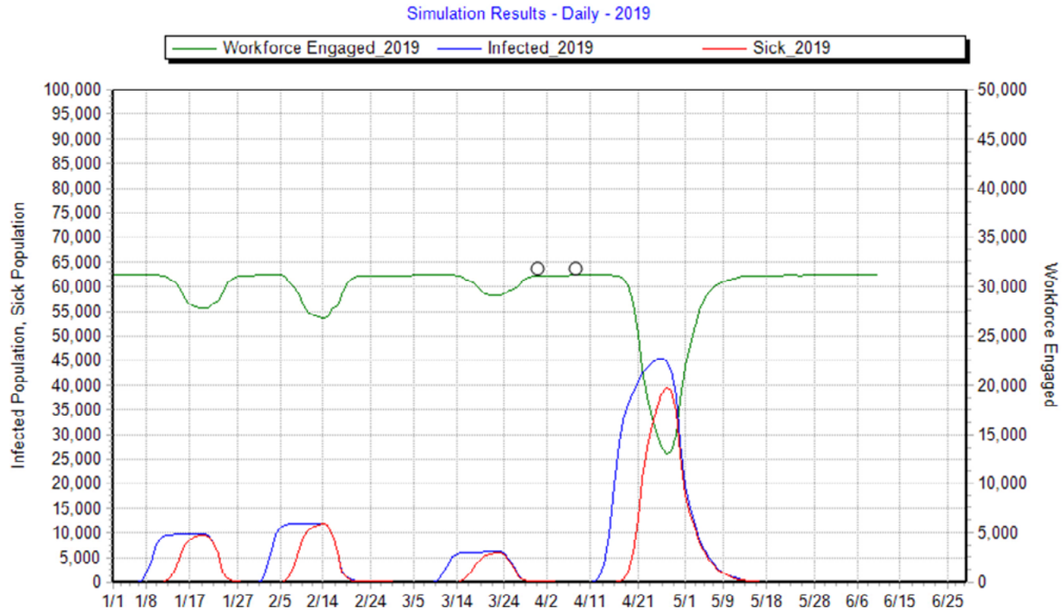

Figure 7: Social distancing for 84 days with 100% compliance gives the lowest initial peaks in cases. The high peak in the end results from stopping the social distancing at 84 days.

4.3 Social Distancing for the Long Run

Focusing on the best-case, Figure 7 shows how the infection plays out for the 70-day social distancing, 100% compliance run which starts at 100 cases. The chart clearly shows that peaks of 5-10,000 cases occur regularly but are stopped before they reach the large numbers shown in the base run. This is due to social distancing managing the spread. The engaged workforce experiences equivalent drops of 2-5,000 as these managed outbreaks occur.

The chart above shows that a large peak occurs in April. This is due to social distancing being lifted after 84 days and contact and transmission probabilities returning to normal. The next question explored concerned extended social distancing until a vaccine is found. The result is shown in Figure 8. The chart shows that indeed the peaks of infection can be managed to reduce infections to a much smaller percentage of Optima's population than the base run (from 75,000 to 13,000 cases), and a comparable drop in disruption to the engaged workforce is achievable. Most favorably, as time progresses, the peaks begin to drop more and more, reflecting the steady increase in immunity across the community over time.

The video below shows the evolution of the infection under this long-term social distancing approach. Note that, compared to the base run video, the infection is managed and appears and disappears quickly as each successive peak occurs.

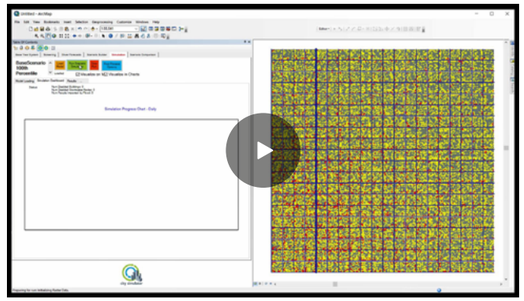

Video 2: Social distancing run

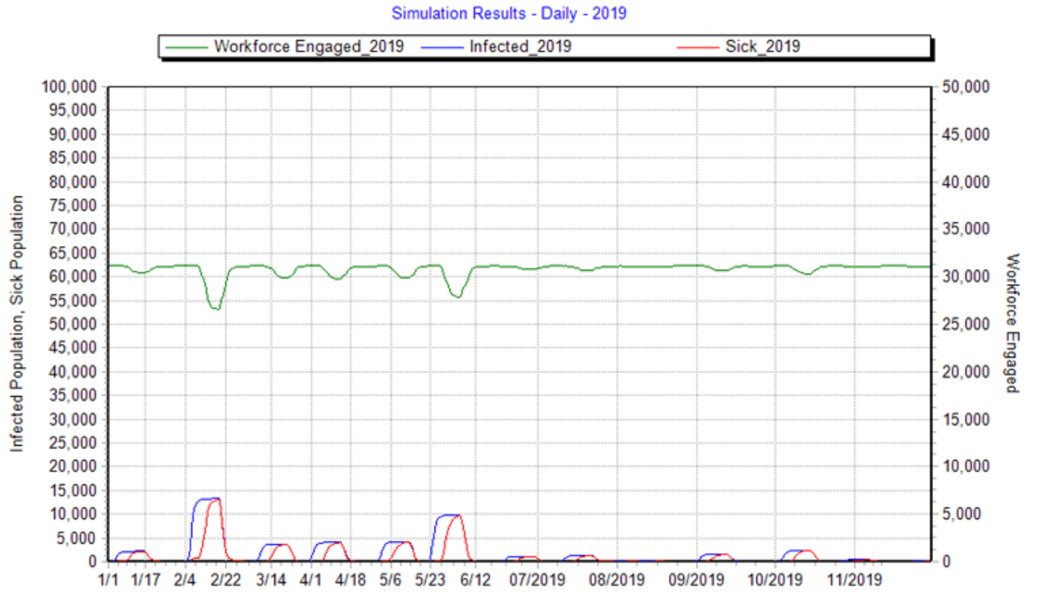

Figure 8: Extending social distancing to 365 days and assuming 100% compliance results in a more manageable series of outbreaks, which diminish in number of cases over time as the population builds immunity.

5. Caveats and Places to Enhance the Model

While the result for social distancing is encouraging, it would require significant, and even impossible, levels of control (100% compliance) to execute. Further, it is important to take results like those laid out above with a grain of salt. The model applied is quite simple and does not capture non-work-related travel and stops residents make along the way. Nor does the model capture infection spread from surfaces. Finally, as the process being modeled is probabilistic in nature, the results are uncertain, and should be treated as estimates of the metrics involved, at best. Still, the dynamics of infection displayed in the results are expected, the results give a valuable picture of how measures like social distancing can empower communities to act.

As Atkins matures the model, it is addressing all of these items. For example, journey-type trips will be added, which include stops along the way to work and back. Further, a person-to-surface-to-person contact model is being added that will capture the impact of surfaces and their varying levels of infectiousness over time.

To tackle uncertainty, cloud-based parallel processing is being employed to do thousands of runs and use the resulting ensemble prediction to estimate error bars around each key metric, allowing identification of best- and worst-cases scenarios.

Finally, while social distancing could be a powerful tool, it certainly should not be the only one that communities should explore. To help, a toolbox of measures is being developed like stay-at-home directives, regular disinfection of gas pump handles, wearing protective masks, and many more. Using this toolbox, communities can replicate the measures they've implemented to date and add more to future weeks and months as a single scenario. The results will allow them to find the best management plan to navigate restarting their economies.

6. Further Information

Please visit the City Simulator web page at http://atkinsglobal.com/citysimulator or contact Stephen Bourne at stephen.bourne@atkinsglobal.com for more information on City Simulator Epidemic modeling and other City Simulator research and development underway.

References

UK Office for National Statistics (2020). GDP first quarterly estimate, UK: April to June 2020. https://www.ons.gov.uk/economy/grossdomesticproductgdp/bulletins/gdpfirstquarterlyestimateuk/apriltojune2020#:~:text=3.-,Headline%20GDP,previous%20quarter%20(Figure%201).&text=Compared%20with%20the%20same%20quarter,UK%20economy%20fell%20by%2021.7%25.

US Bureau of Economic Analysis (2020). Gross Domestic Product, 2nd Quarter 2020 (Advance Estimate) and Annual Update. https://www.bea.gov/news/2020/gross-domestic-product-2nd-quarter-2020-advance-estimate-and-annual-update

Weisstein, Eric W. “SIR Model.” 2020. From MathWorld--A Wolfram Web Resource. https://mathworld.wolfram.com/SIRModel.html

A Hybrid Force/Displacement Seismic Design Method for Planar and Space Steel Building Frames

Angelos S.Tzimas

PhD
Civil/Structural Engineer
Engineering, Design and Project Management
Epsom, UK

Dimitri E. Beskos

Emeritus Prof., Department of Civil Engineering
University of Patras
Patras, Greece

Abstract

A main aspect to consider in seismic design of building structures according to EC8 is the selection of the behaviour factor, *q*, which is directly related to the energy dissipation capacity of the structure. The prescribed values of *q* (1) are referred only to one limit state; (2) depend on the structural system and on the ductility class; (3) are constant; and (4) are not directly related to structural and non-structural demands. This paper proposes a preliminary performance-based seismic design method for planar and space steel building frames within the framework of EC8. The proposed hybrid force/displacement (HFD) method incorporates deformation-controlled *q* factors to better control the structural and non-structural damage, expressed in terms of drift and ductility demands. The main advantages of the HFD method over the EC8 method is that it achieves target performance for more than one seismic event, controls deformation and therefore damage, and requires fewer design iterations. A realistic design example serves to demonstrate the advantages of the proposed method over the seismic design procedure of EC8.

Keywords

Steel frames; Seismic Design; Behaviour Factor

1. Introduction

Current seismic design codes for building structures, such as EC8 (2004), use the force-based design (FBD) method, which employs the seismic force as the basic design parameter. EC8 (2004) adopts two limit states, the ultimate limit state (ULS) and the damage limit state (DLS). The design of the structure is first performed with respect to the ULS by using the design seismic action (475 years return period). At the ULS, the main intent of EC8 (2004) is to ensure the development of a ductile plastic mechanism in case of a major seismic event with the aim being the protection of human life. This is achieved through the application of capacity design principles. According to such an approach, strategic dissipative regions are defined to undergo inelastic behaviour during the occurrence of a seismic event. The design seismic action is represented by the inelastic design spectrum, which is derived from the corresponding elastic one by dividing its ordinates with the behaviour factor q. EC8 (2004) gives constant values of q for different structural systems. Use of the inelastic spectrum in conjunction with a response spectrum analysis leads to the lateral design forces and member dimensioning in a trial and error fashion. The shape of the inelastic design spectrum for a specific value of q is illustrated in Figure 1. It should be noted that the adoption of high values of q factor can result in stiffer and heavier structures, in the case of moment resisting frames (MRF). This is due to the need to comply with the limits specified in EC8 (2004) for the inter-storey drift sensitivity coefficient θ, which is used to control the level of second-order (P-Δ) effects in the structure. Thus, a more rational selection of the q factor can lead to substantial material savings without compromising safety. After the ULS strength-based design, one checks the adequacy of the structural stiffness to limit the deformation under specific target values that satisfy serviceability requirements for the frequent earthquake (95 years return period). If this is not the case, the structure is re-designed for increased stiffness.

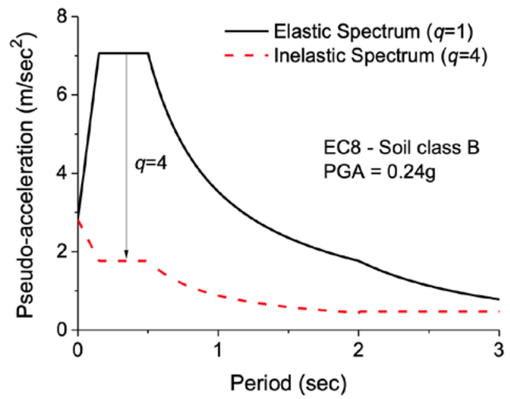

Figure 1: Type 1 elastic and inelastic design spectrum of EC8 (2004).

With a view to better control the seismic damage in a structure, displacement-based design (DBD) methods have also been developed (Priestley et al., 2007). Out of the various DBD methods, the direct displacement-based design (DDBD) method (Priestley et al., 2007) is the most widely used. The DDBD method is based on the equivalent linearization approach, in which the inelastic behaviour of a structural system is accounted for by considering the response of an equivalent linear system with lower equivalent stiffness and higher viscous damping (Priestley et al., 2007). In this way, the multi degree of freedom (MDOF) structure is substituted by an equivalent single degree of freedom (SDOF) structure. The method starts with the target inter-storey drift ratio (IDR) and in conjunction with a displacement design spectrum and the substitute SDOF structure, determines the seismic base shear force required for the structure to experience the desired deformation. The method controls both structural and non-structural damage by imposing limits only on IDR.

The purpose of this paper is to present the hybrid force/displacement (HFD) design method for planar and space regular and irregular steel building frames, which has been recently proposed by the present authors and co-workers (Tzimas, et al., 2013, 2017, 2020). The HFD method combines the advantages of both the FBD and DDBD in a hybrid force/displacement design scheme. The method has been evolved from previous works of the authors and co-workers on planar and spaced steel frames with different mechanical and geometrical characteristics, taking into consideration plan and elevation irregularities. A comparison of the FBD, DDBD, and HFD methods for planar steel MRF carried out by Bazeos (2009) yielded favourable results for the HFD. The HFD method has been studied in association with far-fault ordinary ground motions. The main advantage of the HFD seismic design method over the FBD and DDBD methods is the ability to directly control both structural and non-structural damage at various levels of seismic intensity with fewer design iterations without the use of a substitute SDOF structure (Tzimas, et al., 2013). The HFD starts by using both IDR and local ductility target values and transforms them to a target roof displacement in order to obtain a behaviour factor q. HFD then determines seismic design forces by utilizing an acceleration design spectrum along with response spectrum analysis; similarly to the FBD method. Therefore, the engineer works with familiar concepts and tools, uses a deformation-controlled q factor (and not a constant value of q adopted by EC8 (2004)), and avoids the employment of a highly damped displacement design spectrum, which is used by the DDBD.

2. Steps of the Proposed Design Procedure

The proposed hybrid force/displacement (HFD) seismic design procedure can be summarized in the following steps:

(1) *Definition of the basic building attributes*

With reference to the types of frames depicted in Figure 2, definition of the number of stories, n_s, number of bays, n_b, bay widths and storey heights, presence of setbacks (geometrical irregularity), accidental eccentricity, and use of a specific floor differing to the adjacent ones (mass irregularity).

(2) *Definition of the performance level*

Every pair of seismic action and damage level constitutes a performance level, while the whole set of performance levels comprise the performance objective or design goal. For example, immediate occupancy (IO) under the frequently occurring earthquake (FOE), life safety (LS) under the design basis earthquake (DBE) or collapse prevention (CP) under the maximum considered earthquake (MCE). The earthquake intensity level is represented by the appropriate elastic acceleration response spectrum, as shown in Figure 3.

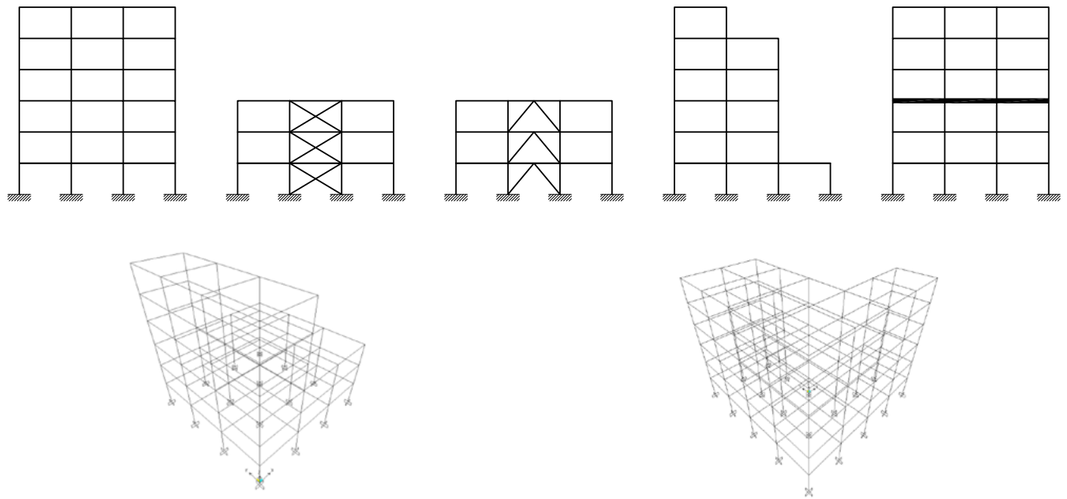

Figure 2: Types of steel building frames considered in the HFD seismic design method

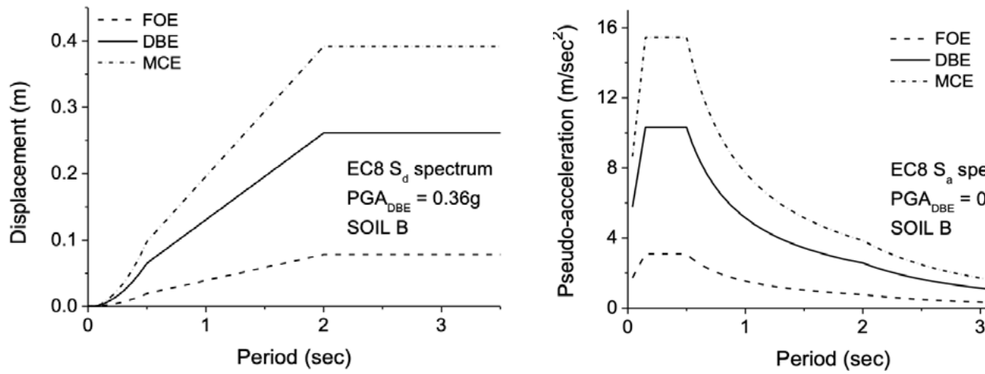

Figure 3: *Design spectra of EC8 (2004) for soil class B and PGA_{DBE} = 0.36g: (a) displacement design spectra; (b) pseudo-acceleration design spectra*

(3) *Definition of input parameters (performance and irregularity metrics)*

Definition of limit values for the maximum inter-storey drift ratio (IDR_{max}) and maximum local ductility (rotation ductility, μ_θ, for beams/columns and cyclic elongation ductility, μ_{cb}, for braces (Tzimas, et al., 2013)) along the height of the frame. The μ_θ is defined as $1+\theta p/\theta y$, where θy and θp are the yield chord rotation and the plastic rotation of the member's ends, respectively. These limit values are selected based on the performance level defined in Step (2) and can be obtained, e.g., from Table 1 taken from ASCE 41-13 (2014).

Table 1: Target Values of Performance Metrics for MRF in Accordance With ASCE 41-13 (2014)

Immediate Occupancy		Life Safety		Collapse Prevention	
Inter-storey Drift	Local Ductility	Inter-storey Drift	Local Ductility	Inter-storey Drift	Local Ductility
0.7% transient; negligible permanent	1.00[a]	2.5% transient; 1.0% permanent	9.00[a]	5% transient; or permanent	11.00[a]
[a] Limit on flange and web slenderness and limit on axial force of columns.					

Description of irregularity metrics of MRF with setbacks, accidental eccentricities and location of mass irregularities can be found in Tzimas et al. (2013, 2017, 2020).

(4) *Estimation of the input variables (yield roof displacement and mechanical characteristics)*

Yield roof displacement, u_{ry}. This displacement corresponds to the formation of the first plastic hinge (for MRF) or to the initiation of buckling (for braced frames). An initial estimation of the yield roof displacement may be obtained by designing the frame only for strength requirements under the FOE by assuming elastic behaviour, i.e., with q=1.

Mechanical characteristics. The definition and estimation of mechanical characteristics of MRF and braced frames, such as the fundamental period T of the structure, column-to-beam strength ratio, a, beam-to-column stiffness ratio, ρ and brace slenderness, λ, can be found in Tzimas, et al. (2013). Initial estimates of these input variables may be obtained by designing the frame only for strength requirements under the FOE by assuming elastic behaviour, i.e., with q=1. The capacity design rules and the gravity load combination should be also considered in order to improve the initial estimation of the input variables of the proposed method.

(5) *Transformation of performance metrics to the target roof displacement*

Transformation of the IDR_{max} to target maximum roof displacement, $u_{r,max}$, using the relation

$$u_{r,max(IDR)} = b_1 \cdot H \cdot IDR^{b_2} \quad (1)$$

where H is the total height of the frame (in m) and b_1 and b_2 coefficients given by Table 2 in terms of the number of stories, ns, and the level of IDR_{max}. It should be noted that the empirical formulae of HFD method has been developed by using the nonlinear dynamic analyses results of several types of steel building frames. More information on the created databank can be found in Tzimas, et al. (2013, 2017, 2020). Due to space limitations, design equations are provided only for regular space MRF (Tzimas, et al. 2017).

Transformation of local ductility, μ_θ, to target roof displacement, $u_{r,max(\mu)}$, by employing the relation

$$u_{r,max(\mu)} = \mu_{r,\theta} \cdot u_{ry} \quad (2)$$

where the roof displacement ductility, $\mu_{r,\theta}$, is defined as the ratio of the maximum roof displacement corresponding to a specific performance level (see Step 2) over the maximum roof displacement at the appearance of the first plastic hinge, and is associated with local ductility through

$$\mu_{r,\theta} = 1 + 0.81 \cdot (\mu_\theta - 1) \quad \text{for } \mu_\theta \le 4.68$$

$$\mu_{r,\theta} = 2.58 + 0.38 \cdot (\mu_\theta - 1) \quad \text{for } \mu_\theta > 4.68 \quad (3)$$

Thus, the maximum design roof displacement $u_{r,max(d)}$ is obtained as

$$u_{r,max(d)} = \min\left(u_{r,max(IDR)},\ u_{r,max(\mu)}\right) \quad (4)$$

Table 2: Indices of Eq. (1) Taken From Tzimas, et al. (2017)

Number of stories	$IDR_y - IDR_{1.8\%}$		$IDR_{1.8\%} - IDR_{3.2\%}$		$IDR > IDR_{3.2\%}$	
	b_1	b_2	b_1	b_2	b_1	b_2
3	0.84	1.01	1.03	1.06	0.99	1.05
6	0.37	0.88	0.93	1.11	1.51	1.25
9	0.29	0.88	2.07	1.37	2.38	1.41
12	0.28	0.91	1.46	1.32	5.58	1.71
15	0.22	0.89	5.04	1.67	6.88	1.76

(6) *Calculation of the behaviour (or strength reduction) factor*

Calculation of the design value of the roof displacement ductility, $\mu_{r,d}$, as

$$\mu_{r,d} = \frac{u_{r,max(d)}}{u_{r,y}} \quad (5)$$

and then computation of the behavior factor, q, from the relation

q=1+1.35·($\mu_{r,d}$ – 1) for e≠0

q=1+1.30·($\mu_{r,d}$ – 1) for e=0 (6)

where e is the accidental eccentricity (up to 10% (Tzimas et al., 2017)).

(7) *Design of the structure*

Divide the ordinates of the elastic design spectrum by the q factor and design the frame on the basis of an elastic response spectrum analysis in conjunction with the capacity and ductile design rules of seismic codes (EC8 (2004)). Use of the behavior factor q makes this design a strength-based one. Stiffness requirements are automatically satisfied through the dependence of q on deformation (step (6)).

(8) *Iterative design procedure*

Iteration with respect to the input variable u_{ry}. The required number of iterations for convergence depends on the initial estimate of the input variable u_{ry} (see step 4 of the method). A good initial estimate of u_{ry} can be easily obtained by designing the frame only for strength under the FOE by assuming elastic behavior, i.e., q=1.

As noticed in Tzimas, et al. (2013), the iterative seismic design of a structure by using response spectrum analysis in conjunction with target damage levels, as is the case here, may not be feasible. Target damage levels are the target values of IDR_{max} and μ_θ, or equivalently the target maximum design roof displacement, $u_{r,max(d)}$. The reason for this lack of convergence is that every design spectrum has a maximum response demand, which may lead to a lower $u_{r,max}$ value than the desirable one. In such a case, one has to modify the target response value of $u_{r,max(d)}$ in order to achieve convergence of the iterative design procedure.

This modification can be accomplished with the aid of the corresponding single degree of freedom (SDOF) system to the multi degree of freedom (MDOF) system under design. This SDOF system is defined to have as its period the fundamental period of the MDOF and as its damping the damping ratio of the MDOF. For this SDOF system, its maximum displacement is calculated with the aid of the displacement design spectrum obtained from the corresponding acceleration spectrum of EC8 (2004). This maximum displacement is then compared against the desirable maximum roof displacement $u_{r,max(d)}$ of the MDOF. If the displacement of the SDOF system is smaller than the $u_{r,max(d)}$, as shown in Figure 4, one has to assume $u_{r,max(d)}$ equal to that of the SDOF and from the design equations of the HFD method determine the new IDR_{max} and μ_θ.

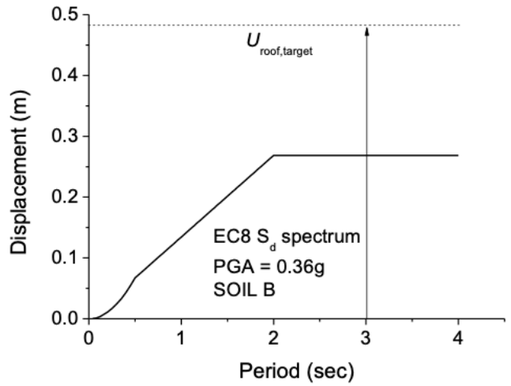

Figure 4: Displacement design spectrum of EC8 (2004) for PGA = 0.36 g and soil class B

A modification factor to relate the spectral displacement of an equivalent SDOF system to the roof displacement of the building MDOF system is required. ASCE 41-13 (2014) on the basis of the coefficient method for calculating the target displacement of a building, proposes an appropriate value of this factor equal to 1.0, 1.2, 1.3, 1.4, and 1.5 for buildings with 1, 2, 3, 5, and ≥10 number of floors, respectively, with which to multiply the resulting spectral displacement. Thus, one can use these multiplier factors to estimate more realistically the response demand of an MDOF system by using an equivalent SDOF system.

3. Application Example and Comparison of the HFD and FBD Methods

3.1. Description of the Building and Design Calculations

The proposed HFD method is applied to the seismic design of a space MRF with nine stories of height 3.0 m each and a rectangular plan view with four bays of 6.0 m and 8.0 m in each direction, respectively (see Figure 5). It is assumed that this space frame has an accidental eccentricity of 5%.

The space frame was designed with the aid of the commercial computer program SAP 2000 and use of the EC8 (2004) and EC3 (2005) provisions. The grade of steel was assumed S235 and S355 for beams and columns, respectively. The column sections were square hollow ones (SHS), while those of beams IPE. The dead and live design loads were assumed to be G=6.5 kN/m^2 and Q=2 kN/m^2, respectively. The G + 0.3Q load combination results in 7.1 kN/m^2. It is assumed here that IO under the FOE, LS under the DBE and CP under the MCE are the appropriate performance levels for seismic design. The FOE, DBE, and MCE are expressed through the Type 1 elastic design spectra of EC8 (2004) (similar to Figure 3) for soil class B by assuming seismic zones which have peak ground acceleration under DBE (PGA_{DBE}) equal to 0.40 g. The peak ground accelerations under the FOE and the MCE are equal to 0.3 x PGA_{DBE} and 1.5 x PGA_{DBE}, respectively. Table 1 provides limit values for performance metrics according to ASCE 41-13 (2014), which were used to determine the q factor of the HFD method at the various performance levels.

The design process of the nine-storey MRF in accordance with the HFD method can be summarised as: 1) FOE analysis and design with estimates of the LS and CP performance levels under the DBE and MCE, respectively; 2) DBE analysis and design with estimates of the IO and CP performance levels under the FOE and MCE, respectively; 3) MCE analysis and design with estimates of the IO and LS performance levels under the FOE and DBE, respectively; and 4) selection of the lighter designed structure which complies with the limit values of all performance levels.

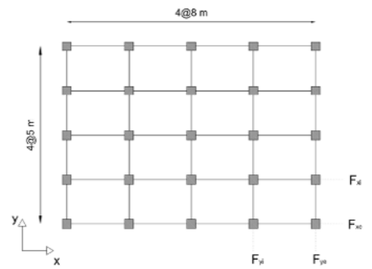

Figure 5: Plan view of the nine storey MRF

An initial elastic design for the FOE yields the dimensions of Table 3. Table 3 also provides the first three natural periods of the designed MRF, with the fundamental period to be translational and equal to 1.65 sec. The roof displacement under the FOE is $u_{r,y}$ = 0.130 m, while IDR_y = 0.69%, which fulfils the IO demands of Table 1. The above values serve as initial estimates for the input variables of the HFD. In addition, an assessment of the designed structure for the LS and the CP performance levels is made. The q factor of the space MRF under the DBE is easily obtained as (PGA_{DBE}/PGA_{FOE}) = 3.33. This value is used in order to estimate the response of the space MRF under the DBE, i.e., by employing Eq. (6) $\mu_{r,d}$ = 1+(3.33-1)/1.35 = 2.73, by employing Eq. (5) $u_{r,max}$ = 2.73×0.130 = 0.355 m, by employing Eq. (3) μ_θ = 1+(2.73-1)/0.81 = 3.14 and by employing Eq. (1) IDR_{max} = (0.355/(2.07×3*9))1/1.37 = 2.49%. The q factor of the space MRF under the MCE is easily obtained as (PGA_{MCE}/PGA_{DBE})×q_{DBE} = 5. This value is used in order to estimate the response of the space MRF under the MCE, i.e., by employing Eq. (6) $\mu_{r,d}$ = 1+(5-1)/1.35 = 3.96, by employing Eq. (5) $u_{r,max}$ = 3.96×0.130 = 0.515 m, by employing Eq. (3) μ_θ = 1+(3.96-1)/0.81 = 4.65 and by employing Eq. (1) IDR_{max} = (0.515/(2.38×3*9))1/1.41 = 3.26%. According to the above results, using the limit values of Table 1, the space MRF which satisfies the IO performance level satisfies also the LS and CP performance levels.

The target values of the IDR_{max} and μ_θ for the LS performance level are equal to 2.5% and 9, respectively (Table 1). By employing Eq. (1), the target roof displacement $u_{r,max(IDR)}$ = 9×3×2.07×0.0251.37 = 0.356 m and therefore, the target roof displacement ductility $\mu_{r,IDR}$ becomes equal to 0.356/0.130 = 2.74. Employing Eq. (3), the target roof rotational ductility $\mu_{r,\theta}$ is calculated as 2.58+0.38×(9-1) = 5.62 m. Thus, the design roof ductility $\mu_{r,d}$ is equal to the min ($\mu_{r,IDR}$, $\mu_{r,\theta}$) = min (2.74, 5.62) = 2.74 m and therefore, drift controls the LS performance level design. According to EC8 (2004) displacement design spectrum, for an SDOF system which has the same period as the space MRF, the maximum displacement would be equal to 0.246×1.48 = 0.364 m for the case of the DBE, where the above multiplier 1.48 is proposed by ASCE 41-13 (2014) for nine storey buildings. This means that there is no need to revise the target values of the IDR_{max} and μ_θ, because the demand displacement of 0.364 m as obtained by the displacement design spectrum is higher than the $u_{r,max(IDR)}$ = 0.356 m. The required behaviour factor q is calculated equal to 3.35 m based on Eq. (6). By using this factor, the DBE design spectrum is reduced and the space frame under the DBE is designed with spectrum analysis. This q factor does not change the sections of the designed space MRF for the IO (Table 3). This design fulfils the demands of Table 1. Therefore, both the IO and the LS performance levels leads to the same design.

The target values of the IDR_{max} and μ_θ for the CP performance level are equal to 5% and 11%, respectively (Table 1). By employing Eq. (1), the target roof displacement $u_{r,max(IDR)} = 9\times3\times2.38\times0.051.41 = 0.941$ m and therefore, the target roof displacement ductility $\mu_{r,IDR}$ becomes equal to 0.941/0.130 = 7.24 m. Employing Eq. (3), the target roof rotational ductility $\mu_{r,\theta}$ is calculated as 2.58+0.38×(11-1) = 6.38 m. Thus, the design roof ductility $\mu_{r,d}$ is equal to the min ($\mu_{r,IDR}$, $\mu_{r,\theta}$) = min (7.24, 6.38) = 6.38 m and therefore, local ductility controls the CP performance level design and $u_{r,max(d)} = 6.38\times0.130 = 0.829$ m. According to EC8 (2004) displacement design, for an SDOF system which has the same period as the space MRF, the maximum displacement would be equal to 0.369×1.48 = 0.546 m for the case of the MCE, where the above multiplier 1.48 is proposed by ASCE 41-13 (2014) for nine storey buildings. This means that there is a need to revise the target values of the IDR_{max} and μ_θ, because the demand displacement of 0.546 m as obtained by the displacement design spectrum is smaller than the $u_{r,max(d)} = 0.829$ m. By employing Eqs. (5, 3, and 1) and by adopting as target displacement the 0.546 m, the demand values of IDR_{max} and μ_θ of this structure cannot be much higher than 3.40% and 5.26%, respectively. These values fulfil the demands of Table 1. In addition, the response spectrum analysis/design under the FOE spectrum fulfils the demand of Table 1. The use of $IDR_{max} = 3.40\%$ as design input will lead to more flexible structure compared to the designed structure under the FOE spectrum (estimated $IDR_{max} = 3.26\%$ under the MCE), thus the demands of Table 4 for the IO will be violated. Therefore, the IO performance level controls the design of the space MRF and there is no need for a new design in the case of MCE.

Using SAP 2000 in conjunction with EC8 (2004) and EC3 (2005) the space MRF of this example was also designed by the FBD method. The behavior factor $q = 6.5$ was chosen in accordance with EC8 (2004), which represents steel MRF with high ductility demands. Table 3 provides the dimensions of the space frame and its three first natural periods. According to FBD, the LS performance level controls the design. The space frame remains elastic under the IO earthquake and experiences $u_{r,y} = 0.120$ m, $IDR_{max} = 0.69\%$ and $\mu_\theta = 1$. Under the DBE, the space frame will experience $u_{r,max} = 0.120\times PGA_{DBE}/PGA_{FOE} = 0.120/0.3 = 0.400$ m and $IDR_{max} = 0.69\%\times PGA_{DBE}/PGA_{FOE} = 0.69\%/0.3 = 2.30\%$. Under the MCE, the space frame will experience $u_{r,max} = 0.400\times PGA_{MCE}/PGA_{DBE} = 0.400\times1.5 = 0.600$ m and $IDR_{max} = 2.30\%\times PGA_{MCE}/PGA_{DBE} = 2.30\%\times1.5 = 3.45\%$.

3.2. Comparison and Seismic Assessment Using Semi-Artificial Accelerograms

In order to conduct a more detailed comparison of the two design methods (HFD and FBD), the two designed structures by the above methods were seismically analysed through dynamic nonlinear analyses performed by the Ruaumoko program (2005). Table 4 shows comparisons of the two methods with the "exact" nonlinear dynamic analysis employed with the aid of 10 accelerograms compatible with the EC8 (2004) seismic spectra for the three performance levels considered here. The Ruaumoko (2005) computer program was used for this analysis. Furthermore, a comparison of the results of nonlinear time-history analyses of the designed frames according to HFD and FBD methods, with the limit values of Table 1 shows that both designed frames satisfy these limits. In addition, the HFD method in this worked example gives better estimates of inelastic deformation demands and led to a 10% lighter structure.

It should be noted that the inter-storey drift sensitivity coefficient θ of EC8 (2004) governs the design of the nine-storey building for the FBD method. Thus, the initial choice of the q factor plays a direct role in the design solution by FBD and lighter solutions can very likely be adopted if a lower q factor was adopted instead. HFD appears to be more rational in estimating a q factor which satisfies both the targeted performance levels and drift requirements without implying later any indirect revision.

Table 3: Sections for Columns, Beams and Vibration Periods of the Nine Storey Space Steel Frames Designed According to the HFD and FBD Methods (The Indices "i" and "E" Mean Internal and External Beam/Column Sections, Respectively)

Floor	Designed according to the HFD method			Designed according to the FBD method		
	IPE		SHS	IPE		SHS
	F_{xe} - F_{ye}	F_{xi} - F_{yi}	C_i - C_e	F_{xe} - F_{ye}	F_{xi} - F_{yi}	C_i - C_e
1	450-400	550-500	400x20	600-550	600-550	450x22
2	500-450	600-550	400x20	600-550	600-550	450x22
3	500-450	600-550	400x20	600-550	600-550	450x22
4	450-400	550-500	400x16	550-500	600-550	400x20
5	450-400	550-500	400x16	550-500	600-550	400x20
6	450-400	550-500	400x16	450-400	500-450	400x16
7	450-400	500-450	400x16	450-400	500-450	400x16
8	400-360	500-450	350x16	400-360	450-400	350x16
9	400-360	500-450	350x16	400-360	450-400	350x16
	Steel Weight = 3588 kN T1=1.65sec - T2=1.60sec - T3=1.54sec			Steel Weight = 3960 kN T1=1.45sec - T2=1.41sec - T3=1.27sec		

Table 4: Time History Analyses Results and Comparison With Design Estimations (TH: Time History Analysis; EST: Estimations of HFD; EC8: Estimations Using the Equal Displacement Rule)

Nine storey space MRF - $PGA_{DBE} = 0.40g$												
	HFD						FBD (EC8)					
Example	FOE		DBE		MCE		FOE		DBE		MCE	
	TH	EST	TH	EST	TH	EST	TH	EST	TH	EST	TH	EST
IDR (%)	0.70	0.69	2.11	2.49	3.37	3.26	0.69	0.69	2.19	2.30	3.10	3.45
$u_{r,max}$ (m)	0.133	0.130	0.335	0.355	0.535	0.515	0.121	0.120	0.332	0.400	0.455	0.600
μ_θ	1.11	1.00	4.05	3.14	7.61	4.65	1.38	1.00	4.34	-	5.73	-

4. Conclusions

On the basis of the previous developments as well as additional ones to be found elsewhere (Tzimas, et al., 2013, 2017, 2020), the following conclusions can be drawn:

1. The HFD method: (1) treats both drift and ductility demands as input variables for the initiation of the design process; (2) does not use a substitute SDOF system done by the DDBD; (3) makes use of the conventional elastic response spectrum analysis and design; and (4) can be applied to different type of frames taking into consideration their irregularity metrics and mechanical characteristics.

2. The adopted design criteria (drift and local member ductility) are associated with the IO, LS, and CP performance levels. The HFD method considers both strength and drift demands for all performance levels, while FBD considers strength-based design for the LS and drift-based design for the IO performance levels.

3. The advantages of the HFD method over the FBD method by comparing the inelastic deformation estimates of both methods with the results of the nonlinear dynamic analysis are better estimates of inelastic deformation demands and fulfillment of the limit deformation values in all the performance levels.

4. Based on the design examples presented in Tzimas, et al. (2013, 2017, 2020) and the design example of this work, the HFD method appears to offer significant design efficiencies for high rise buildings and similar designs for low rise buildings compared to the FBD method of EC8.

5. Empirical expressions of the HFD method derived for steel frames can be also used for assessment.

6. Limitations and modelling assumptions of the HFD method can be found in Tzimas, et al. (2013, 2017, 2020).

Acknowledgements

The authors acknowledge with thanks Mr. Dave Cotton (Technical Director of Atkins) for reviewing this paper.

References

1. ASCE/SEI Standard 41–13. Seismic evaluation of retrofit of existing buildings. American Society of Civil Engineers, Reston, Virginia, USA; 2014.

2. Bazeos N. Comparison of three seismic design methods for plane steel frames. Soil Dynamics and Earthquake Engineering 2009;29(3):553–62.

3. Carr AJ. Ruaumoko-3D - A Program for Inelastic Dynamic Analysis. Technical Report, Department of Civil Engineering, University of Canterbury, Christchurch, New Zealand; 2005.

4. Eurocode 8, EC8. Design of Structures for Earthquake Resistance, Part 1: General Rules, Seismic Actions and Rules for Buildings, European Standard EN 1998–1, Stage 51 Draft. European Committee for Standardization (CEN), Brussels; 2004.

5. Eurocode 3, EC3. Design of Steel Structures, Part 1. 1: General Rules for Buildings, European Prestandard ENV 1993-1-1. European Committee for Standardization (CEN), Brussels; 2005.

6. Priestley MJN, Calvi GM, Kowalsky MJ. Direct displacement-based design. Pavia, Italy: IUSS Press; 2007.

7. Tzimas AS, Karavasilis TL, Bazeos N, Beskos DE. A hybrid force/displacement seismic design method for steel building frames. Engineering Structures 2013; 56: 1452-1463.

8. Tzimas AS, Karavasilis TL, Bazeos N, Beskos DE. Extension of the hybrid force/displacement (HFD) seismic design method to 3D steel moment-resisting frame buildings. Engineering Structures 2017; 147; 486–504.

9. Tzimas AS, Skalomenos KA, Beskos DE. A hybrid seismic design method for steel irregular space moment resisting frames. Journal of Earthquake Engineering 2020; In Press.

Benefits of Contractor Prototyping: GFRC Cladding on Crossrail

Jim Abatti

Senior Architect
Infrastructure
London, UK

Jorrin ten Have

Architect & Associate
Principal
Grimshaw
London, UK

Abstract

Extensive prototyping was carried out during the design and delivery of the Elizabeth line for the line-wide architectural components. Previous papers have covered the process of client prototyping and its key benefits. This paper concentrates on the prototyping carried out by the contractors during the construction stage, with focus on the Glass Fibre Reinforced Concrete (GFRC) tunnel cladding. The three suppliers involved were interviewed to share their experiences. In the summary, some conclusions are made about the potential benefits of the prototyping approach for DfMA (Design for Manufacture and Assembly) in architectural design and construction.

Keywords

Prototyping; Contractor; Benefits; GRC Cladding; Crossrail

1. Introduction

Extensive prototyping of the line-wide architectural and engineering components was carried out during the design and delivery of the Elizabeth line in aid of the progressive development of technical requirements, assurance of safety and maintenance, stakeholder engagement and delivery of product value and quality. Previous papers (1) have covered the process of client prototyping and its key benefits. This paper concentrates on the prototyping carried out by the contractors during the construction stage, with focus on the Glass Fibre Reinforced Concrete (GFRC) (2) station tunnel cladding. As a methodology, the key decision makers in each contractor/supplier team were interviewed with the same questions for the purpose of eliciting the value and benefits of the prototyping approach for DfMA (Design for Manufacture and Assembly) (3) in architectural design and construction and for the delivery of outcomes required of large infrastructure projects.

They included David Shillito, director at Laing O'Rourke (LO'R); Patrick Weijers, project manager and currently managing director at Sorba; and; Franz Maidl, department head of CAD and research and development at Lindner.

This paper describes how the process used by the client company Crossrail supported the delivery of consistent outcomes at the new central London stations through the lens of one line-wide component type; the GFRC tunnel cladding. It describes the role of prototyping as a bridge between technical and design objectives on one hand, and contractor design, testing, manufacture and installation on the other. The process relates to the overall benefit and risk strategy for the principal project outcomes required: safety, reliability, usability, low-cost maintenance and passenger experience.

Benefits and risks were progressively integrated into contractors' work informed and benchmarked by highly resolved client requirements in the form of drawings, technical reports and performance specification, validated at design concept stage by trials, prototypes and testing. In this way, contractors were able to draw on an inventory of tools with confidence that they would work in use.

The process described also mitigated risk of construction stage changes, reduced errors and actively promoted collaboration between client, designer, stakeholders and multiple contractors with extended supply chains through shared client-side information that originated at pre-contract stage.

2. Crossrail Project for the Elizabeth Line

Crossrail Limited is the company delivering a new railway for London and the South East, running from Reading and Heathrow in the west, through 42km of new tunnels beneath London to Shenfield and Abbey Wood in the east. The project is being completed in phases and planned to open fully in 2022. The new railway, which will be known as the Elizabeth line, will carry an estimated 200 million passengers per year. Integrating new and existing infrastructure, the project includes the construction of 10 new stations as well as the upgrading of 30 existing stations.

Within central London there are eight new underground stations and two new above ground stations, linked by a common identity created using standardised components. This unified set of architectural components, products and assemblies form part of a line-wide design package for the public areas.

From 2009, a multi-disciplinary design team developed the line-wide design strategy, since forming a working partnership to integrate these essential components of the Elizabeth line. The team comprises engineers and package leaders from SNC-Lavalin's Atkins business, architects from Grimshaw, product designers and wayfinding experts from Maynard, and lighting designers from GIA Equation. The line-wide designs include a range of components such as tunnel cladding, platform-edge screens, furniture, lighting and signage.

Extensive assessment of the global marketplace identified which materials and components would meet Crossrail's project requirements and where customised designs were required. Many of these were then developed using a process of standardisation, prototyping and user testing to refine and enhance the design for manufacturing, installation and future maintenance. This approach is in line with DfMA, an industrial design concept that has gained more prominence recently in architecture with a view to maximise benefits from pre-fabrication.

2.1 GFRC Cladding and Client Prototype

In the five mined central London stations, the escalator barrels and public spaces at platform level are lined with curved Glass Fibre Reinforced Concrete (GFRC) panels. These provide a robust finish to cover the rough surface of the sprayed concrete tunnel engineering. The panels perform well with daily wear and tear as well as in bomb blast scenarios. Another function of the cladding is to distribute reflected light from luminaires and provide acoustic attenuation through perforated GFRC acoustic panels (See Figure 1).

Figure 1: Production of acoustic GFRC panels at the GRCUK factory
© GRCUK

As a cladding material, GFRC is relatively new to the London Underground (LU), so its use required extensive engagement to satisfy its performance in meeting fire safety and maintenance requirements over the project's baseline design life of 120 years. The sheer quantity required (more than 50,000 sq m) meant that a high level of standardisation was imperative to keep capital and lifecycle costs down, production and installation manageable, provide a consistent product performance.

In line with the principles of DfMA, the number of variations was kept as low as possible, both for individual panel

geometries and in the design of the junctions and interfaces. The quantity and value of GFRC and its associated performance requirements justified the case for full-scale prototypes of the tunnel junctions; one full scale client prototype was built during the design phase in a separate facility at Vinci Technology Centre UK in Leighton Buzzard. (4)

Conventionally, an architectural 'mock-up' is used as either an off-site visual benchmark or an installation for specific testing (for example, water tightness testing on external facades during the construction stage). The GFRC client prototype went beyond this in scope and purpose, addressing issues of manufacture, buildability, access and importantly, providing a feedback loop back into the design process that included the client and stakeholders. The prototype tested that concept stage requirements could be met and allowed the design team to progressively develop its technical performance. After the client prototyping at Leighton Buzzard was concluded, the requirement for the construction of a full size GFRC prototype was carried forward in the deliverables of the contractor.

3. Purpose of Contractor Prototype

The Contractor GFRC prototype, as required in the Station Works specification, served a purpose for both the client and the contractor. Each GFRC contractor had to build their own full-scale prototype, as an evolution of the client prototype, validating that their design and construction could meet all requirements. For the client, it was used to monitor visual appearance (i.e. the quality of production and alignment of installation), carry out access and maintenance trials, and limited performance testing (such as soft body impact tests and repair procedure tests). On occasions that the prototype did not perform to the required level in any aspect, amendments were made, and further trials carried out until the desired performance was met – thereby significantly de-risking the construction prior to full production. The second purpose of the prototype was for the Contractor to learn and optimise their systems and quality issues within their supply chains. It allowed the Contractor to coordinate and plan their supply chain in anticipation of full manufacture and installation.

Outside of the prototypes, further assurance was attained by the preceding sample regime that confirmed in progressive steps the general finish, light reflectance, anti-graffiti coating application, quality of panel perforations and edge geometry, and bomb-blast performance. (5) After the Contractor prototypes were completed and the appropriate technical approvals met, further benchmarks on site were used to judge installation quality.

In order to identify the key benefits and lessons to be learned from the Contractor prototyping, as mentioned above the three contractors who supplied GFRC for the tunnel cladding were interviewed. These were GRCUK (part of the Laing O'Rourke group), Sorba (who worked with Concrete Valley), and Lindner. Their experiences of the benefits of the prototyping process are grouped around the relationship to the Crossrail client, the design and construction phase, and the wider long-term benefit for the contractors.

4. Contractor Experience: Client

The GFRC cladding design was developed from concept design in 2009 to tender information by May 2011, with the design information progressively assured through a series of gate reviews. Although the GFRC cladding was designed to be implemented across five central London stations, Crossrail decided to procure the package as part of the individual Station ('Tier 1') contracts. This decision was partly based on procurement evidence in 2011 that there was no single company in the UK with enough capacity to supply all the stations within an acceptable risk profile.

To Laing O' Rourke (LO'R), who won the tender for two of the tunnelled stations (6), the GFRC presented a major risk to the delivery of the stations. David Shillito, director at LO'R and Operations Director at GRCUK, confirms that LO'R set up their own manufacturing facility as a means of establishing control over the finishing of the product and increasing delivery certainty in handover to Crossrail. LO'R purchased a GFRC company, GRCUK, which was one of only three larger suppliers in the UK at the time, with the express purpose of utilising their people, skills and experience.

Of the other Tier 1 contractors, one went with GRCUK and two others awarded the GFRC packages to Sorba and Lindner respectively. (7) These two companies, one based in the Netherlands and the other in Germany, are cladding design and construction specialists, but they had limited experience with GFRC as a product. Sorba partnered with supplier Concrete Valley. Lindner originally worked with Betsinor in France, then GRC Beton in Poland, and ultimately set up their own facility.

For Crossrail as a client, the client prototype developed at Leighton Buzzard provided confidence in the performance of the GFRC system. This was translated into the project requirements as set out in the Station Works specification, drawings, and various guidance reports such as Lessons Learnt, Access and Maintenance Strategy and Cladding Setting-Out Guidelines.

The level of information provided was judged to be appropriate by the contractors while leaving enough room to optimise the detailed design. Patrick Weijers, Sorba, confirms that the technical requirements were clearly communicated from the client to the contractor, with line-wide design guidance showing the outline boundaries of what needed to be designed to and confirming the elements available for subcontractor design.

Crossrail also encouraged the contractors to learn from each other with the purpose of avoiding asymmetric information in the contractors' development process and to aid in achieving consistent contractor's designs. Franz Maidl, Lindner, concurs and adds that Lindner were afforded opportunities to share and collaborate through being shown the prototype produced by LO'R.

All contractors admit that the level of knowledge-sharing between them could have been better, but they point to the attitudes of the Tier 1 contractors getting in the way of this at times. One aspect where they believe they could have learnt more from each other was in the process of material acceptance. Both Sorba and Lindner accept that the collation of MCRs (Material Compliance Records) (8), conducted at each project site, duplicated records for a single component, such as a gasket which equally could be used by another contractor on other station projects within the Crossrail programme. A single accessible repository for the collation of these records on a programme basis (where concessions had been granted), could have ensured more consistent information from client to contactor and avoided some of the issues caused by asymmetric information.

Weijers acknowledges that such a level of knowledge sharing would have been difficult to achieve prior to the award of the last GFRC package on the project due to commercial tensions.

After the initial sample regime and detailed designs had been accepted, all three GFRC contractors built their full-size off-site prototypes of a typical tunnel junction, measuring approximately 8m x 9m to a height of 5m (See Figures 2,3).

Figure 2: Sorba Full scale prototype © Sorba

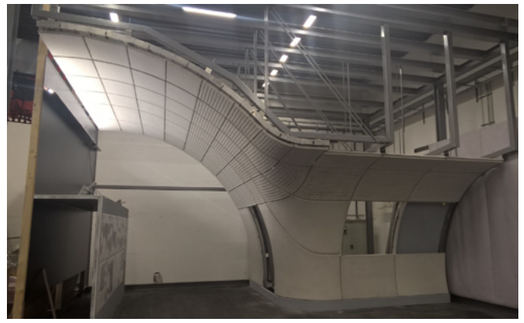

Figure 3: Lindner Full-scale prototype © Lindner

The installation of the physical prototypes provided Crossrail with a level of assurance on the buildability, appearance and operation of the system, thereby significantly de- risking this part of the project. Shillito recounts that LO'R's physical prototype gave the client a level of confidence that he would otherwise not easily have achieved before construction on site. (See Figure 4).

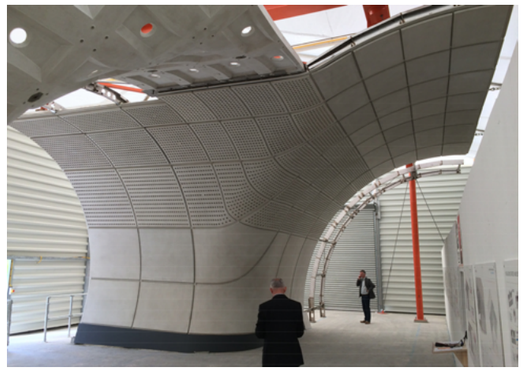

Figure 4: Full scale prototype at LO'R with client Julian Robinson © Jorrin ten Have

For his own business, it helped de-risk buildability and programme, so the prototyping benefits were distributed across the project. A lesson here for future design and build mega-projects is that the combination of consistent information from client to contractor and early construction stage testing, such as prototyping, can bring multiple benefits to enhance outcome certainty.

The prototyping was part of the wider thorough assurance processes followed by Crossrail. The organisation had to satisfy many stakeholders, from representatives of the project sponsors to future Infrastructure Managers (IMs), so prototypes were key in the demonstration that the project could be built and maintained safely and in an efficient manner. This in turn provided the contractors with an element of learning about maintenance planning and quality control.

Specifically, the GFRC prototypes served to demonstrate the access and maintenance strategy to stakeholders like LU (9). Panels were taken off and re-installed during inspections, demonstrating the equipment and methods involved and timing the operations to ensure these would be able to be carried out in the limited time available during engineering hours. As each of the contractors' designs varied in the detail of their fixings and framing, the access strategy had to be proven for all individual systems. Crossrail maintenance planning engineers and LU premises engineers travelled to inspect all the contractor prototypes in the UK, the Netherlands and Germany multiple times between 2015 and 2017 to witness these trials in person and comment in detail. All these procedures were signed off on Inspection Test Plans (10) and became part of the contractors Operation and Maintenance manuals.

For Sorba, the rigorous testing of access and maintenance on prototypes was a novel experience. Weijers asserts that through Crossrail's requirement to demonstrate these strategies in detail, Sorba has become more aware of the importance of this aspect to operators and going forward they will demonstrate and design with asset maintainability at early stage in future projects.

5. Contractor Experience: Design and Construction

A clear aim for the prototyping was for the contractor to learn how to manufacture and install their systems. Like prototyping in product design, this process resulted in many feedback loops into the detailed design to simplify production, minimise waste and optimise material use. For LO'R, it presented a leap in terms of the skills present in the company; both for the GFRC material itself and the cladding design. In contrast with Sorba and Lindner, LO'R is not an experienced cladding specialist. Teaming up with the office of Bryden Wood (11) as technical advisers and through the process of prototyping LO'R managed to overcome this handicap and even optimise material weights and the number of panel variations.

Approximately, 35,000 square metres (some 6.5 football fields) of GFRC panelling and 7,000 types were used across LO'R's three stations. With Sorba, there were approximately 800 panel types on Farringdon station, and on Bond Street station with Lindner some 750 panel types. For LO'R, typical lead times for performance testing, prototypes and mock-ups would be six months. An evolution in learning and development for LO'R over 18 months helped to obtain the handover certainty that Crossrail as client required. It can thus be understood that a tangible benefit for major design and build projects alongside consistent, evidential information is planning in extended timescales to develop the production process and technical understanding with samples and prototypes.

Many trials were conducted with different mould types and materials, methods of sand blasting and cast-in fixings to achieve the desired outcome. So, by the time the first version of the prototype was ready, many of these lessons had been recorded in a large manual for internal use in the company. After the prototype established the physical feasibility of the installation, LO'R could concentrate on further optimising both panel variations across three stations. The moulds proved a critical item for many contractors, in terms of design, sign off, and the time it took for production and delivery. Due to the complex geometry of the junctions, many moulds were required Also, depending on the type of material used, ranging from low- to high-density foam, timber, and GFRP, some moulds were used as one-off, some for series of up to 10, and others to 50 before the mould would become unusable. (See Figure 5).

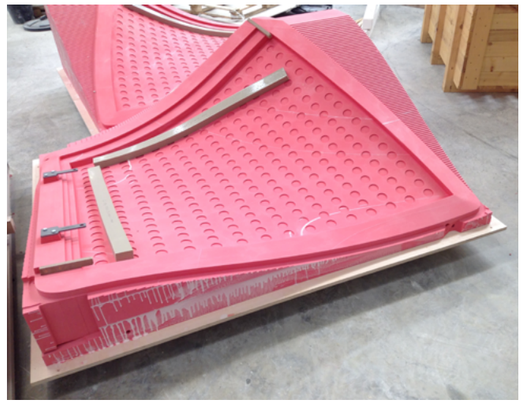

Figure 5: Double curved foam mould © GRCUK

LO'R, with designer Bryden Wood developing their digital models, were able to rationalise the number of moulds. The reduction in the number of moulds (for 27,500 panels) was significant: a 30% reduction – 3,300 moulds reduced to 2,300 moulds. With each mould costing some £3,000 pounds, LO'R were thus able to introduce savings of approximately £3 million. Arguably, as parametric 3D modelling and optimisation is employed on further complex major projects, it will aid the consistency of technical information shared from client to contractor.

Reliance on external suppliers for the moulds pushed several contractors to set up their own in- house mould production. Lindner's experience also shows that the prototyping process allowed them to further refine and rationalise the geometries of tunnel radii and panel types, thus reducing the number of moulds. Sorba and Concrete Valley took an innovative approach to this problem; they cast the single curved panels on a deformable and re-usable steel bed, thereby greatly reducing the number of required moulds. (See Figure 6).

Figure 6: Deformable steel moulds at Concrete Valley © Sorba

This fabrication method was only possible using a poured rather than sprayed GFRC. Generally, poured GFRC is of a lower strength category, so Sorba had to demonstrate that the chosen mix (including high performance concrete), method and panel thicknesses would sufficiently address all of Crossrail's performance requirements. While it took longer to evidence compliance through calculations, test panels, load tests, and full-scale prototyping, Sorba saved time and money later in the process – an example of how early testing and investments is suited to a successful DfMA approach and consistent project outcomes.

While the other contractors did not follow this route, each made their own other innovations on the system. For LO'R, optimisation of panel weights was a key aim. They achieved this through a combination of cast-in stainless steel ribs in the horizontal spanning direction and varying the thickness of the panels according to their size and location. Lighter weight panels were easier to handle and used less concrete. This panel optimisation was combined with a pin hooking system that allowed for a very fast installation of panels once the main frame members were accurately positioned. The system innovation prompted a series of prototype tests to ascertain the effect of this system on access and maintenance. In particular, the system did not allow each acoustic panel to be individually removable – a performance requirement of the design for long term maintenance. After successful time trials at the full-scale prototype in the presence of LU engineers, it was decided to leave the lowest row of acoustic panels individually removable and use the pin hooking system for the upper panels. This process showed that the prototype was not there merely as a finished piece for acceptance, but also functioned as a working test and design development model. LO'R's third innovation was the structural system around the tunnel junctions. Rather than using 3D curved steel members for framing, LO'R used an integral GFRC shell, made up of four connected elements as the structural carrier frame. This unusual approach, called the 'tusk', was calculated in detail and prototyped at full scale in order to give Crossrail the confidence that it was going to perform satisfactorily.

For the client, these innovations presented potential efficiencies in cost and construction, but the specification requirements for access and maintenance had to be closely guarded. The prototype proved to be the most effective way to ensure that the systems could be safely and efficiently maintained.

Lindner's approach to innovation was to base the GFRC framing system on technology developed in their interior cladding business. By using a toggle clamping system accessible through the vertical joints, each panel became fully individually demountable without the need for multiple face fixings on each panel. Although the principles of this system were explored through drawings and models, it was again the prototype that demonstrated the effectiveness of the approach.

The complex geometries of the stations and the technological innovations proposed by the contractors were only possible to achieve through detailed and accurate 3D modelling. Lindner produced a detailed 3D model which was used to pick up details such as additional bracketry to aid the fabrication process. The model served as a general BIM model but it also became a means to determine construction processes and the exchange of information between the Tier 1 contractor/station designer and Lindner as a Tier 2 supplier of the GFRC cladding (See Figure 7).

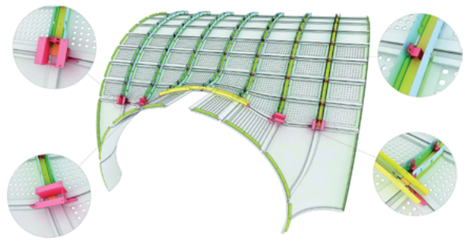

Figure 7: Lindner 3D model © Lindner

In some way, the prototyping was therefore not only a test of the physical objects, but also of the processes required to achieve these. The contractual set-up provided many challenges in the communication and acceptance of proposals. Franz Maidl identifies that Lindner would often receive inconsistent information being passed down the supply chain. Lindner would receive the line-wide design in parts, amended with updates from the Tier 1 contractor via their designer. Lindner experienced numerous changes and new instructions which became a challenge to manage due to the lag-time in information being received by Lindner as a Tier 2 supplier. Thus, the contractor's designer was not always able to review designs submitted by Lindner as they had changed works information instructed to them. The process of client information being passed along the supply chain became slow at times, alongside an elaborate contractual mechanism which was not acting lockstep with the required information flow. (12)

LO'R's Shillito criticises the process when compared against advanced manufacturing processes such as in the automotive industry - the inspiration behind DfMA in construction - where change requirements are held back by the sponsor before manufacture even commences.

6. Contractor Experience: Wider Benefits

The tunnel cladding on the Elizabeth line-wide design presented a large volume and was complex to deliver because of 3D geometries, demanding performance requirements and restricted installation. The challenges of delivering this package posed such risks to programme and cost that the contractor had to gain a higher degree of control over their own suppliers and manufacturing processes. This was most obvious in the case of LO'R who set up their own new factory as GRCUK and were therefore able to plan out and optimise each step of the production process. But beyond responding to a need on the project this move has transformed part of LO'R's business. LO'R subsequent to the Crossrail programme now possess their own GFRC business where previously they held none and have used lessons learnt on Crossrail to drive forward their manufacturing processes. Already, the firm is looking to use these new capabilities on subsequent projects such as the Sydney Metro. Shillito here does not merely refer to the physical production of the cladding panels; the process of applying a fully digital workflow is still relatively new in the construction industry.

Lessons learnt through the physical prototyping could be fed back into the digital workflow and the client was able to review detailed proposals and variations directly in 3D. This way of working still informs GRCUK's current work but Shillito has found the uptake within the larger organisation of LO'R to be slow.

Lindner was confronted directly with the risks of the package when their initial GFRC supplier went into administration. Relatively late in the programme, they had to change supplier (13). The experience motivated them to take even more control of the process and set up their own GFRC business.

Although the decision by both Contractors to set up their own GFRC facilities seems primarily driven by risk reduction and future business opportunities, the process of prototyping and design development presented by Crossrail enabled LO'R and Lindner to get familiar with the product. It allowed them to build up enough of a knowledge base to understand the risks and opportunities related to the material as well as the digital processes involved in the making of the panels.

It is clear from the points above that the process of the Contractor developing the GFRC production design has indirectly hugely benefited their own capabilities regarding future work. In contrast, the Contractors were initially reluctant to engage in a thorough design and prototyping process. At several points the client requirement for prototyping was challenged and the need for maintenance trials was questioned. Although the process at that time may have seemed to the Contractor to be time consuming and costly and the benefits unclear or limited, they gained from the knowledge built up in the process to improve their own operations and business. A better understanding of these indirect benefits could help to overcome the initial reluctance.

7. Conclusions

In summary, the prototyping process for the GFRC cladding on Crossrail presented various benefits for the contractor in relation to different aspects of the process:

7.1 Client

The level of information provided by Crossrail was consistent, effective and evidential, allowing three different Tier 2 contractors to understand the performance requirements of the cladding system while allowing them enough room for individual innovation to optimise their detailed design and manufacture. Consistent information combined with the planned prototyping process provided the client with a level of assurance that the different solutions developed by the contractors would all meet the requirements of the system. The physical prototype helped de-risk the GFRC cladding by providing the client with a level of assurance on the buildability, appearance and operation of the system. The prototype was used to demonstrate safety and access as part of this assurance.

The prototyping process allowed the Contractor to learn how to include maintenance planning and quality control in their design and manufacturing processes.

7.2 Design and Construction

The prototype aided the contractor to learn how to manufacture and install their systems prior to full production and site installation. This resulted in simplified production, minimised waste and optimised material/mould use, thereby saving money on the production costs. The process allowed the contractor to build up the necessary skills and knowledge including advanced 3D parametric modelling with geometric outputs that could be used directly for production of moulds.

7.3 Wider Benefits

The quantity and complexity of delivering the GFRC with its associated risk led contactors to use their learning for their own business development, with two of them setting up new production facilities in the process. This means the benefits from learning on Crossrail can be carried forward to future opportunities.

The contractors all developed in-depth knowledge about the materials and production processes that were not previously part of their core business. Having proven their systems by physical prototype, the contractors were able to develop their digital workflow to a high accuracy, setting up processes seamlessly linking design development and design changes to rationalisation, production design and manufacture.

7.4 Key Learning for Other Major- and Mega-Projects

Crossrail's approach to line-wide design was informed by client expertise across a wide range of UK mega-projects such as St Pancras, HS1 and the Jubilee line extension. It forms relevant learning for most future major- and mega-projects, as a design and procurement process but also as a risk assignment approach in contrast to more traditional methods.

In Crossrail's case, the client acknowledged project risks at an early stage and mitigated these through collaborative working relationships. This approach involved the progressive disinvestment of risk from client to contractor, ultimately benefiting operational cost, reliability of quality and durability. Important aspects of this approach were defining the line-wide requirements, allowing for design iterations and testing early in the process, and reducing complexities to a level where the supply chain could effectively resolve the remaining ones. Designs were then carried through with client and contractor prototyping and benchmarks for collaborative working, input from supply chain expertise and sponsor engagement and buy-in. This paper has focussed on the contractor prototyping aspect of the approach.

In summary, the GFRC contractor prototyping provided a test of the physical objects, but also of the processes required to achieve these. Having identified the above benefits, the relevance of these to the wider industry and DfMA approaches can only be understood by looking at the project conditions and the challenges overcome. The GFRC cladding on Crossrail presented a potential economy of scale, through reduction of the time on site and the complexity of product. Sectors that feature a comparable scale, complexity of construction, and maintenance critical operations would all be likely candidates, such as the transport and energy sector, and to a lesser extent large commercial or residential development with a high degree of repetition.

Crossrail also provided a project condition where the long civil works programme allowed for time to engage in prototyping and testing of the fit-out. Budgets were allocated to support this process from, initially with client prototypes and throughout with client-side technical advice and guidance.

Challenges were both the management of information and the management of variation. Some of the information flow processes, such as MCRs and 2D versus 3D technical submissions, were only developed throughout the process and at times suffered from complicated contractual relationships between the different tiers of contractors and consultants. In order to allow contractors room for optimisation and innovation, Crossrail had to actively manage the quality and consistency of the outcomes through continued guidance from the original design team (See Figures 8,9).

Figure 8: Consistent finishes and quality across Elizabeth line stations © Crossrail

Figure 9: Installation of GFRC cladding in a station tunnel © Crossrail.

The main lesson from the GFRC prototyping on Crossrail is how this process supports de-risking and optimising a large and complex part of the project through the combination of performance requirements and prototyping requirements. It is an approach that aligns with the idea of DfMA and digital workflow in architectural design and production. The necessary level of client involvement, through planning, early investment and continued guidance should not be underestimated. In parallel, many contractors are reluctant to engage in prototyping; it is seen as costly, slow and unnecessary. This was also the case on Crossrail in the initial phases of contractor involvement. However, the benefits that resulted from the prototyping have become clear to the contractors during the process and all three are now strong advocates of Crossrail's approach to this part of the line-wide design; they are already applying the gained knowledge to other major- and mega- projects such as the Sydney Metro and London Underground extensions.

Perhaps further industry guidance on prototyping as part of DfMA in construction could be developed to help to educate and communicate this process for future projects. The authors of this paper certainly hope that these lessons from Crossrail will inform future clients and contractors to organise their processes using the full benefits that prototyping can bring.

Acknowledgements

The authors would like to thank David Shillito from GRCUK, Franz Maidl from Lindner and Patrick Weijers from Sorba for sharing their experiences and insights that form the basis of this paper.

References

1. Neill McClements, 'The Value of Common Design – C100 Crossrail Architectural Components' and Simon Atherton, Stuart Moxon, 'The Importance of Construction Mock-ups and Trials' in Crossrail Project: infrastructure design and construction Vol. 1, ed. by Mike Black and others (London: ICE Publishing, 2014)

2. Glass fibre-reinforced concrete consists of a composite of high-strength, alkali-resistant glass fibres embedded in a concrete matrix.

3. The concept of Design for Manufacture and Assembly originates from the manufacturing industry as a form of lean engineering with the aim of reducing manufacturing and assembly costs and to quantify improvements through decisions in the design process.

4. After an initial visual mock-up of a section of platform was completed in 2010, Crossrail constructed a full scale GFRC cladding prototype working with GFRC manufacturer BCM during 2012-2013.

5. A series of prescribed tests on panels of varying sizes was carried by each contractor out prior to building the full prototype. GFRC as a material has varying properties depending on the types and amount of aggregates used as well as the glass fibre length, method of manufacture etc. Light reflectance, acoustic performance and blast performance could not be accurately calculated for this type of cladding and therefore required physical laboratory testing.

6. Tottenham Court Road station and Liverpool Street station.

7. GRCUK, Sorba and Lindner acted as Tier 2 contractors responsible for the design, manufacture and installation of the GFRC cladding. They in turn used different material suppliers and installation contractors.

8. As part of the Quality Assurance plan on Crossrail, Tier 1 contractors were contractually obliged to summit material compliance records on each component/material to be utilised on the project. These provided evidence for compliance on issues such as fire resistance and durability and were checked against the Employer's requirements.

9. The future operation and maintenance of the central Elizabeth line stations falls under the Infrastructure Managers, London Underground and RfL (Rail for London).

10. Inspection Test Plans (ITPs) were part of a rigorous process to check against requirements and gain acceptance from the IMs.

11. Bryden Wood is a design and engineering practice focussed on developing DfMA solutions and off- site construction.

12. Dan Harvey, 'Crossrail May Not Open Until 2021 – Reports on Problems with the Project Identified in a Report From the NAO' Modern Railways, June 2019 pp 17-20.

13. Lindner changed supplier twice, from Betsinor to GRC Beton to their own in-house production facility, now named Lincrete.

Biodiversity Net Gain: One Policy, Many Metrics - Comparing Different Metrics Because the Maths Matters

Claire Wansbury

MA MSc FCIEEM CEcol CEnv CMLI
Associate Director of Ecology
Infrastructure
London, UK

James Hicks

MBiolSci MCIEEM CEnv,
Senior Ecologist,
Infrastructure,
Birmingham, UK

Matt Wainhouse

BSc MSc MCIEEM
Cardiff University
Cardiff, UK

Abstract

Biodiversity Net Gain is an approach that means development leaves biodiversity in a better state than before. Net gain policies and the use of biodiversity metrics are on the rise. It is easy to forget that the seemingly simple maths at the heart of metric tools can have real-world outcomes. Several metrics have been developed to meet the specific needs and situations of public bodies, local authorities, and developers in the UK. Here we compare some of these metrics to illustrate how subtle differences in the metrics can influence the biodiversity balance sheet. This article does not attempt to judge whether any particular approach is the “best” of those currently in use; it simply signals that there can be substantive differences in units and therefore the requirements placed on developers depending on which metric is used.

Keywords

Ecology; Biodiversity Net Gain; Metrics; Offsetting; Policy

1. Introduction

Biodiversity Net Gain is an approach that means development leaves biodiversity in a better state than before. In the United Kingdom (UK), there has been increasing recognition that Biodiversity Net Gain is a policy approach that could contribute to creating ecological benefits from development (Ministry of Housing, Communities and Local Government 2018, Defra 2018a).

Achieving genuine net gain relies on an objective method for measuring some proxy for biodiversity in a transparent and replicable way. Biodiversity metrics are simple conceptual tools for doing just this. They attempt to represent the complexity of nature using tangible values through a calculation based on factual survey data. When supported by underlying good practice in respect of habitat equivalence and additionality (CIRIA, CIEEM, IEMA 2016), the calculation of losses and gains can then be used by non-specialists to inform better decision making.

In the UK, the biodiversity metrics used to-date are habitat rather than species orientated. Defra's Biodiversity Offsetting Metric 2012 (Defra 2012) is perhaps the best known and most widely used. Its introduction set the precedent for similar metrics used by HS2, Network Rail's Biodiversity Calculator (NRBC), The Warwickshire, Coventry and Solihull Biodiversity Impact Assessment Tool (WCSBIA), and the update to the Defra biodiversity metric ('2.0') that Natural England published as a Beta version in late 2019, drawing on experience across the industry and studies, including this comparative study (Defra 2018b and Natural England 2018).

These metrics are broadly similar in the method of calculation, multiplying values of habitat distinctiveness, condition, and area to produce a figure of pre-construction biodiversity value. Post-construction biodiversity value is calculated in the same way (i.e., multiplying values for habitat distinctiveness, target condition and area, with negative multipliers for time to reach target condition, delivery risk and spatial relevance).

Despite their similarity, each metric takes a subtly different approach. This ultimately reflects the context in which they were intended to be used. Both the original 2012 draft Defra method and the subsequent Defra biodiversity metric 2.0 (2019 Beta version) are designed to be used across the breadth of England and in a range of infrastructure projects. Other metrics have been developed with a greater degree of relevance to their situation. Network Rail's Biodiversity Calculator was designed specifically for rail projects, most of which occur almost entirely within the rail estate. HS2's metric was developed specifically for the scheme and the circumstances unique to such a large-scale, linear infrastructure project. In contrast, the WCSBIA metric was designed with local conservation priorities in mind and use at County scale.

Despite the increasing application of a Biodiversity Net Gain approach to development, the UK metrics have rarely, if ever, been openly compared. The nuances of each metric mean that the net balance of biodiversity has the potential to vary quite significantly depending on which is used. This is an important issue because a net gain approach must be transparent in order for stakeholders to have faith in the process and so that genuine benefits to biodiversity can be attained.

An exercise was carried out to compare four biodiversity metrics currently used in the UK:

1. Defra's Biodiversity Offsetting Metric 2012

2. HS2 Phase 1 Biodiversity Offsetting Metric (HS2 2015)

3. Network Rail's Biodiversity Calculator (Version 5.10)

4. The Warwickshire, Coventry and Solihull Biodiversity Impact Assessment (WCSBIA) Tool (Version 19.0)

The authors also reviewed a working draft version of Defra's biodiversity metric 2.0 for context. In comparing these metrics, we aim to highlight the similarities and differences in how net gain is calculated in three areas: offsite habitat creation; distinctiveness and condition values; and trading down corrections. The comparison is not exhaustive and there are several facets of these metrics that add to the variation in Units but are not discussed. In identifying these points, we hope to emphasise the importance of the sums with the aim of making the Biodiversity Net Gain process more transparent.

2. Comparing the Metrics

For each metric, there are two distinct types of inputs: user-specified values and metric-specified values. User-specified values are those where there is more than one value option to choose from and this is defined by the person using the tool. An example is choosing whether a semi-natural woodland is of Good, Moderate or Poor condition. The person inputting the values reviews the survey data and chooses the appropriate option.

Metric-specified values are fixed within the metric tool itself or by metric rules and cannot be changed or edited by the user. The spreadsheet tools for the NRBC and WCSBIA, for example, have automatic formulae, drop-down boxes, and restricted cells that cannot be overwritten or changed by the user. These values are entirely metric-specified and vary between the two. An example of a metric-specified value common to all metrics would be lowland beech-yew woodland, which is automatically defined as high value.

3. Calculating Offsets

Maths is at the heart of the metric-based net gain approach and so, to understand the metric outputs, we need to understand the equations. The order of the calculation matters because subtleties within them can cause quite different outcomes. At its most basic we can say:

Biodiversity Net Change = After Works Units – Baseline Units

When we expand this to include the multipliers, all the metrics were consistent in their approach to calculating on-site units, but approaches differed for offsets (i.e., off-site habitat compensation). Two schools of thought begin to emerge from the metrics we looked at: whether to deduct baseline Units before negative multipliers have been applied, or after (Box 1).

Calculating off-site offsets

Equation 1

Biodiversity Net Change=

$$\frac{((\text{After Works Distinctiveness} \times \text{Condition} \times \text{Area}) - \text{Baseline Biodiversity Units})}{((\text{Delivery Risk} \times \text{Time to Condition} \times \text{Spatial Risk}))}$$

Equation 2

Biodiversity Net Change=

$$\left(\frac{\text{After Works Distinctiveness} \times \text{Condition} \times \text{Area}}{\text{Delivery Risk} \times \text{Time to Condition} \times \text{Spatial Risk}}\right) - \text{Baseline Biodiversity Units}$$

For example, an off-site habitat compensation scheme will create one hectare of unimproved grassland (High distinctiveness, 6) with a Moderate target condition (2). This will replace one hectare of poor semi-improved grassland (Low distinctiveness, 2) in Moderate condition (2). The new unimproved grassland is of Medium delivery risk (1.5), will take 20 years to reach its target condition (2), and is spatially well connected to the habitat it is replacing (1).

The pre-construction value of the poor semi-improved grassland habitat is calculated as:

$$2 \times 2 \times 1 = 4 \text{ Biodiversity Units}$$

Using Equation 1, the net change is a positive increase of 2.66 Units, calculated as:

$$((6 \times 2 \times 1) - 4) / (1.5 \times 2 \times 1) = 2.66 \text{ Biodiversity Units}$$

Using Equation 2, there is a net balance of 0 Units. There is no net loss in Units, but no net gain either, calculated as:

$$((6 \times 2 \times 1)/(1.5 \times 2 \times 1)) - 4 = 0 \text{ Biodiversity Units}$$

The Defra 2012 metric guidance is somewhat vague on this and it is easy to see how it has been interpreted differently in different metrics. The worked example in the Defra 2012 guidance does at least show their line of thought: baseline Units are subtracted before negative multipliers are applied (Equation 1, Box 1). This is the approach taken in the NRBC and some of biodiversity offsetting pilot study areas. The alternative approach (Equation 2, Box 2) has been taken up in other metrics used by HS2, WCSBIA, The Environment Bank, and provisionally used in Defra biodiversity metric 2.0 (Natural England 2018).

The difference this makes is best illustrated through the worked example in Box 1. Using equation 1 to calculate the value of offsets, the habitat creation scheme would be predicted to result in a 66% net increase in biodiversity Units. An equivalent increase in Biodiversity Units using Equation 2 would require a commitment to achieving a "Good" target condition (3) and an increased area of 0.35 ha (i.e., a third extra land or habitat needs to be acquired or managed).

Defra's net gain public consultation suggests that Biodiversity Net Gain may be identified as an increase of at least 10% above the baseline value (Defra 2018b), which in this example would mean a positive increase of 0.4 Units. Using an Equation 1 metric, this could be reached with 0.5 ha of the created unimproved grassland in Moderate condition. Using an Equation 2 metric hitting the same net gain target needs a minimum 0.75 ha of Good condition habitat, again a third extra in both area and condition for the same result.

4. Distinctiveness and Condition

A less subtle difference between the metrics is that both user- and metric-specified values differ between them. The WCSBIA, for example, uses five distinctiveness scores (2, 3, 4, 5, 6) compared to three in the Defra 2012 and NRBC (2, 4, 6) and four in HS2 and (anticipated) Defra biodiversity metric 2.0 (2, 4, 6, 8) (Natural England 2018). High distinctiveness habitats are rarely encountered on most developments and throw up an entirely different set of issues to those discussed here. However, three common habitats do warrant some discussion because of their prevalence and lack of other legislative protection. Dense scrub is valued Medium-low (3) in the WCSBIA and Medium (4) in the other metrics, amounting to a 25% difference in the Units available for this habitat depending on which metric is used. Similarly, tall ruderal vegetation is valued as Low distinctiveness (2) in the NRBC, HS2 and Defra metrics and Medium-low (3) in the WCSBIA, a 25% difference in the Unit outcome of this habitat. Poor semi-improved grassland was considered to be of Medium (4) distinctiveness by HS2, but valued Medium-low (3) in the WCSBIA and Low (2) in the NRBC, again resulting in a 25-50% difference in the Unit score that this habitat will contribute to the biodiversity balance sheet.

Applying condition values can also exacerbate the differences between metrics. The Defra 2012 metric used the Farm Environment Plan (FEP) Manual (Natural England 2010) as the basis for its condition assessment. However, the consensus now is that it is not particularly suitable for this purpose, with many habitats typically encountered on development sites either not included or covered inadequately, particularly for Low distinctiveness habitats.

A creative method for getting over this issue was devised for use with the NRBC. This bespoke method uses a default condition assessment derived from common themes in the FEP (e.g., presence of non-native invasives) (Network Rail 2017). Other metrics have removed the variable condition weighting of habitats altogether. The HS2 metric gives all Low distinctiveness habitats an automatic Poor condition, *"recognising that condition has a negligible effect on the overall value of those habitats"* (HS2 2015). The WCSBIA takes a similar stance, using metric-specified condition multipliers for some Low distinctiveness habitats. In these three metrics, again we begin to see differences emerging in how the Unit score might vary between them. A patch of arable land would have a standard Poor condition (1) using the WCSBIA or HS2 metrics and up to Good condition (3) using the NRBC, a difference of up to 66% depending on the flexibility of the metric. Similar variation will also occur in the post-construction calculation with the time to reach the target condition multiplier. An interesting point drawn from HS2's metric is that creating habitat of High distinctiveness was capped at a Moderate (2) condition, limiting the overall value of much of their compensatory habitat. By contrast, other metrics do not enforce a condition cap in the same way. The new bespoke condition assessment in the Beta testing version of Defra biodiversity metric 2.0 uses five condition values (1, 1.5, 2, 2.5, 3) (Natural England 2018) and this may level the playing field with a consistent protocol for describing habitat condition.

5. Trading Down

One of the key net gain principles is of equivalency in habitat compensation. High distinctiveness habitats cannot be offset with the creation of habitats of lower value. The loss of one hectare of unimproved grassland, for example, should not be replaced with larger areas of habitats of lower distinctiveness such as semi-improved grassland or dense scrub (i.e. trading down). However, this then raises the question of what to do when a project does result in trading down. A facet unique to the WCSBIA tool is that it includes an automatic "trading-down correction," which the others do not. The WCSBIA calculates the net change in biodiversity Units and then deducts the number of Units that are not accounted for through equivalency. While all other metrics should apply a similar correction, it is not automatically deducted. So, without skilled interpretation, the metric tools can appear to allow trading down to occur without penalty. This can make the WCSBIA appear to be far less favourable than other metrics where equivalency can be poorly accounted for.

6. Conclusion

It is difficult to disentangle the extent that these differences contribute to the overall variation that we see between the metrics. There are, of course, many other idiosyncrasies not discussed here that add to the variation. The specifics of the site and situation where a metric is used will no doubt contribute to any disparity. What is clear is that the individual metric rules that account for distinctiveness and habitat condition, together with trading down and differences in the calculation itself will all contribute to the overall Unit variance between metrics.

In a comparison like this, subtle differences like those outlined above may seem innocuous at first glance. However, we need to recognise that Biodiversity Net Gain strategies do affect real-life projects. A third extra habitat may equate to a third extra cost, which, on large developments, can be substantial. In the Defra 2.0 metric consultation, an indicative tariff rate of £9,000 - £15,000/ Unit was estimated (Defra 2018b). With this figure in mind, we can see that calculating Units inaccurately, or using an unsuitable metric, can lead to substantial differences in the cost of offsets, with the total sum scalable to the size of the project. Using an inappropriate metric could be bad news for project balance sheets if excessive costs result from over compensation, but even worse news for biodiversity if it results in failure to deliver genuine net gain. Such large differences in Units don't only translate to cash but also to the biodiversity outcomes that we, as an industry, are trying to promote through Biodiversity Net Gain policies.

Acknowledgements

This paper is an updated version of one originally published as: Wainhouse M, Wansbury C and Hicks J (2019) One Policy, Many Metrics: Comparing Different Metrics Because the Maths Matters. In Practice – Bulletin of the Chartered Institute of Ecology and Environmental Management (CIEEM) 104: 17-21. It is re-published with kind permission from CIEEM. The original article has been shortlisted for the "2020 CIEEM InPractice Award".

The authors would like to express thanks to Network Rail, Julia Baker (Balfour Beatty), Nick White (Natural England) and Rachel Blount (SNC Lavalin's Atkins) for valuable comments on a previous draft of the manuscript.

References

CIRIA, CIEEM, IEMA (2016). Biodiversity Net Gain: Good practice principles for development. Available at: https://www.cieem.net/data/files/Publications/Biodiversity_Net_Gain_Principles.pdf. [Accessed Feb. 2019]

Defra 2012. Technical Paper – metric for the biodiversity offsetting pilot in England. Available at https://assets.publishing.service.gov.uk/government/uploads/system/uploads/attachment_data/file/69531/pb13745-bio-technical-paper.pdf. [Accessed Feb. 2019).

Defra (2018a). A Greener Future: Our 25 Year Plan to Improve Environment. https://assets.publishing.service.gov.uk/government/uploads/system/uploads/attachment_data/file/693158/25-year-environment-plan.pdf. [Accessed Feb. 2019].

Defra (2018b). Net Gain Consultation Proposal. Available at: https://consult.defra.gov.uk/land-use/net-gain/supporting_documents/netgainconsultationdocument.pdf [Accessed Feb. 2019].

HS2 (2015). HS2 London-West Midlands No net loss in biodiversity calculation Methodology and results. Available at: https://assets.publishing.service.gov.uk/government/uploads/system/uploads/attachment_data/file/490928/No_net_loss_in_biodiversity_calculation_-_methodology_and_results_v2.pdf. [Accessed April 2019].

Ministry of Housing, Communities and Local Government (2018). National Planning Policy Framework. Available at: https://assets.publishing.service.gov.uk/government/uploads/system/uploads/attachment_data/file/740441/National_Planning_Policy_Framework_web_accessible_version.pdf [Accessed Feb. 2019].

Natural England (2010). Higher Level Stewardship Farm Environment Plan (FEP) Manual. Available at: http://publications.naturalengland.org.uk/file/2819648. [Accessed March 2019]

Natural England (2018). Updating the Defra Biodiversity Metric. Available at http://publications.naturalengland.org.uk/publication/6020204538888192. [Accessed April 2019, and Beta version of Defra biodiversity metric available at http://nepubprod.appspot.com/publication/5850908674228224?cache=1564421772.98].

Network Rail (2017). Biodiversity Calculator User Guide Version 2. Available at https://safety.networkrail.co.uk/wp-content/uploads/2017/12/NR-Biodiversity-Calculator-User-Guide_V2.pdf. [Accessed April 2019].

Ecological Uplift Through Engineering – Tidal Circulation and Old Tampa Bay

Shayne Paynter

PhD, PE, PG
Vice President, Atkins
Fellow, Senior Technical Manager, Technical Professional Organization Engineering, Design and Project Management
Tampa, FL, USA

Ed Cronyn

PWS
Technical Manager, Technical Professional Organization Engineering, Design and Project Management
Tampa, FL, USA

Mike Salisbury

PE
Senior Engineer, Technical Professional Organization Engineering, Design and Project Management
Melbourne, FL, USA

Abstract

In lieu of traditional site-specific stormwater Best Management Practices (BMP's) for large infrastructure projects, Atkins and the Florida Department of Transportation (FDOT) looked at a regional solution in an area of Old Tampa Bay that has historically had poor water quality. After in-situ study, modelling and coordination with multiple agencies, Atkins and FDOT have established a new tidal connection through the SR 60/ Courtney Campbell Causeway to improve water quality north of the causeway and created ecological conditions that are conducive to seagrass recovery and benthic habitat. The project removes an equivalent of 10,161 Kg of nitrogen due to tidal flushing and is expected to increase seagrass coverage and density over an area of approximately 300 acres. Atkins and FDOT set up a first-of-its-kind water quality credit leger as well as a seagrass mitigation ledger to track improvements and offset future impacts for project that drain to the bay. The water quality improvements have already offset approximately $100 million in acquisition, construction and maintenance costs. The project has won multiple state and national awards, including the 2019 Federal Highway Administration (FHWA) Environmental Excellence Award.

Keywords

Nitrogen removal; Seagrass; Water quality; Residence time

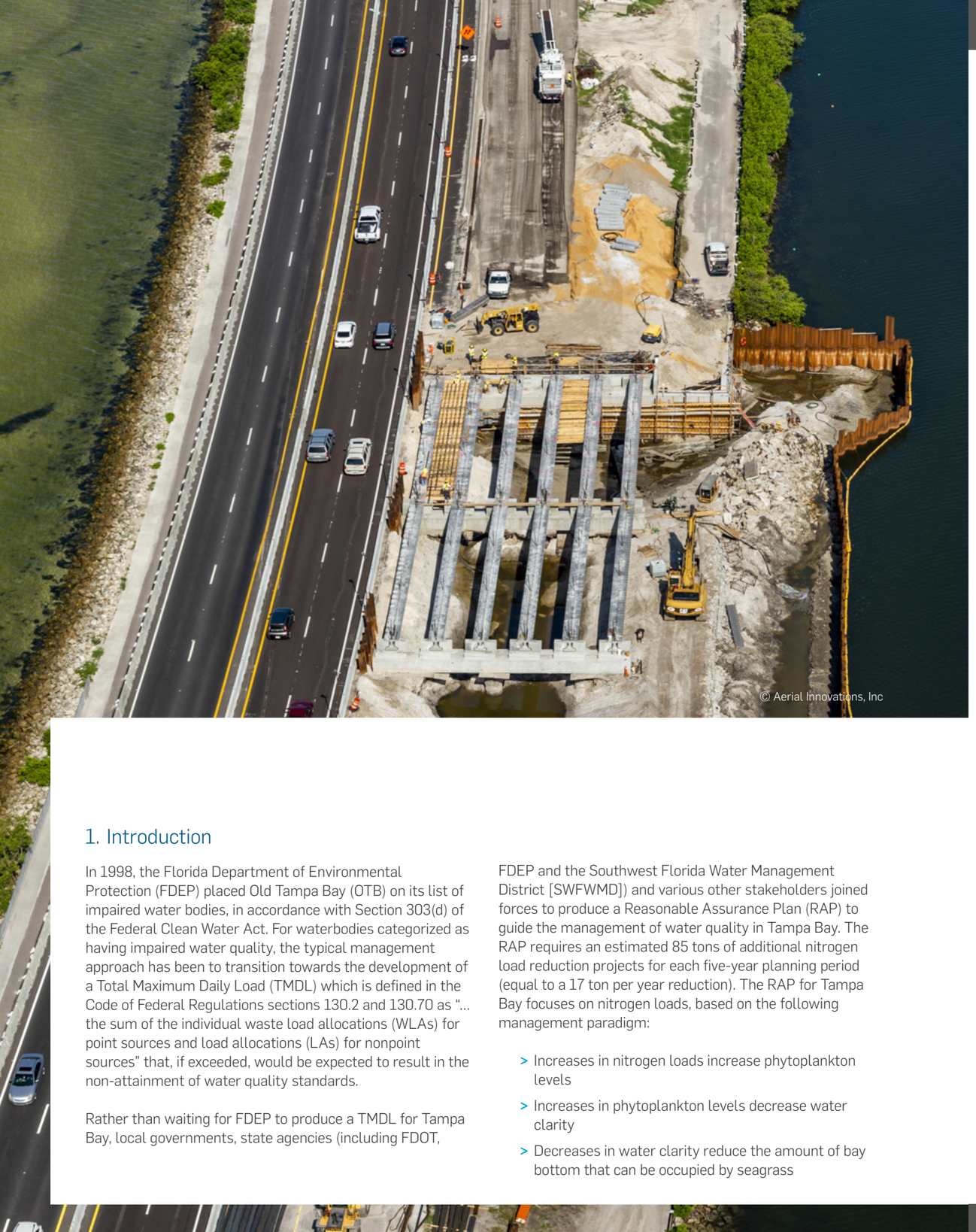

1. Introduction

In 1998, the Florida Department of Environmental Protection (FDEP) placed Old Tampa Bay (OTB) on its list of impaired water bodies, in accordance with Section 303(d) of the Federal Clean Water Act. For waterbodies categorized as having impaired water quality, the typical management approach has been to transition towards the development of a Total Maximum Daily Load (TMDL) which is defined in the Code of Federal Regulations sections 130.2 and 130.70 as "... the sum of the individual waste load allocations (WLAs) for point sources and load allocations (LAs) for nonpoint sources" that, if exceeded, would be expected to result in the non-attainment of water quality standards.

Rather than waiting for FDEP to produce a TMDL for Tampa Bay, local governments, state agencies (including FDOT, FDEP and the Southwest Florida Water Management District [SWFWMD]) and various other stakeholders joined forces to produce a Reasonable Assurance Plan (RAP) to guide the management of water quality in Tampa Bay. The RAP requires an estimated 85 tons of additional nitrogen load reduction projects for each five-year planning period (equal to a 17 ton per year reduction). The RAP for Tampa Bay focuses on nitrogen loads, based on the following management paradigm:

- Increases in nitrogen loads increase phytoplankton levels
- Increases in phytoplankton levels decrease water clarity
- Decreases in water clarity reduce the amount of bay bottom that can be occupied by seagrass

The most widely adopted stormwater treatment system in Florida, wet detention ponds, only remove about 30 to 40 percent of incoming nitrogen loads from stormwater. Dry retention ponds have nitrogen removal efficiencies in excess of 90 percent, but they often require much larger construction costs or areas of land to meet design standards and are often impossible in areas with poor soils or high water tables. Given the continuous rise in costs associated with acquisition of property for stormwater management as well as the associated costs of construction and maintenance, many clients are beginning to seek regional, innovative solutions that can address stormwater water quality needs of more than one project.

One such alternative treatment system involves the Courtney Campbell Causeway (CCC). The CCC was constructed in the early 1930s during a time when OTB was considered to have good water quality. Aerial photographs show evidence of extensive seagrass meadows in most of Old Tampa Bay in 1948. However, the shallow waters of OTB north of the CCC at its eastern terminus appear to be devoid of seagrass in 1948. These findings indicate that the construction of the CCC changed the environment to the extent that seagrass could not grow in that area, even while adjacent waters supported extensive meadows of these underwater plants.

2. Feasibility Study

In January 2015, a field study characterizing existing seagrass, water quality, sediments, and other parameters was completed in OTB (north of the CCC Figure 1). The results of this preliminary study revealed a pattern of seagrass species and presence that is best explained by the altered salinity regime that currently occurs in the area north of the CCC. Hydrologic flow and residence times have also been altered by the CCC, which has placed stressors on seagrass meadows within the assessment area. The current state of the seagrass resources in the assessment area can be most likely attributed to the lack of tidal flushing causing the differences in seagrass species and abundance. The current pattern of seagrasses is such that shoal grass (*Halodule wrightii*) and widgeon grass (*Ruppia maritima*) are the dominant species north of the CCC, while mixtures of turtle grass (*Thalassia testudinum*), shoal grass, and manatee grass (*Syringodium filiforme*) dominate the seagrass areas south.

This study was initiated to evaluate if the replacement of a portion of the CCC with a conveyance structure such as a bridge would likely bring about an ecological response in OTB similar or greater than that which would be expected to occur by treating stormwater runoff alone.

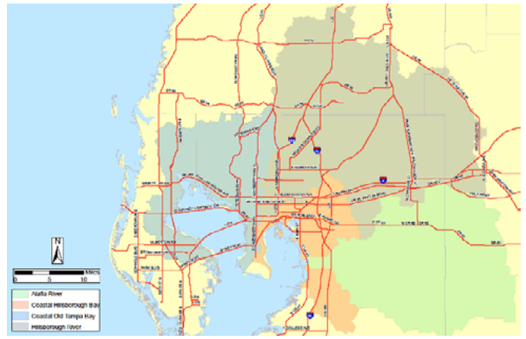

Figure 1: Map of Tampa Bay showing main transportation features and the watersheds of coastal drainage to Old Tampa Bay, the Hillsborough River, the Alafia River, and coastal drainage to Hillsborough Bay.

Tampa Bay suffered significant declines in seagrass coverage between 1950 and 1980, but these initial losses have been followed by substantial increases in recent years (i.e., Johansson, 1991; Johansson and Greening, 1999; Tomasko et al., 2005; and Greening and Janicki, 2006).

The removal or modification of causeways (as opposed to bridges) has been promoted worldwide as an environmental restoration tool. Examples include Cockburn Sound, Australia (Cockburn Sound Management Council, 2003), Fidalgo Bay, Washington State (Samish Indian Nation, 2007), Lake Victoria, Kenya (Patrick et al., 2005), and Missisquoi Bay, Vermont (Mendelsohn et al., 1997). In Tampa Bay, the removal of the 50-year-old causeway leading to Ft. Desoto Park was completed in 2004, restoring tidal flow between two lagoons in this high-profile public park. The removal of the causeway and its replacement with a bridge appears to have helped improve water quality over an area in excess of 1,000 acres (NOAA, 2006). After the removal of the 100-year old causeway across Lake Surprise, which was part of Flagler's railroad, water quality improved over an area in excess of 300 acres (PBS&J, 2009).

In OTB, the CCC represents a potentially significant impact to seagrass resources. The CCC was constructed during the Great Depression and was completed in the early 1930s, during a time when Tampa Bay as a whole, and OTB as well, was considered to have had good water quality, based on photographic evidence of extensive seagrass resources. Aerial photography from 1948 shows evidence of extensive seagrass meadows to the south of the CCC along Rocky Point (Figure 2).

Figure 2: Aerial photograph from 1948 showing extensive seagrass meadows in Old Tampa Bay. Area shown is north and south of the CCC, at the eastern terminus of the causeway.

However, in the area north of the CCC shown in Figure 3, the photographic signature of seagrass meadows found in areas to the west and south is reduced or absent. While no ground-truthed data are available, it would appear that seagrass meadows were already impacted in the areas shown in Figure 3 at least as far back as 1948.

Figure 3: Aerial photograph from 1948 showing apparent impacts to seagrass meadows north of the CCC at the eastern terminus of the causeway. The yellow oval indicates the photographic signature of shallow areas devoid of seagrass.

2.1 Feasibility Study Methods

A comprehensive data collection effort was completed to characterize the study area north and south of the CCC. The data collection effort conducted here consisted of the following parameters for each of the four strata:

- Seagrass and macroalgal presence and abundance
- Depth of the deep edge of seagrass meadows
- Surface and near bottom water quality
- Sediment characterization
- Flora and fauna observations

Four representative areas (strata) were identified: three to the north of the causeway and one to the southeast (Figure 4). The strata were selected based on available biannual seagrass maps produced by SWFWMD.

Figure 4: Experimental design layout with the four strata delineations

The presence and abundance of seagrass and macroalgae were quantified at 30 randomly chosen sites within each stratum. In addition to evaluating the presence and absence of seagrass within each stratum, the distance from each sampling site to open water was calculated as a surrogate for tidal influences, to see if "distance" correlated with indicators of ecosystem health. For the purposes of this study, "open water" was defined as areas with a water depth of six feet or greater and located 500 feet or more from land or other structures.

A line shapefile was then generated, snapping the ends of each line to the points and the edges of the open water. The lengths of each line were calculated and assigned to the points from which they were measured in order to show the distance of each sampling point to open water (Figure 5).

Figure 5: Graphic depicting distance from sampling sites to nearest open water

Surface and near-bottom water quality samples were collected at randomly selected sites within each stratum and are shown in Table 1.

Table 1:Parameters and Analytical Method Used to Analyze Surface and Near-Bottom

Parameter	Method
Chlorophyll-a	445.0
Ammonia Nitrogen	350.1
Nitrate+Nitrite	353.2
Ortho-Phosphorus	365.3
Total Kjeldahl Nitrogen	351.2
Total Nitrogen	351.2+353.2
Total Phosphorus	365.3

Sediment characterization was conducted at randomly selected sites within each stratum and is summarized in Table 2.

Table 2: Parameters and Analytical Method Used to Analyze the Collected Sediment Samples

Parameter	Method
Color	
Grain size	ASTM D-4464-85
Percent organic content	SM 2540G
Hydrogen sulfide	Colorimetric test kit
Total Kjeldahl Nitrogen	351.2
Total Phosphorus	365.4

2.2 Feasibility Results

Four species of seagrass were identified within the overall study area: Halodule wrightii, Ruppia maritima, Syringodium filiforme, and Thalassia testudinum (Figure 6).

Figure 6: Seagrass species observed within each stratum

In regards to seagrass abundance, (Figure 7) strata A and D, closer to open water, have significantly greater seagrass presence.

Figure 7: Average percentage of seagrass coverage at each sampling site

In order to ascertain if distance to open water correlated with ecosystem health (or seagrass abundance), the relationship between seagrass abundance and the calculated distance to open water was evaluated (Figure 8). The average seagrass abundance observed less than 8,000 feet from open water (81 percent) was found to be significantly greater than the abundance (36 percent) for locations greater than 8,000 feet from open water.

The results shown in Figure 8 strongly suggests that artificially reduced tidal influences and/or increased residence times are important stressors to seagrass health in this region of OTB as areas farthest removed from tidal influences (i.e., those farthest from open water) are the

areas with the lowest probability of occurrence and abundance.

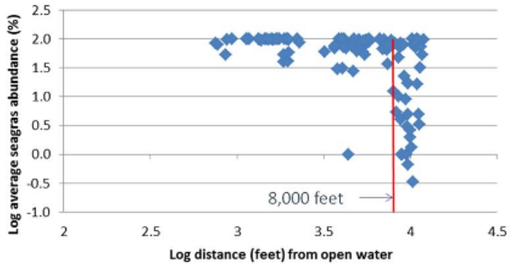

Figure 8: Seagrass abundance compared to the calculated distance from open water

Five genera of macroalgae were identified within the overall study area: *Entermorpha, Gracilaria, Hypnea, Laurencia* and *Uva*. The offshore edge of seagrass meadows was located in deeper waters within Stratum D compared to the areas north of the CCC ($p<0.001$; Strata A, B and C; Figure 9). The median water depth at the deep edge was 1.34 meters below MSL in Stratum D compared to 0.45 meters below MSL in Stratum C. This discrepancy indicates that seagrasses grow to a deeper water depth in Stratum D than elsewhere, reflective of better water clarity in this stratum.

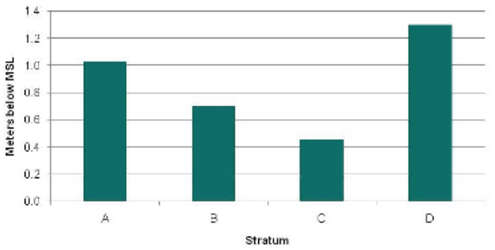

Figure 9: Median water depth (meters) of the seagrass meadow deep edge for each Stratum

Multiple long-term surface water monitoring locations were identified within the area of interest. These data represent monitoring efforts conducted for more than 30 years by the Hillsborough County Environmental Protection Commission. These stations provide a long-term dataset from 1972 to the present. Data from stations 62 (North of CCC) and 63 (South of CCC) were compared to identify if there are discernable differences in water quality between the two locations.

The average salinity north of the CCC has significantly lower salinity, 10 percent lower, than the area directly south of the CCC ($p<0.001$). Additionally, the annual average coefficient of variation of salinity is statistically greater (more variable) north of the CCC than south of the CCC ($p<0.003$). This finding shows that there is greater variation in salinity north of the CCC (36 percent more variable) than south of the CCC (Figure 10).

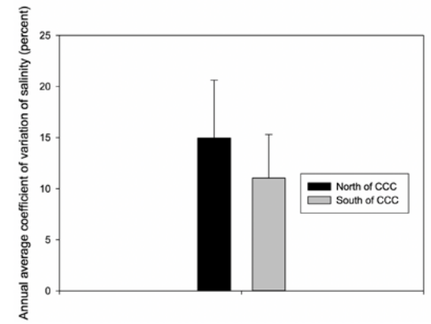

Figure 10: Comparison of annual average coefficient of variation of salinity north and south of the CCC over the period of 1983 to 2013

Chlorophyll-a, a measure of phytoplankton production, and nutrient concentrations were also compared for stations north and south of the CCC. Chlorophyll-a concentrations were significantly higher north of the CCC (43 percent higher) when compared to south of the CCC ($p<0.001$; Figure 11). Total nitrogen concentrations were 23 percent higher north of the CCC compared to south of the CCC ($p<0.001$; Figure 12).

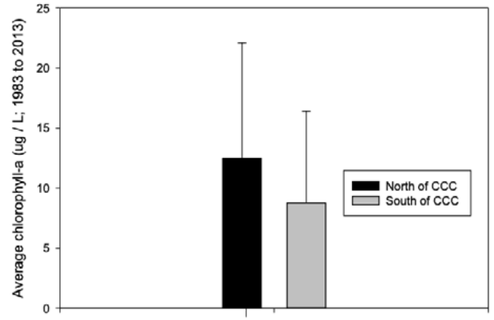

Figure 11: Comparison of average chlorophyll-a concentrations north and south of the CCC over the period of 1983 to 2013

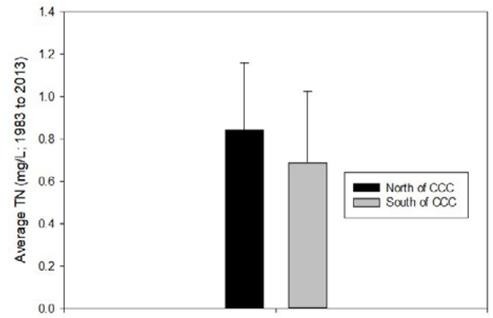

Figure 12: Comparison of average total nitrogen concentrations north and south of the CCC over the period of 1983 to 2013

3. Hydrodynamic Modeling

Based upon the results of the feasibility study, including demonstration of significant differences in nitrogen, salinity, seagrass type and abundance as well as a link between lack of seagrass and distance to open water, it was deemed by FDOT, Atkins, and permitting agencies that placing a cut within the CCC would likely result in significant ecological uplift. As such, a hydrodynamic model and further data collection was provided to help size and locate a bridge cut through the causeway as well as to evaluate anticipated changes in salinity, nitrogen and residence time.

The hydrodynamic model utilized in this effort was the Delft3D model, a widely used and validated numerical model which incorporates the effects of astronomic tides, wind, waves, and meteorological forces to simulate time-varying hydrodynamics in two or three dimensions. The grid associated with the model is depicted in Figure 13, Figure 14, and Figure 15, respectively, illustrating the bathymetric contours for the Tampa Bay and nested domains.

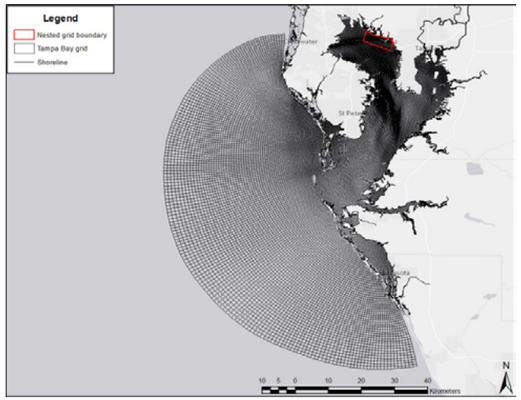

Figure 13: Tampa Bay (black) and nested (red) model domains

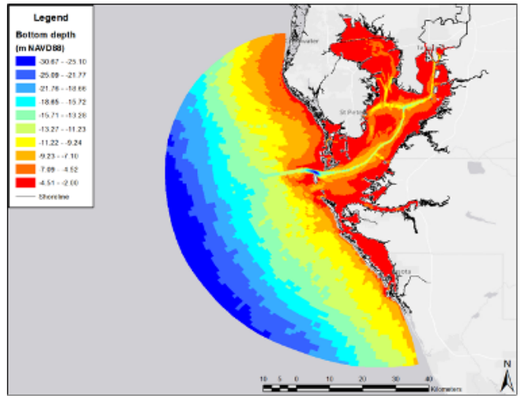

Figure 14: Bathymetric contours for the Tampa Bay model domain

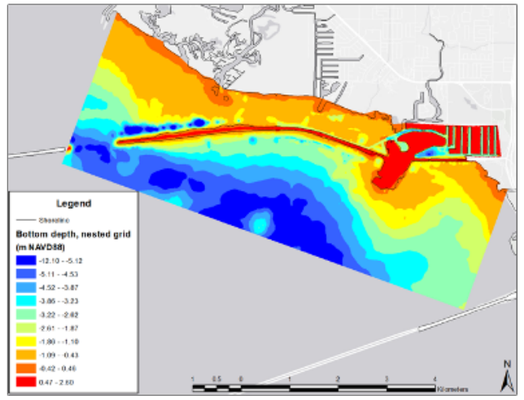

Figure 15: Bathymetric contours for the nested model domain

Models were driven by tides, wind, and precipitation, and the nested domain included a conservative tracer to simulate residence time in the area of interest. Model predictions were validated against actual data prior to running bridge simulations.

Modelling scenarios of various bridge opening lengths and locations along Courtney Campbell Causeway were evaluated. The intent was to balance costs versus having an opening long enough to exchange sufficient water to significantly reduce residence time north of the causeway and improve water quality.

Figure 16 illustrates the initial distribution of a 1 kg/m3 concentration of the conservative tracer. This distribution is identical for all model simulations. Figure 17 and Figure 18 represent the final tracer concentration for the existing and proposed conditions at the end of the seven-day model run.

After seven days, the highest concentration in the area of concern is 0.25 kg/m3 under existing conditions and 0.15 kg/m3 with a modelled 200 ft opening.

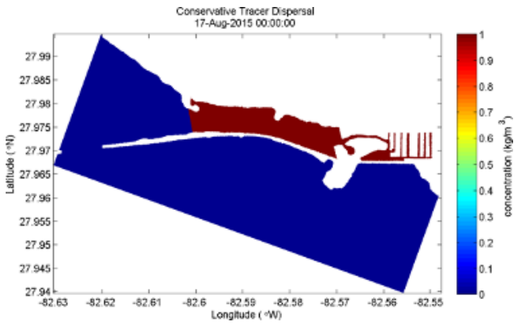

Figure 16: Initial tracer concentration; all scenarios

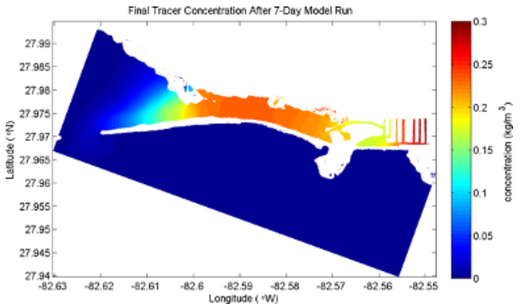

Figure 17: Tracer concentration after 7 days; existing conditions

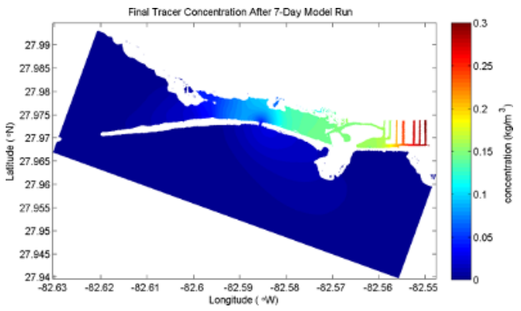

Figure 18: Tracer concentration after 7 days; 200 ft opening

The addition of the modelled 200 ft opening generally decreases peak velocities to the north of CCC compared to existing conditions except in the immediate vicinity of the opening, while the opening itself experiences a peak depth-averaged velocity of 2.5 ft/s. A sediment analysis was also performed to ensure no significant impacts on erosion or siltation would be caused by the bridge or changes in velocities. After seven days, the peak concentrations in the area of concern are about 50 percent lower with the 200 ft opening versus without. Within the area of concern, the modelled 200 ft opening reduces residence time (defined at time to reach 50 percent of initial concentration) from about three days to about one day, location dependent (Table 3).

Table 3: Summary of Modelled Residence Time for Strata A, B, and C

Location	Residence time (days)	
	Existing conditions (no alternative)	With proposed 200 ft opening
Stratum A	2.50	0.50
Stratum B	2.75	0.50
Stratum C	3.00	1.50

4. Design and Permitting

Because both the field study and hydrodynamic modeling demonstrated that adding a bridge cut under CCC was extremely likely to significantly improve water conditions, the design and permitting phase was begun. A final bridge length of 229 ft was developed and permits with the SWFWMD, FDEP, Tampa Port Authority, United States Army Corps of Engineers, Florida Fish and Wildlife, and the United States Coast Guard were obtained. As part of the permitting conditions, a two-year water quality monitoring program and success criteria for releasing both water quality and seagrass credits were developed. Credits could be applied, on a case-by-case basis, to any FDOT projects within the Tampa Bay Coastal Floodplain. The water quality success criteria and release schedule are in Table 4.

Table 4: Water Quality Success Criteria and Release Schedule

Success Criteria	Release	Compensatory Impervious Area Credits (Acres)	Compensatory Total Nitrogen Credits (Kg N/year)
A. Tidal Flux Established	20%	612.00	2,032.20
B. Dissolution Rate Improvement	20%	612.00	2,032.20
C. Salinity Improvement	30%	918.00	3,048.30
D. to E. Chlorophyll-a and TN Improvement	20%	612.00	2,032.20
F. Restoration vs. Reference Differences Reduced by 50%	10%	306.00	1,016.10
	Total	**3,060.00**	**10,161.00**

5. Construction

In the summer of 2019, the OTB project was completed. The location is shown in Figure 19 and construction photos, including a tracer test to establish tidal flux, are included in Figures 20 and 21.

Figure 19: Bridge location

Figure 20: Bridge construction aerial

Figure 21: Dye tracer test for initial release of credits

6. Monitoring and Success Criteria

Water quality monitoring as part of the permit success criteria has been ongoing since the opening of the bridge in December of 2018. The majority of the success criteria look for Strata A, B, and C north of the bridge to improve sufficiently to approach values at the reference site, Strata D, south of the bridge which has excellent seagrass coverage, abundance, and water quality. As of spring 2020, tidal flux, salinity, Chlorophyll-a, total nitrogen, seagrass coverage, and seagrass species variation have all met their targets and 80 percent of water quality and seagrass credits have been requested or released. In fact, while a residence time reduction of 50 percent was modeled and was generally the basis for parameter improvement, all of the parameters improved by over 50 percent. The difference in monthly mean values between Stratum C and D for Chlorophyll-a reduced by over 82 percent. In addition, multiple residents and boaters have indicated visually improved water clarity and more abundant wildlife north of the new bridge. Figure 22 demonstrates a clear reduction in Chlorophyll-a north of the causeway after the bridge opening, which is represented by the vertical black line.

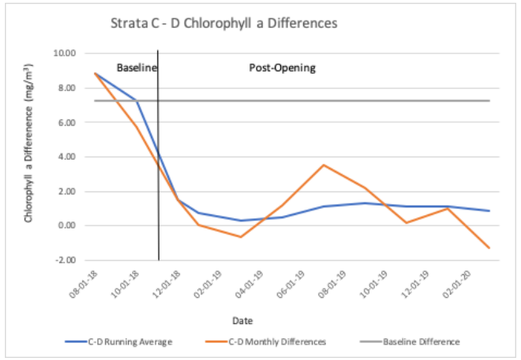

Figure 22 – Pre/post Chlorophyll a concentrations

7. Conclusions

An area totaling 321 acres evidences a reduction in residence time from 50 percent to 80 percent, depending on location in proximity to the proposed opening and existing bridge. The improvement of water quality in 321 acres would result in conditions favorable to the growth and expansion of seagrass. It was determined that the resulting water quality improvements would be equivalent to constructing over 200 traditional ponds.

The completed project (Figure 23) is a win-win for the environment and for FDOT. The project has already saved $100 million by internal FDOT cost analysis; it improves water quality and ecological habitat far more than more expensive ponds could possibly have; and the local public residents, boaters, and water enthusiasts receive direct benefit. This benefit will exist in perpetuity and not require the ongoing maintenance costs that traditional ponds would have. Also, if seagrass growth and abundance increase over time, as anticipated, a significant long-term ecological benefit for benthic organisms, seagrass, and marine life is anticipated. Due in part to the success of this project, FDOT and Atkins are developing state-wide guidance promoting the use of similar innovative, regional projects in lieu of traditional project-by-project stormwater management solutions as a first option.

Figure 23: Completed OTB bridge

References

Calleja, M.L., N. Marba, and C.M. Duarte. 2007. The relationship between seagrass (Posidona oceanica) decline and pore-water sulfide pools in carbonate sediments. Estuarine Coastal and Shelf Science 73: 583-588.

Cockburn Sound Management Council. 2003. Influence of the Garden Island Causeway on Mangles Bay, Cockburn Sound. Community Summary Paper for: Cockburn Sound Management Council. Rockingham, Western Australia. 8 pp.

Greening, H.S. and A. Janicki. 2006. Toward reversal of eutrophic condi¬tions in a subtropical estuary: Water quality and seagrass response to nitro¬gen loading reductions in Tampa Bay, Florida, USA. Environmental Manage¬ment. 38:163–178.

Greening, H.S., Cross, L.M. and E.T. Sherwood. 2011. A multiscale approach to seagrass recovery in Tampa Bay, Florida. Ecological Restoration. 29: 82-93.

Johansson, J.O.R. 1991. Long-term trends in nitrogen loading, water quality and biological indicators in Hillsborough Bay, Florida, p. 157–176. In S. F. Treat and P. A. Clark (eds.), Proceedings, Tampa Bay Area Scientific Information Symposium 2. Tampa Bay Regional Planning Council, St. Petersburg, Florida.

Johansson, J.O.R. and H.S. Greening. 1999. Seagrass restoration in Tampa Bay: A resource-based approach to estuarine management, p. 279–293. In S. A. Bortone (ed.), Seagrasses: Monitoring, Ecology, Physiology, and Management. CRC Press, Boca Raton, Florida.

Mendelsohn, D.L., H.R. Hines and T. Isaji. 1997. Missiquoi Bay Field Study and Hydrodynamic Model Verification. Final Report to: Vermont Geological Survey, Waterbury, VT.

National Oceanic and Atmospheric Administration. 2006. Fort DeSoto Tidal Hydrology Restoration Project, Fort DeSoto Park, Pinellas County, Fl. Pp. 110-115. In: Returning the Tide: Tidal Hydrology Restoration Guidance Manual. NOAA Restoration Center and NOAA Coastal Services Center Report.

NOAA. 2015a. Tampa Bay Operational Forecast System. http://tidesandcurrents.noaa.gov/ofs/dev/tbofs/tbofs_info.html

NOAA. 2015b. Climate Data Online, Daily Summaries, KTPA. http://www.ncdc.noaa.gov/cdo-web/datasets/GHCND/stations/GHCND:USW00012842/detail

NOAA Tides & Currents. 2015. Meteorological Observations, Station 8726607, Old Port Tampa, FL. https://tidesandcurrents.noaa.gov/met.html?id=8726607

Patrick, K., Romero, J.R., Imberger, J., Ewing, T., Antenucci, J., Nijuguna, H., and J. Okungu. 2005. The effect of the Mbita Causeway on water currents in the region of Rusinga Channel, Winam Gulf, Lake Victoria: a 3D modelling study with ELCOM. Report to: Centre for Water Research for the Kenya Agricultural Research Institute and the Lake Victoria Environmental Management Project. Kisumu, Kenya. 5pp.

PBS&J. 2009. Responses of Water Quality and Seagrass Coverage to the Removal of the Lake Surprise Causeway. Report to FDOT District 6, Miami, FL. 34 pp.

Samish Indian Nation. 2007. Fidalgo Bay Causeway Feasibility Study. Anacortes, WA. 14 pp.

Swart, P.K., G.F. Healy, R.E. Dodge, P. Kramer, J.H. Hudson, R.B. Halley, and M.B. Robblee. 1996. The stable oxygen and carbon isotope record from a coral growing in Florida Bay: a 160-year record of climatic and anthropogenic influence. Palaeo. 123: 219-237.

Tampa Bay Estuary Program. 2000. Seagrass Management: It's not just nutrients! Tampa Bay Estuary Program Technical Publication # 04-02. Tampa Bay Estuary Program, St. Petersburg, FL 257 pp.

Tomasko, D.A., Corbett, C.A., Greening, H.S., Raulerson, G.E., 2005. Spatial and temporal variation in seagrass coverage in Southwest Florida: assessing the relative effects of anthropogenic nutrient load reduction and rainfall in four contiguous estuaries. Marine Pollution Bulletin. 50: 797-805.

Tomasko, D.A. and E.H. Keenan. 2010. Potential impacts of sea level rise on Sarasota Bay seagrasses. Pp. 463-477. In: S.T. Cooper (ed.). Proceedings, Tampa Bay Area Scientific Information Symposium, BASIS 5. October 20-23 2009. St. Petersburg, Florida. 538 pp.

Tyler, D., Zawada, D.G., Nayegandhi, A., Brock, J.C., Crane, M.P., Yates, K.K., and Smith, K.E.L., 2007, Topobathymetric data for Tampa Bay, Florida: U.S. Geological Survey Open-File Report 2007-1051 (revised). http://pubs.usgs.gov/of/2007/1051.

United States Army Corps of Engineers and South Florida Water Management District. 2002. Central and Southern Florida Project – Comprehensive Everglades Restoration Plan: Project Management Plan – Florida Keys Tidal Restoration Project. 104 pp.

Continuous Monitoring and a Statistical Approach to Ground Gas Risk Assessment at a Substation Site

Bala Palananthakumar

PhD, BSc.Eng (Hons), CSci, C.WEM, MCIWEM
Senior Environmental Engineer, Contaminated Land and Hydrogeology
Infrastructure
Epsom, UK

Kristian Fox

MSci MSc FGS
Hydrogeologist, Contaminated Land and Hydrogeology
Infrastructure
Epsom, UK

Abstract

This paper details an innovative approach to ground gas risk assessment using a statistical approach in the fault tree analysis applied to an operational electrical substation compound in the south of England.

The site is one of the most complicated brownfield sites operated by National Grid. Historical maps indicated that, prior to development, a landfill crossed the site boundary near a substation. The ground investigations undertaken by Atkins and others at the site had identified elevated concentrations of ground gases (both methane and carbon dioxide) in the vicinity of and directly beneath the relay room of substation.

Atkins has recently reassessed this site using additional continuous monitoring of ground gas (including gas flow) collected using the latest available technology and by applying a statistical approach involving probability density functions of gas data as recommended in the latest guidance. This has reduced the level of conservatism in the previous assessment and increased confidence in the estimated risk level such that the ground gas risk has been demonstrated to be acceptably low. As a consequence, the requirement for ongoing gas control and mitigation measures has been shown to be unnecessary enabling closure of the project and the lifting of operational controls.

Keywords

Ground gas; Methane; Quantitative risk assessment; Fault tree analysis; Continuous monitoring

Philip Harrison

MEng (Hons) CEng, MICE NECReg
Principal Consultant, Contaminated Land and Hydrogeology
Infrastructure
London, UK

Jonathan Steeds

BSc (Hons), CSci, CEnv, FCIWEM, MCIWM, SiLC
Technical Director, Contaminated Land and Hydrogeology
Infrastructure
Epsom, UK

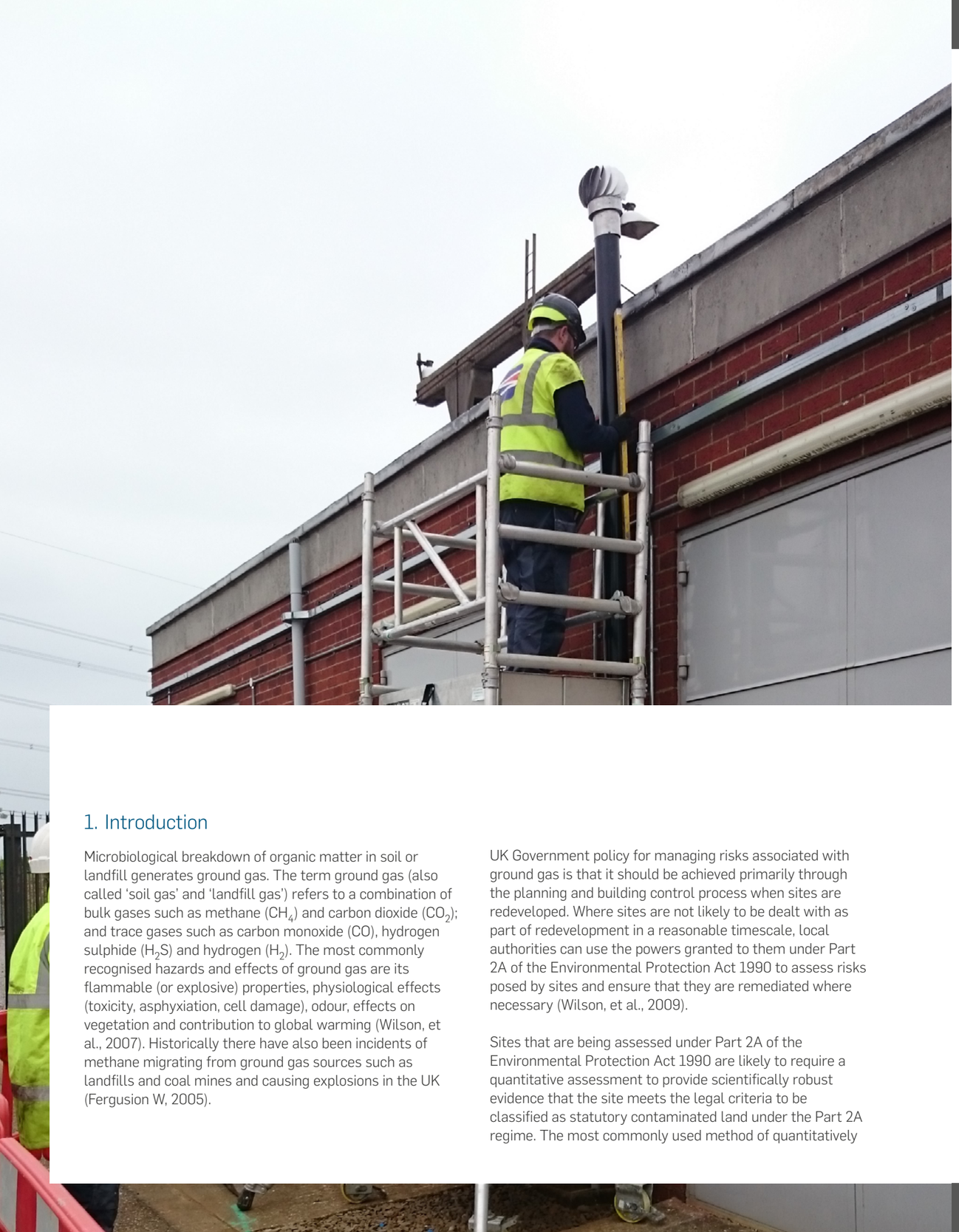

1. Introduction

Microbiological breakdown of organic matter in soil or landfill generates ground gas. The term ground gas (also called 'soil gas' and 'landfill gas') refers to a combination of bulk gases such as methane (CH_4) and carbon dioxide (CO_2); and trace gases such as carbon monoxide (CO), hydrogen sulphide (H_2S) and hydrogen (H_2). The most commonly recognised hazards and effects of ground gas are its flammable (or explosive) properties, physiological effects (toxicity, asphyxiation, cell damage), odour, effects on vegetation and contribution to global warming (Wilson, et al., 2007). Historically there have also been incidents of methane migrating from ground gas sources such as landfills and coal mines and causing explosions in the UK (Fergusion W, 2005).

UK Government policy for managing risks associated with ground gas is that it should be achieved primarily through the planning and building control process when sites are redeveloped. Where sites are not likely to be dealt with as part of redevelopment in a reasonable timescale, local authorities can use the powers granted to them under Part 2A of the Environmental Protection Act 1990 to assess risks posed by sites and ensure that they are remediated where necessary (Wilson, et al., 2009).

Sites that are being assessed under Part 2A of the Environmental Protection Act 1990 are likely to require a quantitative assessment to provide scientifically robust evidence that the site meets the legal criteria to be classified as statutory contaminated land under the Part 2A regime. The most commonly used method of quantitatively assessing risk on gassing sites is to apply a fault tree analysis which provides a numerical estimate of the risk (i.e. a probability that an adverse effect will occur in any year or other specified period).

This paper details an innovative approach to ground gas risk assessment using fault tree analysis as applied to an operational electrical substation compound in the south of England.

2. Conceptual Site Model (CSM)

The site is approximately 1.02 ha and includes three electrical substation compounds (400 kV, 132 kV and 33 kV) operated by National Grid as shown in Figure 1. The site is underlain by Made Ground (including in part a historically infilled gravel pit) and Superficial Deposits (Glaciofluvial sandy clay) over the Holywell Nodular Chalk Formation as shown in Figure 2.

Gravel pits were identified both on site and extending to the north of the site on historical maps prior to 1964 and were infilled with landfill waste prior to construction of the 132kV substation compound in 1972. The waste types input into this historical landfill are listed on the UK Environment Agency website as inert, industrial, commercial and domestic.

Biodegradable materials such as domestic refuse, wood and paper which had been identified within the infill materials are capable of generating landfill gas including methane. Therefore, there was potential for ground gas to migrate through the ground and then via gaps or cracks in the floor construction and accumulate in the buildings on site. If methane concentrations exceed the Lower Explosive Limit (LEL) of 5% v/v. within a building or confined space such as an electrical cabinet, then this has the potential to ignite. The resulting explosion could cause damage to the structure and its contents and, if the building is occupied, injury or even loss of life.

The potential pollutant linkage of the source-pathway-receptor is presented in Table 1.

Table 1: Potential Pollutant Linkages

Source	Receptor	Pathway
Methane produced from biodegradable material within the landfill under and adjacent to the site.	On site workers at the 132kV compound Plant and building structure of the 132kv compound	Migration of methane from the ground into the building, accumulation within confined spaces followed by ignition leading to an explosion.

3. The Challenge

The site had been characterised by a series of historical ground investigations and assessments undertaken since the earliest pre-construction investigation in 1966. Monitoring locations within the historical landfill, which is considered to be the potential source of ground gas, had reported methane concentrations between 41.8 and 97.2% v/v. Boreholes located next to the relay room of the 132kV substation (i.e. HW02 as shown in Figure 3, along the potential migration pathway of ground gas) had reported lower methane concentrations up to 16.2% v/v but which still exceeded the LEL (5% v/v).

Continuous gas monitoring was undertaken for a period of three months under the floor slab of the 132 kV building relay room (at the receptor) in 2013. Methane was measured above the LEL, up to 29.3% v/v, directly beneath the slab. The estimated risk of methane explosion (using 95th percentile site conditions and applying forward modelling method as per Construction Industry Research and Information Association (CIRIA) Report 152 (O'Riordan, et al., 1995) identified a potential annual frequency of an explosion event to be outside of a 'tolerable risk range'.

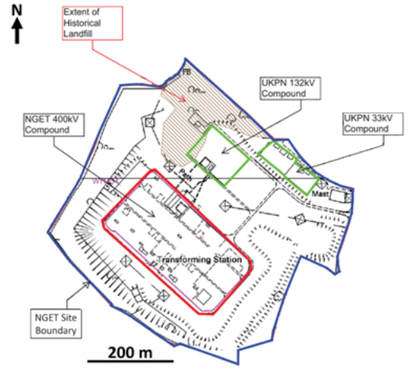

Figure 1: Site layout

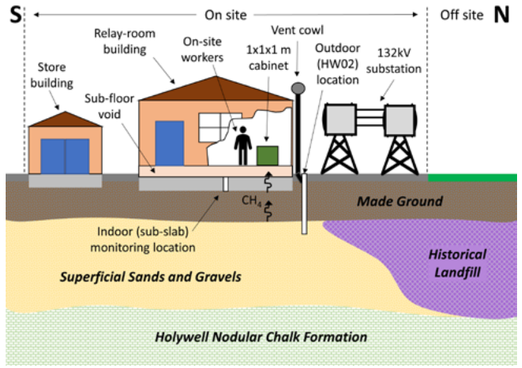

Figure 2: Schematic diagram of conceptual site model

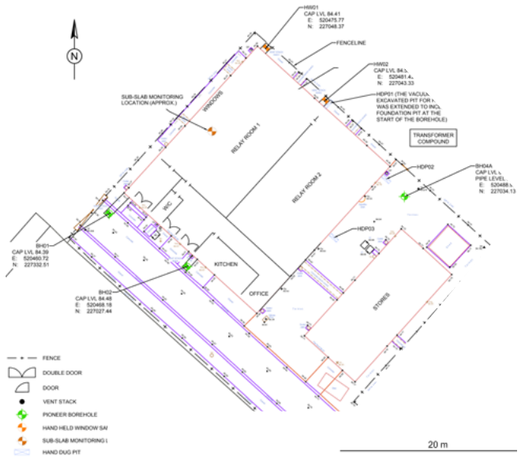

Figure 3: Supplementary gas monitoring locations

Figure 4: Venting cowls installed around the perimeter of the relay room building

As a result of the potential risk identified from ground gas, a temporary gas alarm was installed within the sub-floor void of the relay room on a precautionary basis and an emergency plan was implemented. This arrangement remained operational for over five years from May 2014.

Meanwhile, following a remediation appraisal undertaken for the site, four venting cowls were installed connected to gas wells and extended to above roof level around the perimeter of the relay room building in 2017 to mitigate the risk from the possible accumulation of elevated concentrations of ground gas (as shown in Figure 4).

In 2018, the sub-slab monitoring of the relay room reported a maximum methane concentration of 1.7% v/v, which was significantly lower than the concentrations reported in 2013.

Further, the gas alarm installed above the sub-slab also had not reported methane concentrations above 20% of the LEL.

Although some of these gas monitoring results indicated that the likelihood of the pollutant linkages being realised was low, the risk from ground gas was not able to be discounted due to the lack of gas flow monitoring from beneath the building and the inherent conservatism of the conventional risk assessment methodology.

The challenge was to understand better the residual risks to site users and to reduce or remove the operational costs, disruption and administration complexities involved in maintaining the gas alarm, either through physical remediation or further detailed risk assessment based on additional gas monitoring data.

Figure 5: Sub-slab monitoring (Indoor)

4. The Solution

To resolve the challenge, Atkins undertook a programme of supplementary gas monitoring, which included innovative continuous gas monitoring (including gas flow rates) and conventional spot monitoring, to inform an unconventional detailed quantitative risk assessment (QRA).

The continuous monitoring was undertaken using the Ambisense GasfluX™, which is the world's first device able to monitor real time continuous gas and flow including ambient conditions such as barometric pressure, temperature and humidity (Ambisense). The in-built technology of telemetry in the device enables access to the monitoring data remotely and to check whether critical pressure drops have been achieved.

A total of seven weeks of continuous monitoring (at hourly intervals) was carried out from April to June 2019 at two locations on site (indoor and outdoor as shown in Figure 3). The outdoor unit was attached directly to an existing monitoring location (borehole HW02) along the potential ground gas migration pathway as shown in Figure 6. The indoor unit was attached to the same sub-slab monitoring location as shown in Figure 5 (at the receptor) that was used previously for continuous gas concentration monitoring in 2018.

The supplementary investigation also included three rounds of conventional spot monitoring at six locations (BH01, BH02, BH04A, HW01, HW02, and the indoor sub-slab location as shown in Figure 3) across the site using a hand-held GA5000 gas analyser unit during the same period as the continuous monitoring was undertaken.

5. Supplementary Monitoring Results

Statistical summaries of the continuous and spot monitoring results for 2019 are presented in Table 2 and Table 3 respectively. It can be seen that the methane concentrations and gas flow rates below the building (indoor sub slab) were generally lower than those recorded in boreholes adjacent to the building. The exception was BH02 which was located adjacent to the south-west of the building and further from the historical landfill and ground gas source. Continuous monitoring at the indoor (sub-slab) location identified methane concentrations to be in good agreement with previous monitoring undertaken in 2018 (average 0.6%vol. and maximum 1.7%vol.) and was significantly lower than the concentrations reported in 2013.

Figure 6: Borehole monitoring (Outdoor)

Table 2: Statistical Summary of Continuous Monitoring Results, 2019 (Ambisense, GasfluX™).

Monitoring Location	Number of Readings	Methane (%vol.)		Flow (l/hr)	
		Average	Maximum	Average	Maximum
Outdoor (borehole HW02)	994	3.2	7.0	0.11	2.09
Indoor (sub-slab)	868	0.6	2.0	<0.01	0.48

Table 3: Statistical Summary of Spot Monitoring, 2019 (Gas Analyser, GA5000).

Monitoring Location	Number of Readings	Methane (%vol.)		Flow (l/hr)	
		Average	Maximum	Average	Maximum
Outdoor (HW02)	3	4.1	6.5	<0.1	<0.1
Indoor (sub-slab)	1	1.0	1.0	<0.1	<0.1
BH01	3	1.6	2.4	<0.1	0.1
BH02	3	0.3	0.6	<0.1	0.1
BH04A	3	3.3	4.2	<0.1	0.1
HW01	3	8.4	9.1	<0.1	0.1

6. Continuous Monitoring Validation

Spot monitoring data and continuous monitoring data for the outdoor (HW02) and indoor (sub slab) locations were compared for quality assurance purposes. Table 4 demonstrates the good level of agreement between conventional spot monitoring and continuous monitoring undertaken at the site. Flow readings taken on the GA5000 (spot monitoring) have a resolution of 0.1 l/hr whereas the Ambisense GasfluX™ unit has a resolution of 0.01 l/hr. There was some discrepancy between the flow readings for the outdoor (HW02) location. This may reflect actual changes in ground gas flow regime during the 25-minutes between readings. Alternatively, this may be due to inherent differences in the accuracy of the two monitoring systems with the continuous monitoring system reporting a higher gas flow reading which can be assumed to be more conservative.

Table 4: Continuous Monitoring Validation.

Location	Date	Spot monitoring			Continuous monitoring		
		Time	Methane (%vol.)	Flow (l/hr)	Time	Methane (%vol.)	Flow (l/hr)
Outdoor (HW02)	2 May 2019	11:00	6.5	<0.1	11:25	5.83	0.70
Indoor (sub slab)	2 May 2019	11:40	1.0	<0.1	11:58	0.72	0.08

7. Continuous Monitoring Results: Initial Assessment

7.1. Gas Screening Values

Figure 7 presents the continuous gas monitoring results and gas screening values (GSVs) calculated as per the modified Wilson and Card methodology (Wilson, et al., 2009) for both the outdoor (borehole) and indoor (sub-slab) monitoring locations. This method uses the following formula to calculate the GSV and can be extended to continuous monitoring data.

GSV (l/hr) = gas flow rate (l/hr) x gas concentration (%vol.)

The characteristic situation (CS) rating based on the calculated continuous monitoring data GSVs demonstrated that at least 12% of the monitoring period was CS2, which implies low risk but still requires gas protection measures to be incorporated into new developments (British Standard, 2019).

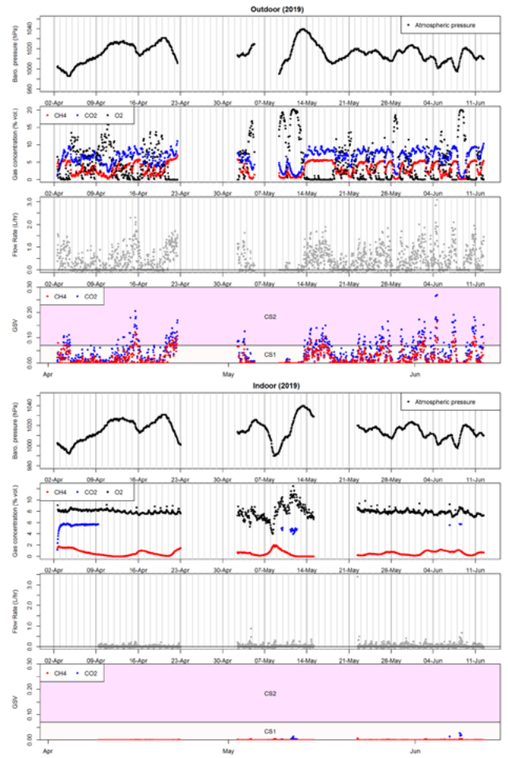

Figure 7: Indoor (sub-slab) and outdoor (borehole) continuous gas monitoring results

7.2. Critical Pressure Drops

Rates of ground gas emission are likely to be highest when there are sharp and/or large falls in barometric pressure. The latest Contaminated Land: Applications in Real Environments (CL:AIRE) guidance (Wilson S., 2018) proposes that a critical pressure drop occurs when the rate and duration of a pressure drop fall within a 'worst case zone'. It is recommended that continuous monitoring should ideally be undertaken to capture at least two significant barometric events (Talbot S., 2019). A significant barometric event is when a critical pressure drop occurs.

The pressure drops that occurred during the indoor (sub slab) monitoring period on different time-scales ranging from one hour (short term) to two days (long term), were also compared against the worst case zone associated with the critical pressure drop presented in the CL:AIRE guidance (Wilson S., 2018) as shown in Figure 8. It clearly showed that the worst-case zone was encountered during the latest continuous gas monitoring period as recommended in the latest CL:AIRE guidance (Talbot S., 2019); therefore, the continuous monitoring data were considered to be sufficient to support a robust ground gas risk assessment.

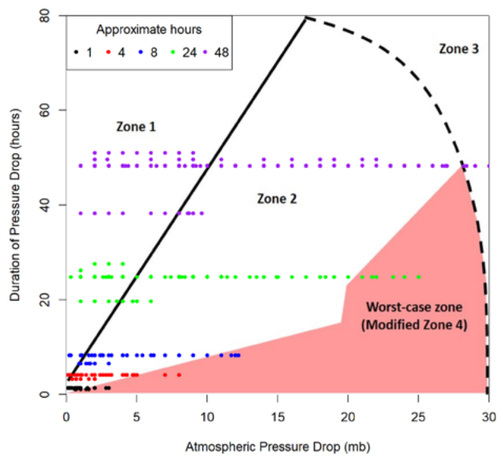

Figure 8: Indoor monitoring record: pressure drops against 'worst-case zone'.

8. Quantitative Risk Assessment (QRA)

While the calculated GSVs (shown in Figure 7) are useful for initial screening of potential gas risks, GSVs do not assess quantitatively the risk posed by extreme events which are unlikely to occur in a given monitoring period. Under the acceptability of risk presented in the CIRIA report (Wilson, et al., 2007), an event causing total loss of life is considered to be of little concern if it has an annual likelihood of less than 1×10^{-7} (one in 10 million years). Therefore, a robust detailed QRA was undertaken to assess the risk.

Only methane was considered in this assessment because the maximum recorded carbon dioxide concentration beneath the building (6.9% v/v) was significantly below the concentration at which it potentially becomes fatal by asphyxiation or by intoxication (22% v/v) (Wilson, et al., 2009). In addition, the explosive risks posed by methane are more acute and occur at lower concentrations, which have previously been exceeded beneath the building. Therefore, assessing methane gas risks was considered to be sufficiently precautionary to also address the risk from carbon dioxide at this site.

The most commonly used method of quantitatively assessing risk on gassing sites is that described in the CIRIA Report (O'Riordan, et al., 1995). This uses a combination of forward modelling (to evaluate the gas concentration at the receptor) and fault tree analysis to provide a numerical estimate of the risk (i.e. a probability that an adverse effect will occur in any year or other specified period) given by:

Risk = (frequency of exposure to hazard) x (probability of hazard occurring)

The method used in this assessment varied from the method described in CIRIA report (O'Riordan, et al., 1995) and included backward modelling (to evaluate the gas flow required to result in ventilation failure) and the statistical approach of considering the PDFs for gas flow based on the latest guidance (Wilson, et al., 2009) and Atkins' extensive experience of undertaking gas risk assessments.

8.1. Fault Tree Analysis

A fault tree is developed by working backwards from the hazard or undesirable event (the top event) and listing in reverse order the things that must happen for the hazard to be realised (contributory events). This continues until a basic event is arrived at where no further events can be developed. The events in a fault tree are connected by logic gates. Probabilities are estimated for the sub events and then the overall probability of the top event (i.e. methane cloud present) occurring can be estimated as shown in Figure 9.

The fault tree analysis aimed to determine the probability of an undesirable event (i.e. explosion from methane) occurring based on estimates for the likelihood or frequency of independent, but necessary conditions (contributory events) arising. For the purposes of this assessment, a number of contributory events to a potential explosion were considered including:

- probability of ventilation failure;
- frequency of ignition; and
- probability of occupation.

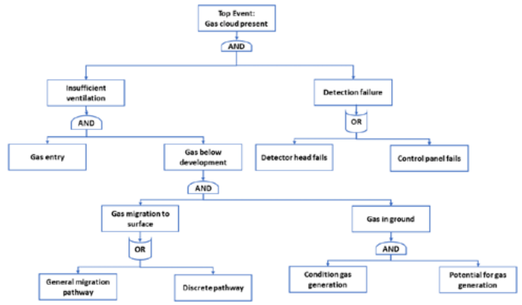

Figure 9: Development of fault tree.

8.1.1. Statistical Approach: Application of Probability Density Function (PDF)

The probability of failure to ventilate the building adequately was derived using a statistical approach made possible by the collection of continuous gas flow and methane concentration data from the sub-slab monitoring location. Under this approach, a set of PDFs (such as exponential, normal, log normal, gamma, Weibull) were fitted to the methane flow rate (i.e. product of gas flow rate and methane concentration,) which is equivalent to the continuous GSV of methane in Figure 7.

Each of the probability density functions can be specified by one or two parameters, for example the PDF of normal distribution P(x) is described by a mean (μ) and a standard deviation (σ) as follows:

$$P(x) = \frac{1}{\sigma\sqrt{2\Pi}} e^{-\frac{(x-\mu)^2}{2\sigma^2}}$$

Similarly, PDFs of other distributions are given by:

Exponential distribution $P(x) = \lambda e^{-\lambda x}$

Gamma distribution $P(x) = \frac{x^{\alpha-1}e^{-\frac{x}{\theta}}}{\Gamma(\alpha)\theta^{x}}$

Weibull distribution $P(x) = \frac{k}{\lambda}\left(\frac{x}{\lambda}\right)^{k-1} e^{-\left(\frac{x}{\lambda}\right)^{k}}$

Where λ and θ are rate parameters; and α and κ are shape parameters.

Appropriate selection of these parameters is required to 'fit' the probability density function to the dataset. The optimal parameters were estimated by maximising the corresponding likelihood function. For the normal, log-normal and exponential distributions likelihood functions were maximised analytically, whereas for the gamma and Weibull functions they were maximised numerically. The maximum likelihood parameters for each of the probability density functions are presented in Table 5.

Table 5: Parameters of Good Fit PDFs

Probability Density Function (PDF)	Parameter	Value	Parameter	Value
Normal	Mean (μ)	0.00043	Standard Deviation (σ)	0.00068
Log Normal	Mean Log (μ)	-8.8	Standard Deviation Log (σ)	1.7
Gamma	Rate (θ)	1400	Shape (α)	0.6
Exponential	Rate (λ)	2300	Specific-case of the gamma probability density function with shape parameter = 1)	
Weibull	Shape (k)	0.21	Scale (λ)	0.1

By comparing a set of five PDFs with a histogram and empirical density function of the observed data (as shown in Figure 10), the gamma distribution (with shape parameter 0.6 and rate parameter 1400) was identified to be the best fit PDF.

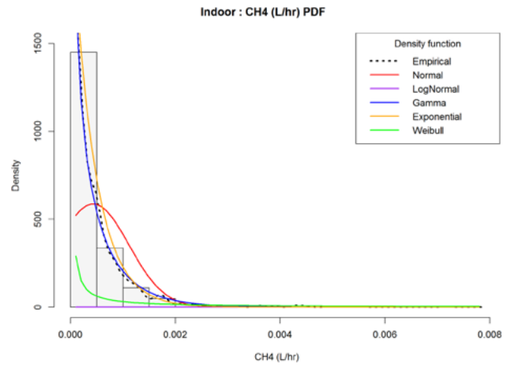

Figure 10: Indoor (sub-slab) methane GSV histogram and probability density functions.

8.1.2. Failure to Ventilate Adequately

The sensitive receptor considered for this detailed QRA is a 1 m x1 m x1 m cabinet, such as the electrical control cabinets present within the relay room building. These are opened infrequently for maintenance operations only and are therefore not routinely ventilated. However, the cabinets are not air-tight and therefore it can be expected that some air exchange will take place with air in the wider building.

Guidance in CIRIA Report 152 (O'Riordan, et al., 1995) estimates the air exchange rate of an unventilated space with an access door (as with the electrical cabinet receptor) to be one air change per hour. However, for the reasons given above, the air exchange rate has been conservatively assumed to be closer to that of an unventilated space with well-sealed doors and windows, i.e. one air change per day.

The threshold for a yellow alert under the current gas alarm system is a methane concentration of 1% vol. Given a 1 m x 1 m x1 m cabinet and an air exchange rate of once per day, a minimum methane gas inflow of 0.4 l/hr is required to exceed the yellow alert threshold of 1%vol. Gas migration into the cabinet is assumed to be through a 2 mm crack extending around the perimeter of the cabinet base. Comparison of this 0.008 m^2 crack with the cross-sectional area of the indoor (sub slab) monitoring location (0.002 m^2) results in a critical flow of 0.1 l/hr. This approach is considered more robust than applying Pickson's law (Peckson G.N, 1985) because it directly compares like-for-like sub-slab ground gas ingress and avoids assumptions about an external borehole area of influence.

This critical flow rate can be compared to the probability density functions fitted to the continuous monitoring data. Based on the best fitting (gamma) probability density function, the probability of exceeding the critical flow rate is 1.1×10^{-63}.

8.1.3. Frequency of Ignition

In the context of the site, this has been assumed to be a spark from a malfunction in the automatic operation of the electrical equipment control cabinets within the building. It is conservatively assumed that such a spark event would occur once a week and therefore the frequency of ignition is assumed to be 52 times in a year. Using a frequency in the fault tree analysis means the resulting calculation will also be expressed per unit of time.

8.1.4. Probability of Occupation

Anecdotal evidence from the current site manager indicated that the site was not continuously occupied. It was suggested that the typical frequency of visits to the site would be once a week for a typical period of an hour (equivalent to an occupancy of 0.006). For this assessment a

conservative assumption has been made, based on the possibility of repair or maintenance works, that occupation could be up to one eight hour day a week (equivalent to an occupancy of 0.05).

8.2. Risk of Explosion Event

From a combination of all the above contributory events, the annual probability of a methane explosion event that would result in harm to human health was calculated as 2.7×10^{-63} (1 in 3.6×10^{62} years).

According to the CIRIA guidance (Wilson, et al., 2007), an event such as a methane explosion in an occupied building, that has the potential for loss of life, is considered to be of little concern if it has an annual likelihood of less than 1 in 10 million years. Events with an annual likelihood less than 1 in 100 million years are considered to be of no concern. Therefore, this assessment suggests that there is not an unacceptable risk from methane explosion within the relay room building.

8.3. Sensitive Analysis: Choice of Probability Density Function

The choice of which probability distribution best represents the data is subjective and while probabilities may be similar for likely events (typical GSVs) the choice of probability distribution can have large impacts on the probabilities of more extreme events (very high GSVs) in the tail of the distribution. The best fitting probability density function (gamma) has been used in this assessment and sensitivity analysis has been undertaken on the impact of selecting the normal and exponential distributions with results presented in Table 6.

Table 8-2 - Sensitivity analysis: choice of probability density function for methane

Probability density function	Annual probability of explosion event	Comment
Exponential $P(x) = \lambda e^{-\lambda x}$	2.5×10^{-103}	Good fit probability density function.
Gamma $P(x) = \frac{x^{\alpha-1}e^{-\frac{x}{\theta}}}{\Gamma(\alpha)\theta^{\alpha}}$	2.7×10^{-63}	Best fit probability density function used in main assessment.
Normal $P(x) = \frac{1}{\sigma\sqrt{2\pi}}e^{-\frac{(x-\mu)^2}{2\sigma^2}}$	$< 1.0 \times 10^{-200}$	Poorly fit probably density function.

The sensitivity analysis indicates that the result (annual probability of methane explosion resulting in harm to human health) is sensitive to the choice of the underlying probability density function. However, the best-fit probability density function (gamma) is also the most conservative, which supports the use of the gamma distribution to model methane GSV in the main assessment.

9. Conclusion

The combination of using a statistical and fault tree analysis approach and use of the innovative continuous gas monitoring technology, conclusively demonstrated that there was not an unacceptable risk of methane explosion within the relay room building. Therefore, Atkins was able to recommend that the existing monitoring activities and other control measures including a temporary gas alarm system could safely be discontinued at the site.

Acknowledgement

The authors gratefully acknowledge the support of National Grid Property Holdings Limited for this project.

References

Ambisense. [Online] [Cited: 01 April 2020.] https://ambisense.net/gasflux/.

British Standard. 2019. BS 8485:2015+A1:2019 : Code of practice for the design of protective measures for methane and carbon dioxide ground gases for new buildings. s.l. : British Standard, 2019.

Fergusion W, and Palananthakumar B. 2005. A fully coupled finite element model of landfill gas migration in a partially saturated soil. Computer Modeling in Engineering and Sciences. 2005, Vol. 8, 3.

O'Riordan, N J and Milloy, C J. 1995. Risk Assessment for methane and other gases from the ground. CIRIA Report 152. ISBN 0-86017-434-4. 1995.

Peckson G.N. 1985. Methane and development of derelict land. s.l. : London Scientific Services, 1985.

Talbot S., Card G. 2019. Technical Bulletin 18: Continuous Ground-Gas Monitoring and the Lines of Evidence Approach to Risk Assessment. s.l. : CL:AIRE, 2019.

Wilson S., Card G., Collins F. and Lucas, J. 2018. Technical Bulletin 17. Ground Gas Monitoring and 'Worst Case' Conditions. London, UK : CL:AIRE, 2018.

Wilson, S, Card, G and Haines, S. 2009. Ground Gas Handbook. ISBN 978-1904445-68-5. 2009.

Wilson, S., et al. 2007. Assessing risks posed by hazardous ground gases to buildings. CIRIA C665. 2007.

New Piling Method in Denmark

Morten Carøe Rasmussen

M.Sc. Ph.D.
Senior Specialist
Broer & Konstruktioner
Aarhus, Denmark

Abstract

Historically, bored piles have been used very seldomly in Denmark as the Danish Codes and Regulations have required that only 30% of the calculated skin friction may be used for the characteristic bearing capacity. Over the past 5-10 years, there has been growing consensus that this is incorrect for cased bored piles. For bored piles in sand there has been no method for determining the bearing capacity so bored piles are not normally used in Denmark and never in frictional materials. At a project in Aarhus Denmark, full displacement bored Fundex piles, a new method in Denmark, was suggested by Keller Funderingsteknik Danmark. Atkins was asked to develop a method to determine the ultimate load bearing capacity for the production piles by evaluating the CPT- tests carried out and compare these with the results of 4 static load tests carried out in different areas in the construction excavation. The method needed to take into account the unloading of the area as excavation for a basement was carried out after installation and testing of the test piles.

Keywords

Bored piles; Static load test; Bearing capacity; CPT tests; Fundex piles

Figure 1: The drilling rig for Fundex piles.

1. Introduction

The calculated bearing capacity of bored piles in Denmark is usually determined as the geostatic determined bearing capacity with a reduction to only 30% of the skin friction in cohesive layers. For frictional material the bearing capacity for driven piles shall be determined using the driving resistance during installation and the “Danish driving formula” to determine the bearing capacity. That is not possible for bored piles. So, in accordance with Danish Codes it is not possible to determine the pile bearing capacity for displacement piles.

As an estimate of the bearing capacity of driven piles in friction material the results of CPT tests are normally used.

For this project driven piles were not an option, as driving was not allowed due to adjacent buildings founded on spread foundations on very loose sand with layers of peat. Any vibrations could lead to compaction of the soil below the footings of the adjacent buildings resulting in settlement.

The project in the centre of Aarhus contains a 6-story building with a basement.

For reduction of vibrations during installation, Keller suggested installation as full displacement driven Fundex piles with toe level in sand. As there is no approved method for determining the bearing capacity in Denmark, Atkins was asked to develop a method to determine the bearing capacity of the production piles based upon the CPT tests conducted, the results of the static load tests and the unloading after the tests were carried out.

2. Soil Conditions

The soil conditions were similar over the complete construction area, but the relative density of the sand layers differed considerably across the construction pit.

The soil conditions at the location were:

+2,6 - -1,4 Fill with peat layers

-1,4 - -5,5 Clay/silt post glacial (w≈70%)

-5,5 - -11,5 Sand/gravel Postglacial

-11,5 - Clay Tertiary

The ground water level is expected in +0,4.

The foundation principle was to install piles in the sand/gravel formation to reduce settlements.

For the project a total of 15 boreholes and 12 CPT tests were carried out. The results of the density of the sand formation was variable so it was decided to locate the 4 test piles for static load testing in different areas of the construction site.

The piles were installed and tested from an excavated level of +1,1 mAOD.

In the final situation the base slab should be cast at level -1,9 mAOD and have a thickness of 0,6 m corresponding to an unloading of the underlying soil of:

$\Delta\sigma' = -(1{,}1-0{,}4)\cdot 18-(0{,}4+1{,}9)\cdot 9+14\cdot 0{,}6$

$= 24{,}9\ \text{kN/m}^2$

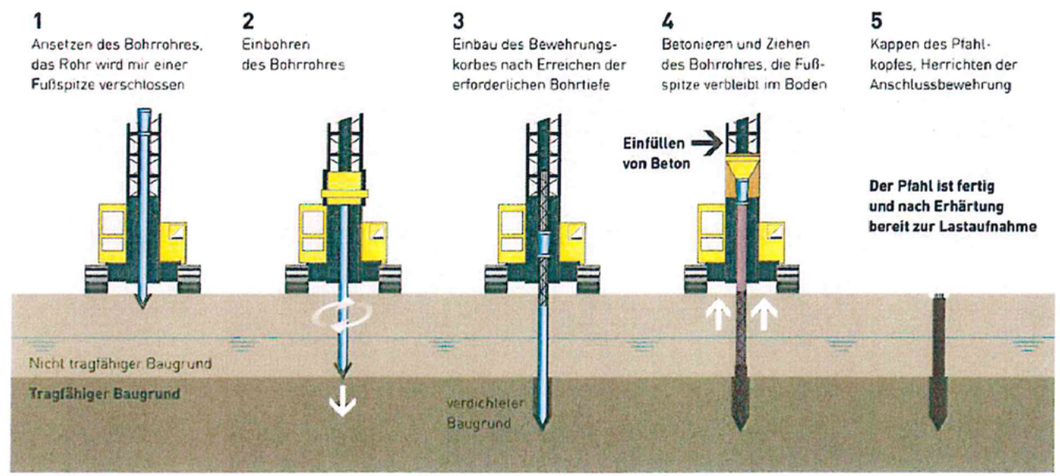

Figure 2: The drilling rig for Fundex piles.

3. Full Displacement Piles

The full displacement piles that were installed were Fundex 560/440 mm, where the tip has a diameter of 560 mm, while the casing has a diameter of 440 mm. When the toe is drilled to the final toe level a reinforcement cage is installed inside the casing after which the casing is retrieved while the pile is filled with concrete. The concrete level in the pile bore is always above the tip level of the casing to avoid inflow of soil material. The method for installation is shown in Figure 2.

Figure 3:The tip of the Fundex pile.

The tip of the piles, see Figure 3, are left in place. The gap between the soil and the casing is filled with concrete, as the casing is always filled with 2-3 m more concrete than outside. This to ensure that the concrete will push out and to avoid inflow of soil material, which will "destroy" the pile.

The installation method will give a tip diameter of 560 mm, while the shaft pile diameter will be between 440 and 560 mm. In sand, the shaft diameter is most likely 440mm, while in hard clay the shaft diameter is expected to be approximately 560mm since in the brief period between drilling and casting of the pile, the clay will be able to hold without support.

In the current project, the piles are installed in sand and hence are end bearing piles. The bearing capacity was therefore determined based on a tip diameter of 560 mm or A_{tip} = 246300 mm².

4. The Test Piles

A total of 4 test piles were installed. The installation data for each of the piles and the representative borehole/CPT test are shown in Table 1

	Pile 1	Pile 2	Pile 3	Pile 4
Top [m]	+1,1			
Length [m]	8,0	9,5	9,5	7,5
Toe [m]	-7,0	-8,5	-8,5	-6,5
Width [m]	0,56			
Future level [m]	-1,9			
Profile	CPT6	CPT12A	CPT10	CPT7

The soil conditions near each of the test piles were evaluated. At each location the tip resistance of the CPT test near the toe to 3x (Diameter of pile) = 3 x 0,56 ≈ 1,5 m was evaluated and a mean and a cautious mean value was determined. As an example, the CPT result for CPT12A, near test pile no. 2 is shown in Figure 4.

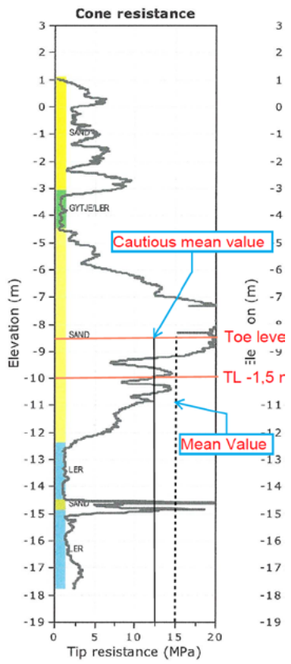

Figure 4: The tip resistance near test pile no.2 - CPT12A

5. Determination of the Bearing Capacity

In Denmark, there is no method for estimating the bearing capacity for Fundex piles. Furthermore, there is no "standard" method to estimate the bearing capacity for a driven pile in sand based upon the results of CPT tests.

In Atkins Denmark, our experience has shown a correlation between tip resistance, qc, and bearing capacity of the pile, q_{pile} of:

q_c/q_{pile} =1,1 for q_c = 10 MPa

q_c/q_{pile} =2,0 for q_c = 30 MPa

Kempert & Becker [1] have evaluated the bearing capacity of a driven based upon CPT. They have also evaluated the bearing capacity of Fundex piles. Atkins correlation (orange) for driven piles, Kempert & Becker's correlation for driven piles (yellow) and K&B's correlation for Fundex piles (blue) are all shown in Figure 5.

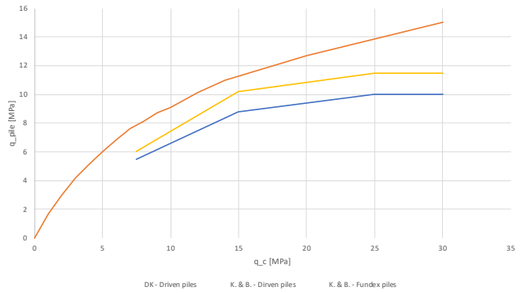

Figure 5: Correlation between qc and qpile for driven and Fundex piles

When evaluating the bearing capacity, it is necessary to be aware of the stress level in the sand. Both the CPT tests and the static load tests were carried out from level +1,1, while the final excavation level is -1,9. This will reduce the bearing capacity of the piles as the effective stress is reduced. According to NGI [2] the correlation between q_c and σ' can be determined as:

$$N_q = q_{c/\sigma'}$$

$$N_q = \tan^2(45+\varphi'/2)\, e^{(\pi/3+4\varphi')}\ \tan^{(\varphi')}$$

q_c is measured and σ' can be calculated. With those known, the friction angle of the sand can be determined. The friction angle and Nq will not change due to unloading. This makes it possible to determine the bearing capacity of a pile after unloading. The excavation after testing can therefore be considered as a reduction of qc. This reduction can be determined as:

$$q_{(c,red)} = q_c\ \sigma'_{red}/\sigma'$$

The bearing capacity that is derived from the above is a measured/calculated pile bearing capacity. The characteristic bearing capacity can then according to DS/EN1997-1 DK NA:2020 [3], be determined as:

$$R_{(c,k)} = R_{(c,m)}/\xi$$

For the test pile itself ξ is 1,1. For the piles where the test pile is representative ξ=1,25 and for other piles ξ=1,5.

For this project, with minimal experience with Fundex piles, ξ=1,5 was used for all production piles.

The design bearing capacity is determined as:

$$R_{(c,d)} = R_{(c,k)}/\gamma_t \text{ , hvor } \gamma_t = 1{,}3.$$

6. Results of Static Load Tests

Four static load tests were carried out at four different locations in the excavation area. At each location the mean and cautious mean value was determined for the representative CPT tests carried out.

	Pile 1	Pile 2	Pile 3	Pile 4
Toe [m]	-7,0	-8,5	-8,5	-6,5
$q_{c,mean}$ [MPa]	12,5	15,0	14,0	4,0
$q_{c,cau}$	11,0	12,5	12,5	3,0

Table 2: Tie tip resistance at the location of the test piles.

The test piles were loaded in 3 load cycles. After each load cycle the pile was unloaded and the settlement of the pile could be determined (No elastic settlement when the pile is unloaded).

In Denmark, failure in a pile is determined as the load where the pile has a settlement of 10% of the diameter of the pile, when unloaded or the load that gives a deformation rate of 20 mm/hour. The deformation rate was not reached in the load tests carried out.

For Fundex piles, the tip diameter is 560 mm and the shaft diameter minimum 440 mm. The failure criteria are then somewhere between 44 and 56 mm. We have conservatively used 44 mm deformation as failure criteria.

Each load cycle contained several load steps. For each test pile the load-displacement curve (Working curve) was produced. As an example, the working curve for test pile no. 2 is shown in Figure 6.

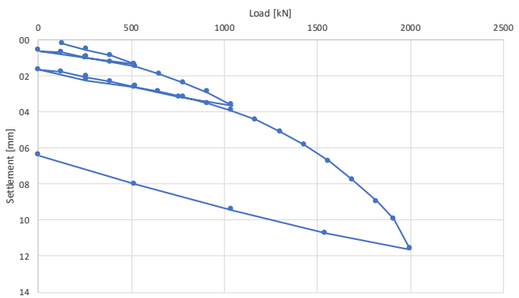

Figure 6: Load displacement curve - Test pile no.2.

Each load step should be maintained until the settlement rate was reducing for a significant time interval. This was not the case for some of the load increments. This was taken into account in the estimate of the bearing capacity.

Based upon the settlements for each unloading, the bearing capacity plots are drawn and shown in Figure 7.

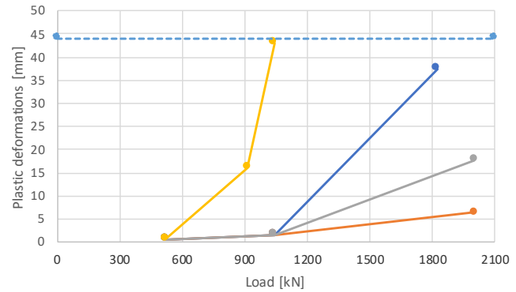

Figure 7: The bearing capacity plots of the four test piles.

The test setup was limited to a maximum test load of 2000 kN.

Figure 7 shows that failure was reached for test piles P1 and P4, while failure was not reached for piles P2 and P3.

The settlement curves are very flat until very close to failure, where the settlement increases rapidly.

The bearing capacity of the four piles are summarized in Table 3.

	Pile 1	Pile 2	Pile 3	Pile 4
F_{pile} [kN]	1800	>2000 ≈2100	2000	914
q_{pile} [MPa]	7,3	>8,1 8,5	8,1	3,7

The results of inserting the q_{pile} vs q_c for the test piles into Figure 5 are shown in Figure 8.

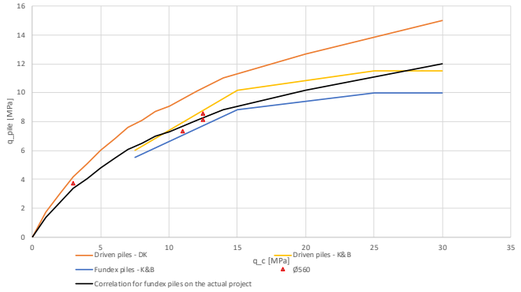

Figure 8: The q_{pile} vs q_c relation for the test piles.

As shown, the test results are better for the actual project than given by Kempert & Becker, but less than the bearing capacity for driven piles.

That makes sense, as no dynamic compaction of the soil takes place during installation.

In the actual project it was decided to use 80% of the expected correlation for driven piles in Denmark. This correlation is shown in Figure 8 as the “black” line. As demonstrated, it suitably corresponds to the test results.

7. The Bearing Capacity of the Test Piles After Excavation

As previously described, an excavation to -1,9 was carried out after the tests had been conducted. This will reduce the bearing capacity.

The design bearing capacity of the test piles are determined in Table 4.

	Pile 1	Pile 2	Pile 3	Pile 4
F_{pile} [kN]	1800	2100	2000	914
$q_{pile,meas}$ [MPa]	7,31	8,53	8,12	3,70
$q_{c,meas}$ [MPa]	10,08	13,25	12,11	3,47
σ'_{ins} [kPa]	87,5	101	101	83
σ'_{red} [kPa]	62,5	76,1	76,1	58,1
$q_{c,meas,red}$ [MPa]	7,2	9,98	9,12	2,43
$q_{pile,red}$ [MPa]	6,16	7,27	7,0	2,81
$F_{pile,red}$ [kN]	1517	1791	1724	692
F_k [kN]	1379	1628	1567	629
F_d [kN]	1061	1252	1206	484

For the production piles the safety factor is higher ξ=1,5 instead of 1,1. The design pile bearing capacity was determined according to the graph shown in Figure 9.

Figure 9: The design bearing capacity for Fundex piles in sand.

8. Production Piles

During installation of the test pile, a full drilling journal showing drilling speed, torque and rotation speed are made and forwarded to the Consultant for approval.

For the production piles it is necessary to verify that the same behaviour is found in all drilling journals as received for the test piles.

In case one shows a different result than expected, the pile shall be further investigated before being approved.

9. What Have We Learned?

The results from the static load tests show that it is possible to evaluate and determine the bearing capacity of full displacement bored Fundex piles in sand, if CPT tests have been carried out on site.

If the soil conditions vary on site it is necessary to carry out a larger number of tests to ensure that all “soft areas” are located. Furthermore, it is necessary to undertake a comprehensive verification of the drilling journals to make sure that all piles are installed in the expected soil types.

It will be recommended to carry out static load tests for the first projects to verify that the established q_c vs q_{pile} correlation is also appropriate for new projects.

The test setup for one of the test piles is depicted in Figure 10.

Figure 10: Possible test setup.

Acknowledgements

The test results and geotechnical information was provided by Keller Funderingsteknik Aps, Jesper Petersen.

References

[1] B. Wrana. Pile load capacity – calculation methods, Studia et Mechanica, vol 37, No.4, pp 83-93, 2015.

[2] NGI Publikasjon nr. 156, Lunne & Christoffersen,1985

[3] DS EN1997-1 + DK NA:2020 Eurocode 7 – Del 1: Generelle regler

SNC·LAVALIN

snclavalin.com

Contact information
Akshaye Sikand
Manager, Knowledge Management
Akshaye.Sikand@snclavalin.com

5629_SL20